

# 國立交通大學

電子工程學系 電子研究所碩士班

## 碩士論文

以 Polyimide 高分子材料/Nafion<sup>TM</sup> 質子交換膜  
為結構作為 pH-ISFET 之微小化固態電極之研究

The study of Polyimide/Nafion<sup>TM</sup> based structures as a  
miniaturized solid-state reference electrode on pH-ISFET  
applications



研究生：何彥忠

指導教授：張國明 教授

桂正楣 教授

中華民國九十七年七月

以 Polyimide 高分子材料/Nafion<sup>TM</sup> 質子交換膜為結構作為  
pH-ISFET 之微小化固態電極之研究

The study of Polyimide/Nafion<sup>TM</sup> based structures as a  
miniaturized solid-state reference electrode on pH-ISFET  
applications

研究生：何彥忠

Student：Yen-Chung Ho

指導教授：張國明

Advisor：Kow-Ming Chang

桂正楣

Cheng-May Kwei



電子工程學系 電子研究所碩士班

碩士論文

A Thesis

Submitted to Department of Electronics Engineering & Institute of Electronics

College of Electrical and Computer Engineering

National Chiao Tung University

in Partial Fulfillment of the Requirements

for the Degree of

Master

In

Electronics Engineering

June 2008

Hsinchu, Taiwan, Republic of China

中華民國九十七年七月

# 以 Polyimide 高分子材料/Nafion™ 質子交換膜為結構作為 pH-ISFET 之微小化固態電極之研究

學生:何彥忠

指導教授:張國明 博士

桂正楣 博士

國立交通大學

電子工程學系 電子研究所碩士班



離子感測場效電晶體( Ion-sensitive Field Effect Transistor )是由 Bergveld 在 1970 年首先提出，由於它的尺寸小，反應速度快、可承受外部應力，且與現今的 CMOS 製程相容，所以在現在的感測元件開發中具有相當大的潛力。

但是由於缺乏一個穩定且微小化的固態參考電極，使得 ISFET 的應用受到很大的限制。為了要實現一個最簡單且小型結構的 ISFET，在微小化的技術上，必須要整合一個固態參考電極在單一 ISFET 晶片上，不需要額外再使用到 REFET 或玻璃電極。

從過去的實驗結果可知道，Nafion™ 混合 Polymer 的結構具有使 REFET 的感測層維持在一個固定的電位且保護它不受離子的干擾的效果。在本篇論文中，我們成功地以 Polyimide/ Nafion™ 的結構應用到固態參考電極的表面修飾上，使得

固態參考電極因為金屬/溶液接面產生的不穩定電壓被消除。由實驗結果可看出，令人困擾的電壓不穩問題，大幅地獲得改善。一個單一的ISFET整合固態參考電極在不需搭配REFET或玻璃參考電極的情況下，對氫離子的靈敏度可達到56.5 mV/pH而且輸出電壓也展現相當優秀的重線性及線性度，且對鈉離子的靈敏度只有7.5 mV/pNa的低靈敏度。以Polyimide/Nafion<sup>TM</sup>塗佈的固態電極作為參考電極，在24小時下的量測結果顯示，飄移速率更可達到每小時1.05 mV的低程度飄移率。



# **The study of polyimide/Nafion<sup>TM</sup> based structures as a miniaturized solid-state reference electrode on pH-ISFET applications**

Student: Yen-Chung Ho

Advisor: Dr. Kow-Ming Chang

Dr. Cheng-May Kwei

Department of Electronics Engineering & Institute of Electronics  
National Chiao Tung University



ISFET( Ion-sensitive Field Effect Transistor ) was first developed by Bergveld in 1970s, and because of its small size, fast response, rigidity and compatibility with standard CMOS process, ISFET is an attractive candidate of modern sensor device.

Due to the lack of a stable and miniaturized solid-state reference electrode, the applications of ISFET will be restricted seriously. In order to realize the single ISFET integrated with the simple and compact structure solid-state reference electrode by miniaturized technology, the simple and compact structure of ISFET sensor was fabricated without the additional REFET or glass reference electrode.

From the previous experimental results, we can know the Nafion<sup>TM</sup> mix PR structure can maintain a constant voltage for the sensing layer of REFET and prevent it from the disturbance of ions. In this thesis, we successfully apply the Polyimide/

Nafion<sup>TM</sup> structure to modify the surface of the solid-state reference electrode. The unstable voltage generated from the thermodynamically undefined metal/electrolyte interface can be eliminated. From the experimental results, it is obviously that the troublesome and unstable problem can be greatly improved. Without REFET arrangement in differential measurement or glass reference electrode, the H<sup>+</sup> sensitivity of single ZrO<sub>2</sub>-pH-ISFET integrated with solid-state reference electrode still can reach to 56.5 mV/pH and the output voltage also exhibit high reproducibility and linearity. Furthermore, the Na<sup>+</sup> sensitivity can reduce to 7.5 mV/pNa. During a measurement period of 24 hours, the reference electrode with Polyimide/Nafion coating shows a low averaged drift rate of 1.05mV/h.



## 誌 謝

首先誠摯地感謝指導教授張國明老師與桂正楣老師，兩位老師悉心的教導使我得以順利完成碩士論文，不時的討論並指點我正確的方向，使我在這些年中獲益匪淺。老師那豁達開朗的個性，讓我印象深刻，並且也教導了我許多待人處世的道理，讓我的想法觀念成長許多，老師對學問的嚴謹更是我輩學習的典範。而擔任桂正楣老師的課程助教，也讓我從中學習到許多寶貴的經驗。

此外，感謝鄧一中老師、鄭兆楨處長在口試中對我論文內容提出的建議及看法，讓我對研究的題目有更進一步的想法，也讓我見識到了教授思考問題的方法，確實是值得我們學習。

本論文的完成另外亦得感謝張知天學長、趙高毅學長、林建宏學長及林聖欽先生的大力協助，不厭其煩的指出我研究中的缺失，且總能在我迷惘時為我解惑，並在我實驗過程中給於建議及鼓勵，使我對於實驗充滿了信心，而且在平常的交談中也傳受了我許多人生的經驗談，讓我受益匪淺。另外我要感謝昇宇、詩帆、菘宏及其他實驗室同學在儀器考核及實驗上的幫助，有了你們讓我可以很快地進行實驗，順利完成我的碩士論文。因為有你的體諒及幫忙，使得本論文能夠更完整而嚴謹。

兩年裡的日子，實驗室裡共同的生活點滴，學術上的討論、言不及義的閒扯、讓人又愛又怕的宵夜、趕作業的革命情感、因為睡太晚而遮遮掩掩閃進實驗室.....，感謝眾位學長姐、同學、學弟妹的共同砥礪，你們的陪伴讓兩年的研究生生活變得絢麗多彩。

最後要感謝我的父母，在我的求學生涯中，你們不曾給予我任何的壓力，讓我可以自由自在的學習。在我遇到挫折失敗時，你們也都給予我極大的關心與幫助，讓我覺得相當幸福及幸運。因為有你們的支持與鼓勵，讓我可以無後顧之憂，順利完成我的學業，取得碩士學位。

誌于 2008.07

何彥忠

## Contents

<b>Abstract (in Chinese)</b>	.....	<b>i</b>
<b>Abstract (in English)</b>	.....	<b>iii</b>
<b>Acknowledgement</b>	.....	<b>v</b>
<b>Contents</b>	.....	<b>vi</b>
<b>Table Captions</b>	.....	<b>viii</b>
<b>Figure Captions</b>	.....	<b>ix</b>
<b>Chapter 1</b>	<b>Introduction</b>	
1.1	The Importance of pH detection.....	1
1.2	Techniques for pH detection.....	1
1.3	The pH glass electrodes.....	2
1.4	The ISFET-based pH sensors.....	3
1.5	The importance of reference electrode.....	5
1.6	Solid-state reference electrode integrated with ISFET.....	6
1.7	Motivation of this work and thesis organization.....	7
1.8	References.....	8
<b>Chapter 2</b>	<b>Theory Description</b>	
2.1	Definition of pH.....	10
2.2	Fundamental principles of ISFET.....	10
2.2.1	From MOSFET to ISFET.....	11
2.2.2	The oxide-electrolyte interface.....	13
2.2.3	Theory for the pH sensitivity of ISFET.....	18
2.3	Non-ideal phenomena of ISFET.....	19
2.3.1	Hysteresis.....	20
2.3.2	Drift.....	20
2.3.3	Dispersive transport.....	21
2.3.4	Physical model for drift.....	23
2.4	Summary.....	25
2.5	References.....	26
<b>Chapter 3</b>	<b>Experiment and Measurement</b>	
3.1	Introduction.....	29



3.2	The characteristics of the Polyimide and Nafion.....	29
3.2.1	Polyimide.....	29
3.2.2	Nafion.....	30
3.3	Fabrication process flow of ISFET.....	30
3.4	Key steps illustration.....	32
3.4.1	Gate region formation.....	32
3.4.2	Sensing layer deposition.....	32
3.4.3	Polyimide/Nafion membrane-based reference electrodes...	33
3.5	Packing and measurement system.....	34
3.5.1	Current-Voltage (I-V) measurement set-up.....	34
3.5.2	Current-Voltage (I-V) measurement set-up with solid-state reference electrodes.....	35
3.5.3	Drift measurement set-up with solid-state reference electrodes.....	35
3.6	References.....	36
<b>Chapter 4</b>	<b>Results and Discussions</b>	
4.1	Introduction.....	37
4.2	Solid-state reference electrode integrated with ISFET.....	37
4.2.1	Solid-state reference electrode.....	37
4.2.2	The glass reference electrode (GRE).....	39
4.3	The experimental results and discussion of solid-state reference electrodes.....	39
4.3.1	Potential reproducibility and linearity.....	39
4.3.2	pH sensitivity.....	41
4.3.3	Drift characteristics.....	42
4.4	Conclusions.....	43
4.5	References.....	44
<b>Chapter 5</b>	<b>Future Work</b>	45

## Table Captions

### Chapter 1

Table 1-1	Sensitivity for different sensing layers	46
-----------	--	----

### Chapter 3

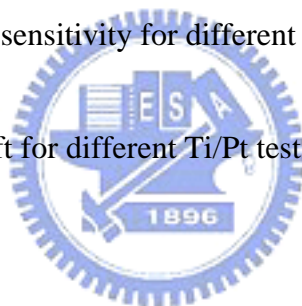
Table 3-1	ZrO <sub>2</sub> Sputtering parameters	53
-----------	--	----

Table 3-2	Test structures of solid-state reference electrode	54
-----------	--	----

### Chapter 4

Table 4-1	Summary of H <sup>+</sup> sensitivity for different test structures	94
-----------	---	----

Table 4-2	Summary of drift for different Ti/Pt test structures	94
-----------	--	----



# Figure Captions

## Chapter 1

Fig. 1-1	Conventional pH glass electrode	46
Fig. 1-2	ISFET cross-section structure of ISFET	47

## Chapter 2

Fig. 2-1	Schematic representation of a MOSFET (a) and an ISFET (b) cross-section structure	48
Fig. 2-2	$I_D$ - $V_{DS}$ curve of an ISFET with $V_{gs}$ (a), and pH (b) as a parameter	48
Fig. 2-3	Electrode and electrolyte interface	49
Fig. 2-4	Schematic representation of site-binding model	49
Fig. 2-5	Hemholtz model	50
Fig. 2-6	Gouy-Chapman model	50
Fig. 2-7	Gouy-Chapman-Stern model	51
Fig. 2-8	Potential profile and charge distribution at an oxide/electrolyte solution interface	51
Fig. 2-9	Schematic representation of carriers hopping through a random array of sites	52
Fig. 2-10	Series combination of the (a) initial (b) hydrated insulator capacitance of sites	52

### Chapter 3

Fig. 3-1	Chemical structure and model of Nafion	55
Fig. 3-2	Fabrication process flow	56
Fig. 3-3	Measurement set-up	59
Fig. 3-4	Detection principle of sensitivity	60
Fig. 3-5	Detection principle of drift	60

### Chapter 4

Fig. 4-1	The $I_{DS} - V_G$ curves and sensitivity linearity of $ZrO_2$ -pH-ISFET measure by glass reference electrode	61
Fig. 4-2	Reproducibility and sensitivity linearity of $ZrO_2$ -pH-ISFET measured by bare Al solid-state reference electrode	62
Fig. 4-3	Reproducibility and sensitivity linearity of $ZrO_2$ -pH-ISFET measured by Al/NF solid-state reference electrode	63
Fig. 4-4	Reproducibility and sensitivity linearity of $ZrO_2$ -pH-ISFET measured by Al/PI solid-state reference electrode	64
Fig. 4-5	Reproducibility and sensitivity linearity of $ZrO_2$ -pH-ISFET measured by Al/PI-mix-NF solid-state reference electrode	65
Fig. 4-6	Reproducibility and sensitivity linearity of $ZrO_2$ -pH-ISFET measured by Al/PI/NF solid-state reference electrode	66
Fig. 4-7	Reproducibility and sensitivity linearity of $ZrO_2$ -pH-ISFET measured by Al/baked PI solid-state reference electrode	67
Fig. 4-8	Reproducibility and sensitivity linearity of $ZrO_2$ -pH-ISFET measured by Al/baked PI-mix-NF solid-state reference electrode	68
Fig. 4-9	Reproducibility and sensitivity linearity of $ZrO_2$ -pH-ISFET measured by Al/baked PI/NF solid-state reference electrode	69

Fig. 4-10	Reproducibility and sensitivity linearity of ZrO <sub>2</sub> -pH-ISFET measured by bare Ti/Pt solid-state reference electrode	70
Fig. 4-11	Reproducibility and sensitivity linearity of ZrO <sub>2</sub> -pH-ISFET measured by Ti/Pt/NF solid-state reference electrode	71
Fig. 4-12	Reproducibility and sensitivity linearity of ZrO <sub>2</sub> -pH-ISFET measured by Ti/Pt/PI solid-state reference electrode	72
Fig. 4-13	Reproducibility and sensitivity linearity of ZrO <sub>2</sub> -pH-ISFET measured by Ti/Pt/PI-mix-NF solid-state reference electrode	73
Fig. 4-14	Reproducibility and sensitivity linearity of ZrO <sub>2</sub> -pH-ISFET measured by Ti/Pt/PI/NF solid-state reference electrode	74
Fig. 4-15	Reproducibility and sensitivity linearity of ZrO <sub>2</sub> -pH-ISFET measured by Ti/Pt/baked PI solid-state reference electrode	75
Fig. 4-16	Reproducibility and sensitivity linearity of ZrO <sub>2</sub> -pH-ISFET measured by Ti/Pt/baked PI-mix-NF solid-state reference electrode	76
Fig. 4-17	Reproducibility and sensitivity linearity of ZrO <sub>2</sub> -pH-ISFET measured by Ti/Pt/baked PI/NF solid-state reference electrode	77
Fig. 4-18	Sensitivity of ZrO <sub>2</sub> -pH-ISFET measured by bare Al solid-state reference electrode	78
Fig. 4-19	Sensitivity of ZrO <sub>2</sub> -pH-ISFET measured by Al/NF solid-state reference electrode	78
Fig. 4-20	Sensitivity of ZrO <sub>2</sub> -pH-ISFET measured by Al/PI solid-state reference electrode	79
Fig. 4-21	Sensitivity of ZrO <sub>2</sub> -pH-ISFET measured by Al/PI-mix-NF solid-state reference electrode	79
Fig. 4-22	Sensitivity of ZrO <sub>2</sub> -pH-ISFET measured by Al/PI/NF solid-state reference electrode	80
Fig. 4-23	Sensitivity of ZrO <sub>2</sub> -pH-ISFET measured by Al/baked PI solid-state reference electrode	80
Fig. 4-24	Sensitivity of ZrO <sub>2</sub> -pH-ISFET measured by Al/baked PI-mix-NF solid-state reference electrode	81
Fig. 4-25	Sensitivity of ZrO <sub>2</sub> -pH-ISFET measured by Al/baked PI/NF solid-state reference electrode	81

Fig. 4-26	Sensitivity of ZrO <sub>2</sub> -pH-ISFET measured by bare Ti/Pt solid-state reference electrode	82
Fig. 4-27	Sensitivity of ZrO <sub>2</sub> -pH-ISFET measured by Ti/Pt/NF solid-state reference electrode	82
Fig. 4-28	Sensitivity of ZrO <sub>2</sub> -pH-ISFET measured by Ti/Pt/PI solid-state reference electrode	83
Fig. 4-29	Sensitivity of ZrO <sub>2</sub> -pH-ISFET measured by Ti/Pt/PI-mix-NF solid-state reference electrode	83
Fig. 4-30	Sensitivity of ZrO <sub>2</sub> -pH-ISFET measured by Ti/Pt/PI/NF solid-state reference electrode	84
Fig. 4-31	Sensitivity of ZrO <sub>2</sub> -pH-ISFET measured by Ti/Pt/baked PI solid-state reference electrode	84
Fig. 4-32	Sensitivity of ZrO <sub>2</sub> -pH-ISFET measured by Ti/Pt/baked PI-mix-NF solid-state reference electrode	85
Fig. 4-33	Sensitivity of ZrO <sub>2</sub> -pH-ISFET measured by Ti/Pt/baked PI/NF solid-state reference electrode	85
Fig. 4-34	Na <sup>+</sup> sensitivity and sensitivity linearity of ZrO <sub>2</sub> -ISFET by Ti/Pt/PI/NF solid-state reference electrode	86
Fig. 4-35	Na <sup>+</sup> sensitivity and sensitivity linearity of ZrO <sub>2</sub> -ISFET by Ti/Pt/baked PI/NF solid-state reference electrode	87
Fig. 4-36	Summary of H <sup>+</sup> -sensitivity for different test structures	88
Fig. 4-37	Summary of H <sup>+</sup> -linearity for different test structures	88
Fig. 4-38	Drift of ZrO <sub>2</sub> -pH-ISFET measured by glass reference electrode for 7 hours	89
Fig. 4-39	Drift of ZrO <sub>2</sub> -pH-ISFET measured by Ti/Pt/PI solid-state reference electrode for 7 hours	89
Fig. 4-40	Drift of ZrO <sub>2</sub> -pH-ISFET measured by Ti/Pt/PI-mix-NF solid-state reference electrode for 7 hours	90
Fig. 4-41	Drift of ZrO <sub>2</sub> -pH-ISFET measured by Ti/Pt/PI/NF solid-state reference electrode for 7 hours	90

Fig. 4-42	Drift of $ZrO_2$ -pH-ISFET measured by Ti/Pt/baked PI solid-state reference electrode for 7 hours	91
Fig. 4-43	Drift of $ZrO_2$ -pH-ISFET measured by Ti/Pt/baked PI-mix-NF solid-state reference electrode for 7 hours	91
Fig. 4-44	Drift of $ZrO_2$ -pH-ISFET measured by Ti/Pt/baked PI/NF solid-state reference electrode for 7 hours	92
Fig. 4-45	Summary of drift for different test structures	92
Fig. 4-46	Drift of $ZrO_2$ -pH-ISFET measured by Ti/Pt/PI/NF solid-state reference electrode for 24 hours	93
Fig. 4-47	Drift of $ZrO_2$ -pH-ISFET measured by Ti/Pt/baked PI/NF solid-state reference electrode for 24 hours	93

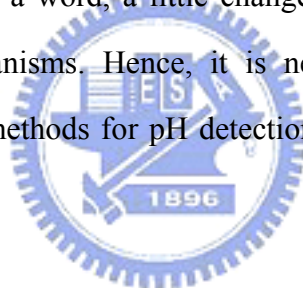


# Chapter 1

## Introduction

### 1.1 The importance of pH detection

pH is one of the most common measurement parameters because so many biological and chemical processes are dependent on pH. We can find the chemical characteristics of a substance by measuring pH. For example, the body fluid of living organisms usually has specific pH range. If the pH of the human blood changes by a little as 0.03 pH units or less the functioning of the body will be greatly impaired [1]. In our surroundings, the pH values of rivers, waters and soils affect the livability of fishes, animals and plants. In a word, a little change of the pH value will result in serious impact to these organisms. Hence, it is necessary to measure pH value accurately. Commonly used methods for pH detection will be introduced in the next section.



### 1.2 Techniques for pH detection

Traditionally, there are many methods for detecting pH value, such as (1) indicator reagents (2) pH test strips (3) metal electrode (4) glass electrode. The methods (1) and (2) are differentiated from colors and are impossible to reach high accuracy. The method (3) is difficult for daily use and reproducing. Because of some limitations in practical applications of the first three methods, the method (4) glass electrode becomes the most widely used method for pH measurement, and is considered to be the standard measuring method. Therefore we will have an introduction for glass electrode.



### 1.3 The pH glass electrodes

In 1906, the first pH glass electrode was developed by M. Cremer with Fritz Haber and many efforts have been devoted to improve its application. The pH glass electrode consists of an electrode membrane that responds to pH, which only permits the passage of hydrogen ions in solution. Generally, a fixed concentration of HCl or a buffered chloride solution inside in contact with an internal reference electrode, which use of Ag/AgCl, as shown in Fig. 1-1.

When the glass electrode is immersed in the solution, the outer bulb surface will be hydrated (the thickness is about 0.3-0.6 nm) and exchange sodium ions for hydrogen ions to build up a surface layer of hydrogen ions [2]. The build up of charges on the inside of the membrane is proportional to the amount of hydrogen ions in the outside solution. The potential difference between inside and outside the thin glass membrane is proportional to this difference in pH value in the external solution, and we can derive the potential difference from Nernst equation:

$$E = E_0 + \frac{RT}{nF} \ln \alpha_{H^+} \quad (1-1)$$

where  $E$  = electrode potential,  $E_0$  = standard potential of the electrode,  $R$  = gas constant ( $8.31441 \text{ JK}^{-1} \text{ mol}^{-1}$ ),  $T$  = temperature (in Kelvin),  $n$  = valence ( $n = 1$  for hydrogen ions),  $F$  = Faraday constant and  $\alpha_{H^+}$  = activity of hydrogen ions.

According to this equation, providing that at one side of the interface the activity of the ion of interest is kept constant, the electrode potential is direct logarithmic function of the ion activity on the other side. Because of its ideal Nernstian response independent of redox interferences, short balancing time of electric potential, high selectivity, reliability and wide pH range, glass electrode is most widely used for pH measurement. However, glass electrode has several drawbacks for many industrial applications. Firstly, they are unstable in alkaline or HF solutions or at temperatures higher than  $100^\circ\text{C}$ . Also, they exhibit a sluggish response and are difficult to

miniaturize. Moreover, they cannot be used in food or in vivo applications due to their fragility of the glass. Finally, due to the need for internal liquid reference solutions, the traditional glass electrode must be used at the vertical position for chemical reproducibility. Consequently, it is very inconvenient in applications. In order to overcome these drawbacks, the all-solid-state electrode sensors have been investigated for a long time. However, it is obvious that the unavailability of a reliable miniature reference electrode hinders many applications. There is an increasing need for alternative pH sensors.

According to ref [1], there are many new techniques for pH detection:

- (1) Optical-fiber-based pH sensors
- (2) Mass-sensitive pH sensors
- (3) Metal oxide pH sensors
- (4) Conducting polymer pH sensors
- (5) Nano-constructed cantilever-based pH sensors
- (6) ISFET-based pH sensors**
- (7) pH-image sensors

As mentioned above, the ISFET-based pH sensor is a new technique for pH detection. Due to the highly advanced IC fabrication techniques, a miniature ISFET-based pH sensor is of particular interest in the field of medical diagnostics for use in implantable devices or on catheter tips and shows a great potential for application in chemical and biological sensing devices.

#### **1.4 The ISFET-based pH sensors**

The ion sensitive field effect transistor (ISFET) was invented by P. Bergveld in 1970 [3] and has been introduced as the first miniaturized silicon-based chemical sensor. The ISFET structure is similar to the Metal Oxide Semiconductor Field Effect Transistor (MOSFET) except that metal gate. In other words, ISFET is a special type of MOSFET without a metal gate, in which the gate oxide is directly exposed to the buffer solution. When the sensing layer of the ISFET contacts with the electrolyte, it will induce a surface potential between the gate oxide and electrolyte. For the

different pH value buffer solution, there are different surface potentials induced at the surface. Hence the electric field at the interface will be changed and the channel conductance that affects the drain current will also be modulated. Since the channel conductance and drain current can be modulated. For instance, the general expression for the drain current of the ISFET in the linear region is

$$I_D = \frac{C_{ox}\mu W}{L} \left[ (V_{GS} - V_T) - \frac{1}{2}V_{DS} \right] V_{DS} \quad (1-2)$$

Therefore, in order to be able to measure the threshold voltage of the ISFET, it is necessary to bias it at constant drain current ( $I_D$ ) and constant drain to source voltage ( $V_{DS}$ ). In such situation there will be only two variables,  $V_G$  and  $V_T$ . When  $V_T$  varies, the gate voltage must adjust by an equal amount to compensate. The circuit to maintain constant  $I_D$  and constant  $V_{DS}$  can be carrying out by using feedback OP amplifiers and current sources and sinks [4]. Different pH concentrations will induce different voltage variation, so we can determine the pH value of the test solution from the potential difference. The more detailed operation mechanisms and theories are presented in Chapter 2. By these method, we can plot a standard linear line between gate voltages and various pH values, and this standard can be taken to measure an unknown acid or alkaline solution [5].

The development of ISFET has been on going for more than 35 years, and the first ISFET sensing layer exploited was silicon dioxide ( $\text{SiO}_2$ ), which showed an unstable sensitivity and a large drift. Recently, there are many materials have been investigated and applied for the ion sensing layer. For example, high dielectric constant insulator materials were used as pH-sensing layers because of their high sensitivity performance and long-term reproducibility. Table 1-1 shows the sensitivities and test ranges of different sensing layers. It is found that pH sensitivity is one of the important characteristic parameters of the ISFET devices and the response of the ISFET is mainly determined with the type of the sensing layer, therefore the sensing material plays a significant role. In the study, we use zirconium

oxide ( $\text{ZrO}_2$ ) as the ion sensing layer. However, because of the poor interface between the high  $k$  sensing layer and silicon substrate, all sensing layers must be deposited on the thermally grown  $\text{SiO}_2$  to improve the interface properties [6], which are low density of interface state, small stress, and good adhesion. Hence, with the study of sensing layer, some material is found can detect different ions, for example,  $\text{K}^+$ ,  $\text{Na}^+$ ,  $\text{Ca}^+$ , and  $\text{H}^+$  ions.

Compare with the conventional pH-meter using glass electrode, ISFET has following features:

- (1) Small size and weight
- (2) Short response time
- (3) Potential of mass production at low cost
- (4) Compatible with the standard CMOS process
- (5) Small sample requirement

However, for most of the sensor devices, it is possible to fabricate a variety of chemical sensors with a small size down to the micrometer scale so that only a small amount of the test solution should be necessary, but this improvement is useless because of the lack of a miniaturized reference electrode [7]. Hence, how to reduce the scale of macroscopic commercial reference electrode is a major challenge. In this study, the problems of the miniaturized solid-state reference electrodes are investigated for practical applications of pH-ISFET. We will discuss the importance of reference electrode in the next section.

## 1.5 The importance of reference electrode

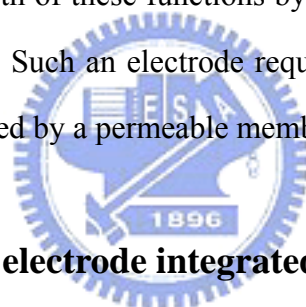
The reference electrode is an important part of electrochemical measurement. The quality of the reference electrode is especially important in the direct potentiometric measurement of pH and blood electrolytes. For a material to be a good reference electrode, the desired parameters are high sensitivity, good linearity, fast response

time, long life, chemical and thermal independence.

An ideal reference electrode for use as the ISFET gate terminal should provide [4]:

- (1) An electrical contact to the solution from which to define the solution potential;
- (2) An electrode/solution potential difference ( $E_{ref}$ ) that does not vary with solution composition.

In other words, it is expected that it is sufficiently stable, that it is not fouled by a sample, and that the reference electrode itself does not contaminate a sample. It is advisable that a reference electrode is easy to manufacture and use, that it is service-free and cheap, and has a long life-time. The conventional silver chloride or calomel electrodes provide both of these functions by maintaining an electrochemical equilibrium with the solution. Such an electrode requires compartments filled with a reference solution and separated by a permeable membrane.



## 1.6 Solid-state reference electrode integrated with ISFET

Due to the lack of metal gate electrode for ISFET, the input gate voltage will be applied through a reference electrode, which provides a stable potential in the electrochemical measuring system, as shown in Fig. 1-2. The most simple and compact structure of ISFET is the all-solid-state reference electrode integrated with ISFET in a single chip. However, very few papers have been devoted to the miniaturization of the reference electrode, although hundreds of papers have been published concerning various sensing devices such as ISFET [8]. For some analytical applications, it is desirable to use all-solid-state pH sensor when the electrode has to work in a non-vertical position. All-solid-state electrodes have several advantages over glass electrode with internal filling solution, one of them being the minimization of the contribution from the liquid junction. Furthermore, all-solid-state electrodes

may be exposed to higher temperatures and pressures than the liquid filling electrodes, and they need not be used in an upright position. They are miniaturizable, do not need refilling with internal solution and can be prepared in various shapes and sizes [9].

Today, due to the frequent applications of potentiometry with ion-selective electrodes in clinical and biological measurements, it is important that a reference electrode is necessary to miniaturize. Hence there has been a considerable effort to develop solid state reference electrodes over the past years. However, it is still a problem to create a long-term stable solid-state reference electrode. Because potential at the solid/liquid interface is thermodynamically undefined, it will lead to significant errors in pH measurement. The unstable problem may come from the redox reaction or other chemical reactions at the metal reference electrode and the liquid interface, i.e. the solid/liquid interface. Hence, providing a stable potential at the interface is a major challenge for miniaturized solid-state reference electrode integrated with ISFET.

## 1.7 Motivation of this work and thesis organization

The presence of the commercial macro reference electrode is unwelcome in clinical and biological measurements. For miniaturization, many groups have been devoted to the development of miniature solid-state reference electrodes. However, these attempts do not seem to be successful with regard to the reproducibility and reliability in comparison with tradition reference electrodes having an internal solution, such as  $\text{Ag}/\text{AgCl}/\text{aq.KCl}$  and  $\text{Hg}/\text{Hg}_2\text{Cl}_2/\text{aq.KCl}$ .

In this study, we will focus on investigating the miniaturization of solid-state reference electrodes with no internal aqueous phase. By directly coating polyimide/Nafion<sup>TM</sup> membrane-based materials on the metal reference electrodes, new reference electrodes with no internal aqueous phase have been carried out. The protective membranes were deposited by using a drop-coating method.

In chapter 2, the basic theory and non-ideal phenomenon of ISFET is introduced.

The entire fabrication process and measurement details will be described in chapter 3. After measuring the characteristics of the devices, we bring up some ideas about the experimental results and show the conclusions in chapter 4. At last, some works are presented to investigate in the future.

## 1.8 References

- [1] Y. Q. Miao, J. R. Chen and K. M. Fang, "New technology for the detection of pH", *J. Biochem. Biophys. Methods*, vol. 63, pp. 1-9, 2005.
- [2] P. Bergveld, "ISFET, Theory and Practice", in *IEEE Sensor Conference*, Toronto, Oct. 2003.
- [3] P. Bergveld, "Development of an ion sensitive solid-state device for neurophysiological measurements", *IEEE Trans. Biomed. Eng.*, vol. BME-17, p.70, 1970.
- [4] Paul A. Hammond, Danish Ali, and David R. S. Cumming, "Design of a Single-Chip pH Sensor Using a Conventional 0.6-um CMOS Process.", *IEEE Sensors Journal*, vol. 4, no. 6, Dec, 2004.
- [5] Kow-Ming Chang, Kuo-Yi Chao, Ting-Wei Chou, and Chin-Tien Chang, "Characteristics of Zirconium Oxide Gate Ion-Sensitive Field-Effect Transistors", *Jpn. J. Appl. Phys.* 46, pp. 4333-4337, 2007.
- [6] Lin, Y-S., Puthenkovilakam, R., and Chang, J. P., "Dielectric property and thermal reproducibility of HfO<sub>2</sub> on silicon", *Applied Physics Letters*, 81(11), pp. 2041-2043, 2002.
- [7] A. Simonis, H. Luith, J. Wang, M.J. Schöning, New concepts of miniaturized reference electrodes in silicon technology for potentiometric sensor systems, *Sens. Actuators B* 103, pp. 429-435, 2004.
- [8] H. Suzuki, T. Hirakawa, S. Sasaki, I. Karube, "Micromachined liquid junction Ag/AgCl reference electrode", *Sens. Actuators B* 46, pp. 146-154A, 1998.

[9] Eine, et al., "Towards a Solid-State Reference Electrode," Sensors and Actuators B, 44, pp. 381-388, 1997.





## Chapter 2

### Theory Description

#### 2.1 Definition of pH

The concept of pH was first introduced by Danish chemist S. P. L. Sørensen in 1909. In simpler interpretation, pH is a measurement of how acidic or how basic a solution is. Solutions with pH more than 7 are considered basic, while those with pH less than 7 are considered acid. pH 7 is neutral because it is the pH of pure water at 25°C. In formal, the definition of pH is expressed as

$$pH = -\log a_{H^+} \quad (2-1)$$

where  $a_{H^+}$  is the hydrogen ion activity, the term activity is used because pH reflects the amount of available hydrogen ions, not the concentration of hydrogen ions.

#### 2.2 Fundamental principles of ISFET

Since the first report of the ion-sensitive field effect transistor (ISFET) by P. Bergveld in 1970, ISFET has developed into a new type of chemical sensing device. This device is similar to MOSFET (Metal Oxide Semiconductor Field Effect Transistor), besides the metal gate electrode is replaced with a reference electrode and inserted in an aqueous solution which is in contact with the sensing layer above gate oxide. A schematic structure of MOSFET and ISFET are shown in Fig. 2-1. The following is the theoretical foundations which are mostly used to characterize the ISFET.

### 2.2.1 From MOSFET to ISFET

It is not difficult to find out the difference between ISFET and MOSFET. The difference in the ISFET is replacement of the metal gate electrode of the MOSFET by the series combination of the reference electrode, electrolyte and chemically sensitive insulator or membrane. For this reason, the best way to comprehend the ISFET is to understand the operating principle of a MOSFET first.

The general expression for the drain current of the MOSFET and thus of the ISFET in the non-saturated mode is

$$I_D = \frac{C_{OX}\mu W}{L} \left[ (V_{GS} - V_T) - \frac{1}{2} V_{DS} \right] V_{DS} \quad (2-2)$$

where  $C_{OX}$  is the gate insulator capacitance per unit area,  $W$  is the channel width and  $L$  is the channel length, respectively, and  $\mu$  is the electron mobility in the channel. If the fabrication process is controlled well and biased in well designed applied electronic circuits, we can keep the geometric sensitivity parameter  $\beta = \mu C_{OX} \frac{W}{L}$ , as well as the drain-source voltage  $V_{DS}$ , and the threshold voltage  $V_T$  constant, then the drain current  $I_D$  will be a unique function of the input voltage  $V_{GS}$  in MOSFET. Thus,  $V_{GS}$  is the only variable.

As well-known, the threshold voltage  $V_T$  of MOSFET is

$$V_T = \frac{\phi_M - \phi_{Si}}{q} - \frac{Q_{OX} + Q_{SS} + Q_B}{C} + 2\phi_F \quad (2-3)$$

where the first term describes the the difference in the workfunction between the gate metal ( $\phi_M$ ) and the silicon ( $\phi_{Si}$ ), the second term is due to the effect of accumulated charge in the oxide ( $Q_{OX}$ ), at the oxide-silicon interface ( $Q_{SS}$ ), and the depletion charge in the silicon ( $Q_B$ ), and the last term  $\phi_F$  is the potential difference between the Fermi levels of the doped and intrinsic silicon.

When immersed in a liquid, the oxide-electrolyte interface will have a chemical reaction and build up charges at the interface which produce an electrostatic potential distribution. The interface potential at the gate oxide-electrolyte interface is determined by the surface dipole potential of the solution  $\chi_{sol}$ , which is a constant, and the surface potential  $\psi_0$  which results from a chemical reaction, usually governed by the dissociation of oxide surface group. And then the interface potential between the liquid and reference electrode is the reference electrode potential relative to vacuum  $E_{ref}$ . Hence the expression for the ISFET threshold voltage becomes

$$V_T = E_{ref} - \psi_0 + \chi_{sol} - \frac{\phi_{Si}}{q} - \frac{Q_{OX} + Q_{SS} + Q_B}{C} + 2\phi_F \quad (2-4)$$

from the Eq. (2-4), the work function of the metal gate  $\phi_M$  seems to be disappeared, but this is not true, because it is “buried” by definition in the term  $E_{ref}$  [2]. Furthermore, we can find that all terms are constant except  $\psi_0$ , it dominates the sensitivity of ISFET to the electrolyte pH. The parameter  $\psi_0$  is a function of solution pH value and is determined by surface chemical reaction at the sensing layer. According to the above-mentioned, we can know that the ISFET drain current  $I_D$  is a function of  $V_{GS}$  and  $V_T$ , i.e.  $I_D(V_{GS}, V_T)$ , and  $V_T$  is a function of surface potential  $\psi_0$ , i.e.  $V_T(\psi_0)$ , where  $\psi_0$  is a function of pH solution. We can see these results obviously in Fig. 2-2. Therefore, detailed investigation of the electrode-electrolyte interface is necessary for designing a high pH sensitivity ISFET.

In brief, An ISFET is electronically identical to a MOSFET, but with one more feature: the possibility to chemically modify the threshold voltage via the interfacial potential at the oxide-electrolyte interface. we will have a statement at the oxide/electrolyte interface in the next section, that is the key point of ISFET.

## 2.2.2 The oxide-electrolyte interface

As mentioned in the preceding section, when we immerse the ISFET in the pH buffer solution, the oxide/electrolyte interface will build up charges and generate an electrostatic potential. The characteristics of the ISFET are completely controlled by the properties of the oxide-electrolyte interface, protonation/deprotonation of the gate material is influenced by the pH solution, which controls the surface potential.

But what is the charging mechanism at the surface? The site-binding model introduced by Yate et al. is the most well-known model to describe the charging mechanism at the oxide/electrolyte interface as illustrated in Fig. 2-3 and Fig. 2-4. The surface of any metal oxide (the sensing layer) always contains hydroxyl groups, for instance, in the case of silicon dioxide is SiOH groups. In this model, the oxide surfaces are assumed to be amphoteric, i.e. the amphoteric sites may donate or accept a proton from the solution, leaving a negatively charged or positively charged surface group, respectively. The surface reactions are:



where A is the metal oxide component, such as Si, Al, Zr, Ta, and  $H_B^+$  represents the protons in the bulk of the solution. From these chemical reactions, it is clear that an originally neutral surface hydroxyl site can be neutral, protonized or deprotonized depending on the pH of the bulk solution. For this reason it is called an amphoteric site. We also have to know that there are a fixed number of surface sites per unit area,  $N_s$

$$N_s = v_{AOH} + v_{AOH_2^+} + v_{AO^-} \quad (2-7)$$

Base on some electrochemical knowledge and math derivation, we can get the surface charge density  $\sigma_0 [C/m^2]$

$$\sigma_0 = q(v_{AOH} - v_{AO^-}) = -qB \quad (2-8)$$

where B is the number of negatively charged groups minus the number of positively charged groups in mole per unit area. We can see that when the number of positively and negatively charged groups on the surface is equal and consequently there will be no net charge on the surface. In this condition, we say the pH value at the point of zero charge is  $pH_{pzc}$ . One more thing we have to know is that different operations of ISFETs (flat band condition and linear region) will yield different value of  $pH_{pzc}$  [3].

Then

$$\sigma_0 = qN_s \left( \frac{a_{H_s^+}^2 - K_a K_b}{K_a K_b + K_b a_{H_s^+} + a_{H_s^+}^2} \right) \quad (2-9)$$

which  $K_a$  and  $K_b$  are intrinsic dissociation constants. A detailed derivation can see the Ref. [4,5]. Equation (2-9) shows the relation between the activity of the protons at the oxide surface  $a_{H_s^+}$  and the surface charge density  $\sigma_0$  in terms of the total number of available sites  $N_s$  and the intrinsic dissociation constants  $K_a$  and  $K_b$ . After we get the surface charge density, we can find the intrinsic buffer capacity  $\beta_{int}$ , the capability of the surface to store charge as result of a small change in the  $H^+$  concentration, defined as

$$\frac{\partial \sigma_0}{\partial pH_s} = -q \frac{\partial B}{\partial pH_s} = -q\beta_{int} \quad (2-10)$$

From equation (2-9) and (2-10), we can get  $\beta_{int}$

$$\beta_{int} = N_s \frac{K_b a_{H_s^+}^2 + 4K_a K_b a_{H_s^+} + K_a K_b^2}{(K_a K_b + K_b a_{H_s^+} + a_{H_s^+}^2)^2} 2.3 a_{H_s^+} \quad (2-11)$$

It is called ‘‘intrinsic’’ buffer capacity, because it is only capable of buffering small changes in the surface pH ( $pH_s$ ) and not in the bulk pH ( $pH_b$ ). We can see that the value of  $N_s$ ,  $K_a$  and  $K_b$  are oxide dependent. More surface sites will have larger  $\beta_{int}$ . According to Ref. [4], Hydrolysis of the surface will create more surface sites

and thus a rise in the intrinsic buffer capacity and the sensitivity.

Not only the surface reaction will affect the surface charge density, but also the background electrolyte will influence the surface charge density [4]. This dependence is ascribed to variations in the double layer capacitance. For reasons of charge neutrality the surface charge  $\sigma_0$  is balanced by an equal but opposite charge,  $\sigma_{dl}$ , in electrolyte. The two opposite charges,  $\sigma_0$  and  $\sigma_{dl}$ , parallel to each other form the electrical double layer structure, and the integral electrical double-layer capacitance is named  $C_{dl,i}$ . The relation between  $\sigma_0$ ,  $\sigma_{dl}$ ,  $C_{dl,i}$  and  $\psi_0$  is given by

$$\sigma_{dl} = -\sigma_0 = -C_{dl,i}\psi_0 \quad (2-12)$$

where the potential difference  $\psi_0 = \psi_s - \psi_B$ , the surface potential subtracts the bulk potential of the electrolyte.

But what is the detailed mechanism for the electrical double layer? The first double layer model is proposed by Helmholtz in 1879. He regards the double layer as a parallel plate capacitance structure as shown in Fig. 2-5. The plate distance “r” is taken as the ion radius and the double layer capacitance  $C_{dl} = \frac{Q}{V}$  will be a constant value, where Q is the surface charge and V is the potential difference of the double layer. But from the experiment, we can know the double layer capacitance is not a constant value, so the Helmholtz is not suitable to describe the exact double layer structure. Therefore the Helmholtz model is merely suitable for the high concentration electrolyte. Because the potential difference will be large in high concentration electrolyte and the double layer structure will be like the parallel plate capacitance.

Because the Helmholtz model only considers the electrostatic force, therefore it can not model the relation between the double layer capacitance and electrolyte concentration. In the beginning of 20th century, Gouy and Chapman proposed the idea of a diffuse layer to interpret the capacitive behavior of an electrode/electrolyte interface as shown in Fig. 2-6. This model made significant improvements by

introducing a diffuse model of the electrical double layer, in which the potential at a surface decreases exponentially due to adsorbed counter-ions from the solution. They think that the ions in the solution are not only electrostatically attracted to the electrode surface but also the attraction is counteracted by the random thermal motion which acts to equalize the concentration through the solution. The ions concentration in the electrolyte will obey the Boltzmann equation:

$$C_i(x) = C_i^0 \exp\left(\frac{-z_i q \phi_x}{kT}\right) \quad (2-13)$$

where  $\phi_x$  is the potential at any distance  $x$  with respect to the bulk of the solution,  $C_i(x)$  and  $C_i^0$  are the molar concentration of species  $i$  at a distance  $x$  and in the bulk of the solution, respectively.  $Z_i$  is the magnitude of the charge on the ions. The relation between ionic activity ( $a_i$ ) and ions concentration ( $c_i$ ) is  $a_i = f_i \times c_i$ , where  $f_i$  is activity coefficient, in diluted electrolyte  $f_i$  will be approach unity. However, the Gouy-Chapman model has one major drawback. The ions are considered as point charge that can approach the surface arbitrarily close in this model. This will cause unrealistic high concentrations of ions near the surface at high values of  $\psi_0$  [4]. Hence, the Gouy-Chapman model only suitable for low concentration electrolyte. This imply that the electrical double layer structure have to combine the Hemholtz and Gouy-Chapman model in certain way.

In 1924, Stern combined these two double layer models, named Gouy-Chapman-Stern model. The Gouy-Chapman-Stern model, which combines the Helmholtz single adsorbed layer with the Gouy-Chapman diffuse layer, is most widely used to describe the electric double layer structure in ISFET literature. The model describes that some of the ions in the electrolyte are next to the electrode surface and because of the finite ions size, the ions couldn't approach the surface arbitrarily close. The other ions are distributed in the electrolyte according to the

Boltzmann equation and form a charge diffuse layer in the electrolyte. There is a distance,  $x_H$ , which is the closest plane for the centers of the ions. Hence, the diffuse layer is starting from  $x_H$ , and will possess the same amount of charge  $\sigma_{dl}$  (of opposite sign) as oxide surface charge  $\sigma_0$ , because the Helmholtz layer is not containing any charge, as shown in Fig. 2-7 and Fig. 2-8. In Gouy-Chapman-Stern model, the double layer capacitance consists of a series network of a Helmholtz layer capacitance (Stern capacitance) and a diffuse layer capacitance. The difference between  $\psi_0$  and  $\psi_1$  is the potential difference across the Stern capacitance and the Stern capacitance has a value of  $\frac{\epsilon_r \epsilon_0}{x_H} [F/m^2]$ . By the Gouy-Chapman-Stern model, we can get the critical parameter : differential double layer capacitance  $C_{dif}$ , the ability of the double layer to store charge in response to a small change in the potential, defined as

$$C_{dif} = \frac{\partial \sigma_0}{\partial \psi_0} = - \frac{\partial \sigma_{dl}}{\partial \psi_0} \quad (2-14)$$



According Ref. [3], for reasons of simplicity, not the expression for  $C_{dif}$  is stated here, but of its inverse. The derived inverse  $C_{dif}$  is made up of two components in series:

$$\frac{1}{C_{dif}} = \frac{\partial \psi_0}{\partial \sigma_0} = \frac{1}{C_{Stern}} + \frac{1}{\sqrt{\frac{2\epsilon_r \epsilon_0 z^2 q^2 n_0}{kT} \cosh\left(\frac{zq\psi_1}{2kT}\right)}} \quad (2-15)$$

where  $\psi_1$  is the potential at  $x_H$ ,  $n_0$  the concentration of each ion in the bulk solution in number/litre, and  $z$  the valence of the ions. The parameters  $\epsilon_r$ ,  $\epsilon_0$ ,  $k$ ,  $q$ , and  $T$  have their usual meaning.



### 2.2.3 Theory for the pH sensitivity of ISFET

From above discussions, the sensitivity of pH ISFET is related to the intrinsic buffer capacity  $\beta_{int}$  and the differential capacitance  $C_{dif}$ . By site-binding model and Gouy-Chapman-Stern model, we can get the values of  $\beta_{int}$  and  $C_{dif}$ , respectively.

The pH sensitivity is the change of the insulator-electrolyte potential,  $\psi_0$ , on a change of the bulk pH,  $\frac{\partial \psi_0}{\partial pH_B}$ . This expression is derived from a separate treatment of both sides of the double layer, i.e., the gate insulator and the electrolyte [8]. Combining equation (2-10) and equation (2-14), we can get the effect of a small change in the surface pH ( $pH_S$ ) on the change in the surface potential  $\psi_0$ ,

$$\frac{\partial \psi_0}{\partial pH_S} = \frac{\partial \psi_0}{\partial \sigma_0} \cdot \frac{\partial \sigma_0}{\partial pH_S} = -\frac{q\beta_{int}}{C_{dif}} \quad (2-16)$$

Combing equation (2-16) with the Boltzmann equation, the activity of the of the bulk protons  $a_{H_B^+}$  can be related to the activity of the protons in the direct vicinity of the oxide surface  $a_{H_S^+}$ , that is

$$a_{H_S^+} = a_{H_B^+} \cdot \exp(-q\psi_0 / kT) \quad (2-17)$$

or in the from of pH

$$pH_S - pH_B = \frac{q\psi_0}{2.3kT} \quad (2-18)$$

then equation (2-16) can be write in the form

$$\frac{\partial \psi_0}{\partial \left( pH_B + \frac{q\psi_0}{2.3kT} \right)} = -\frac{q\beta_{int}}{C_{dif}} \quad (2-19)$$

rearrangement of equation (2-19), we can get a general expression for the sensitivity of the electrostatic potential to changes in the bulk pH,

$$\frac{\partial \psi_0}{\partial pH_B} = -2.3 \frac{kT}{q} \alpha \quad (2-20)$$

with

$$\alpha = \frac{1}{\frac{2.3kTC_{dif}}{q^2 \beta_{int}} + 1}, \quad 0 < \alpha < 1 \quad (2-21)$$

the parameter  $\alpha$  is a dimensionless sensitivity parameter that varies between 0 and 1 depending on  $\beta_{int}$  and  $C_{dif}$ . When  $\beta_{int}$  is high and  $C_{dif}$  is small enough,  $\alpha$  will approaches 1. If  $\alpha = 1$ , the ISFET has a so-called Nernstain sensitivity of precisely -59.2 mV/pH at 298K, which is also the maximum achievable sensitivity.

It appears that the usual SiO<sub>2</sub> from the MOSFET process does not fulfil the requirements of a high value  $\beta_{int}$ . The pH sensitivity of SiO<sub>2</sub> sensing film ISFET is only about 30mV/pH. In order to find high sensitivity sensing film, many sensing layer have been investigated such as Si<sub>3</sub>N<sub>4</sub> [9,10], Al<sub>2</sub>O<sub>3</sub> [9,11], Ta<sub>2</sub>O<sub>5</sub>[9,12], HfO<sub>2</sub> [12], SnO<sub>2</sub> [13].

The ISFET has many advantages over the conventional glass electrode, such as, small size, strong robustness, high input impedance, low output impedance, and rapid response [6,9]. It seems to attractive for biomedical applications. Nevertheless, ISFET has two major time-dependent factors, drift and hysteresis, that will influence the output voltage accuracy and prevent the applications of the ISFET. Therefore, it is importance to understand the mechanism of drift and hysteresis. In the next section, we will have some descriptions for these two unwanted mechanisms.

### 2.3 Non-ideal phenomena of ISFET

The total response of pH-ISFET consists of three parts: fast response, slow response and drift. The response of an ISFET to a fast pH step is general characterized by a fast response, followed by a slow change in the same direction, i.e. slow response,

and ultimately a drift which is linear or logarithmic with time [14]. The fast response time is defined to be the time needed for the output to change from 10% to 90% of the total variation (at the order of ms or faster). The slow response is the extra time needed for the response to reach 100%. The drift is defined as the monotonic change of response after a proper time from the response (ex. 5 hours). However, the technological difficulties in ISFET applications are due to a lack of understanding of the time effects of device. The time-dependent effects of pH-ISFET are characterized by non-ideal mechanisms such as hysteresis and drift, which led to unstable response of the pH-ISFET. Therefore, in order to extend to applications of the pH-ISFET, it is need to measure these non-ideal phenomena.

### 2.3.1 Hysteresis

The amplitude of the slow response is quite small ( 3% to 7% of the total pH response ) but will last for several hours [15]. This is because the slow response is correlated to the response of reactive sites in the bulk, i.e. buried sites of the film, not like the fast response is related to the surface reaction [16,17]. Because the ions diffuse to the buried sites for reaction, it will take a long time for response. The slow response will make small part of the pH response slowly, and occurs with a delay of the order of minutes to hours after the pH variation. There will have different output voltage, when the pH-ISFET was measured many times at the same pH value [18], and we call this phenomena is “Hysteresis” or “Memory effect”, still memory the original pH state.

### 2.3.2 Drift

When the intrinsic response (fast and slow response) is completed, the output voltage of the pH-ISFET still vary with time gradually and monotonically. This

phenomenon is called “Drift”. Drift behavior exists during the entire measurement process. The drift phenomenon has limited the commercial viability of ISFET based sensors. This phenomenon is a complex effect to pH-ISFET which relate to time, sensing film quality, temperature, and pH aqueous solution.

According to Ref [14], it is difficult to identify the cause of this phenomenon, which could be either a surface or a bulk effect, or both. Some possible causes of drift have been proposed. In 1998, Jamasb proposed a physical model quantitatively explains drift in terms of hydration of the silicon nitride surface [19]. This is the first physical model that provides a quantitative description of the drift characteristics.

He proposed that the surface of a silicon nitride film is known to undergo a relatively slow conversion to a hydrated  $\text{SiO}_2$  layer or an oxynitride during contact with an aqueous solution. In other words, as time increases, the thickness of the hydrated layer is increased. Therefore, the oxide capacitance is decreased, results in the threshold voltage increases with time. Since hydration alters the chemical composition of the nitride, then influences the dielectric constant of the overall insulator capacitance, i.e. the series combination capacitance of the superficial hydrated layer. Consequently, the amount of the inversion charge stored in the semiconductor at a given gate bias slowly changes over time, giving rise to a monotonic temporal change in the threshold voltage. The new idea sounds make sense for explaining drift mechanism. The author uses a new diffusion concept, dispersive transport, to model the transport mechanism. We will introduce “dispersive transport” in the next section.

### **2.3.3 Dispersive transport**

Dispersive transport is proposed by Scher and Montroll in 1975 for explaining the phenomenon of the long tail photocurrent  $I(t)$  in photoconductor like  $\text{As}_2\text{Se}_3$ , which can not be explained by traditional Gaussian diffusion theory [20,21]. They use

a stochastic transport model based on time-dependent continuous-time random walk to interpret dispersive transport. Dispersive transport does not depend on the details of any specific mechanisms, but characterizes the motion of a carrier subjected to a broad distribution of event times. The event times include **【1】** hopping times from hopping transport **【2】** trap release times from multiple-trap transport **【3】** or both **【1】** and **【2】** that is from trap-controlled hopping transport. In ISFET, sites may be the buried sites beneath the sensing layer surface and traps may be the dangling bond in the sensing films.

The carriers transport in an amorphous insulating material, which considered as a network of localized sites, by a succession of hops from one site to another, as shown in Fig. 2-9. Each line represents a transition rate  $W(r)$

$$W(r) = W_0 e^{-r/r_0} e^{-\Delta/kT} \quad (2-22)$$

where  $r$  is the difference in position,  $\Delta$  is the energy level of the sites,  $r_0$  is the radius of the local charge distribution. We can know that  $W(r)$  is sensitive to the sites distance and  $\Delta$ , the difference in position and energy levels of the sites, respectively. The sensitivity of  $W(r)$  to small changes in  $r$  and  $\Delta$  means that the site-to-site hopping time in such a disordered system will be a highly fluctuating quantity. It will suffer a wide statistical dispersion. This in turn yields a broad distribution of hopping times [20,21]. We shall quantify these ideas with some of the mathematics of the stochastic model. Therefore, the authors designate a hopping time distribution function  $\psi(t)$  which describes the probability per unit time for a carrier to hop at a time  $t$ , at any sites when the previous hop occurred at  $t = 0$ . The function also can describe a distribution in release times in a multiple trap model of the transport.  $\psi(t)dt$  will be the probability that after a carrier arrives in a given cell.

According to Ref [22], dispersive transport is characterized by a power-law time decay of the mobility or diffusivity of the form  $t^{\beta-1}$ ,  $0 < \beta < 1$ . Dispersive transport

leads to a decay in the density of sites/traps occupied by the species undergoing transport and the hydrated layer is essentially limited by dispersive transport in the presence of these sites/traps. The thickness of this hydrated layer will exhibit a stretched-exponential time dependence. That is

$$\Delta N_{S/T}(t) = \Delta N_{S/T}(0) \exp\left[(-t/\tau)^\beta\right] \quad (2-23)$$

where  $\Delta N_{S/T}(t)$  is the area density (units of  $\text{cm}^{-2}$ ) of sites/traps occupied,  $\tau$  is the time constant associated with structural relaxation, and  $\beta$  is the dispersion parameter characterizing dispersive transport.

### 2.3.4 Physical model for drift

Jamasb proposed the physical model for drift in 1997 [24]. The key point of this model was that employing the dispersive transport theory to express the drift of gate voltage, which is caused by hydration effect at the insulator/electrolyte interface.

Since hydration leads to a change of the chemical composition of the sensing oxide layer, it is reasonable to assume that the dielectric constant of the hydrated layer differs from the dielectric constant of the original sensing oxide. The overall insulator capacitance, which is determined by the series combination of the hydration layer and the underlying sensing film, will exhibit a slow, temporal change. When drift phenomenon occurs, the gate voltage will simultaneously exhibit a change to keep a constant drain current. The change in the gate voltage can be written as

$$\Delta V_G(t) = V_G(t) - V_G(0) \quad (2-24)$$

Since the voltage drop inside of the semiconductor is kept constant,  $\Delta V_G(t)$  becomes

$$\Delta V_G(t) = [V_{FB}(t) - V_{FB}(0)] + [V_{ins}(t) - V_{ins}(0)] \quad (2-25)$$

where  $V_{FB}$  is the flatband voltage and  $V_{ins}$  is the voltage drop across the insulator.  $V_{FB}$  and  $V_{ins}$  are given by

$$V_{FB} = E_{ref} + \chi^{sol} - \psi_0 - \frac{\phi_{Si}}{q} - \frac{Q_{OX} + Q_{SS}}{C_{OX}} \quad (2-26)$$

$$V_{ins} = \frac{-(Q_B + Q_{inv})}{C_{OX}} \quad (2-27)$$

where  $Q_{inv}$  is the inversion charge. If the temperature, pH, and the ionic strength of the solution are held constant,  $E_{ref}$ ,  $\chi^{sol}$ ,  $\psi_0$ , and  $\phi_{Si}$  can be neglected, so the drift can be rewritten as

$$\Delta V_G(t) = -(Q_{OX} + Q_{SS} + Q_B + Q_{inv}) \left[ \frac{1}{C_i(t)} - \frac{1}{C_i(0)} \right] \quad (2-28)$$

In this study, the gate oxide of the fabricated ISFET was composed of two layers, a lower layer of thermally-grown SiO<sub>2</sub> of thickness,  $x_L$ , and an upper layer of sputter-grown ZrO<sub>2</sub> of thickness,  $x_U$ .  $C_i(0)$  is the effective insulator capacitance given by the series combination of the thermally-grown SiO<sub>2</sub> capacitance,  $\epsilon_L/x_L$ , and the sputter-grown ZrO<sub>2</sub> capacitance,  $\epsilon_U/x_U$ .  $C_i(t)$  is analogous to  $C_i(0)$ , but an additional hydrated layer of capacitance make  $C_i$  always smaller than  $C_i$ ,  $\epsilon_{HL}/x_{HL}$ , at the oxide-electrolyte interface must be considered, and the sputter-grown ZrO<sub>2</sub> capacitance is now given by  $\epsilon_U/[x_U - x_{HL}]$ . The series combinations of the capacitances are illustrated in Fig. 2-10. Therefore, the drift is given by

$$\Delta V_G(t) = -(Q_{OX} + Q_{SS} + Q_B + Q_{inv}) \left( \frac{\epsilon_U - \epsilon_{HL}}{\epsilon_U \epsilon_{HL}} \right) x_{HL}(t) \quad (2-29)$$

From this equation, we observed that drift is directly proportional to the thickness of the hydrated layer which may contain both H<sup>+</sup> and OH<sup>-</sup> ions. Other terms at Eq. (2-29) can be considered as constant value no matter what type the substrate is. According to this assume it is possible to eliminate the drift or hold the drift to be a constant at any other pH aqueous solution through the CMOS ISFET. By applying dispersive transport theory, an expression for  $x_{HL}(t)$  is given by [19]

$$x_{HL}(t) = x_{HL}(\infty) \left\{ 1 - \exp[-(t/\tau)^\beta] \right\} \quad (2-30)$$

with

$$x_{HL}(\infty) = \frac{D_{00}\omega_0^{\beta-1}\Delta N_{S/T}(0)}{A_D\beta N_{hydr}} \quad (2-31)$$

where  $A_D$  is the cross-sectional area, and  $N_{hydr}$  is the average density of the hydrating species per unit volume of hydration layer. Substitution of Eq. (2-30) in Eq. (2-29) yields the expression of drift by the following formula:

$$\Delta V_G(t) = -(Q_{OX} + Q_{SS} + Q_B + Q_{inv}) \left( \frac{\varepsilon_U - \varepsilon_{HL}}{\varepsilon_U \varepsilon_{HL}} \right) x_{HL}(\infty) \{1 - \exp[-(t/\tau)^\beta]\} \quad (2-32)$$

## 2.4 Summary

In this chapter, we have introduced the basic concepts and theories of ISFET. The ISFET operational mechanism is similar to the MOSFET. In a constant drain to source voltage  $V_{DS}$ , the drain current will only controlled by  $V_G$ . Furthermore, in ISFET, the drain current will also controlled by different pH values. Because there will be a chemical reaction at the oxide/electrolyte interface, and build up charges and potential to change the drain current  $I_D$ . We introduce the charging mechanism at the surface layer by site-binding model introduced by Yate et al.. We also describe the background electrolyte will also influence the surface charge density, and use the Gouy-Chapman-Stern model to describe this mechanism. By these two models, we can get the critical parameters  $\beta_{int}$ ,  $C_{dif}$  and derive the expression equation of sensitivity  $\frac{\partial \psi_0}{\partial pH_B} = -2.3 \frac{kT}{q} \alpha$ . At the end of this chapter, we also mention the non-ideal phenomena of ISFET, drift and hysteresis, which prevent the widespread application.



## 2.5 References

- [1] Y. Q. Miao, J. R. Chen and K. M. Fang, "New technology for the detection of pH", *J. Biochem. Biophys. Methods*, vol. 63, pp. 1-9, 2005.
- [2] P. Bergveld, "Thirty years of ISFETOLOGY What happened in the past 30 years and what happen in the next 30 years", *Sensors and Actuators B*, vol. 88, pp. 1-20, 2003.
- [3] H.K. Liao, et al. "Study on pH<sub>pzc</sub> and surface potential of tin oxide gate ISFET", *Materials Chemistry and Physics*, vol. 59, pp.6-11, 1999.
- [4] P. Bergveld, "ISFET, Theory and Practice", in *IEEE Sensor Conference*, Toronto, Oct. 2003.
- [5] R.E.G. van Hal et al. , "A general model to describe the electrostatic potential at electrolyte oxide interface", *Advance in Colloid and Interface Science*, vol.69, pp.31-62, 1996.
- [6] Miao Yuqing , Guan Jianguo, Chen Jianrong, "Ion sensitive field transducer-based biosensors", *Biotechnology Advances*, vol. 21, pp.527-534, 2003.
- [7] W. M. Siu, R. S. C. Cobbold, "Basic Properties of the Electrolyte-SiO<sub>2</sub>-Si System: Physical and Theoretical Aspects", *IEEE Transactions on Electron Device*, vol. ED-26, NO. 11, Nov., 1979.
- [8] R.E.G. van Hal, J.C.T. Eijkel, P.Bergveld, "A novel description of ISFET sensitivity with the buffer capacity and double layer capacitance as key parameters", *Sensors and Actuators B*, vol. 24, pp.201-205, 1995.
- [9] Tadayuki Matsuo, Masayoshi Esashi, "Methods of ISFET Fabrication", *Sensors and Actuators*, vol. 1, pp.77-96, 1981.
- [10] Imants R. Lauks, Jay N. Zemel, "The Si<sub>3</sub>N<sub>4</sub>/Si Ion-Sensitive Semiconductor Electrode ", *IEEE Transactions on Electron Devices*, vol. ED-26, no.12, pp. 1959-1964, Dec., 1979.
- [11] J.C. Chou, C.Y. Weng, "Sensitivity and hysteresis effect in Al<sub>2</sub>O<sub>3</sub> gate pH-

- ISFET”, *Materials Chemistry and Physics*, vol. 71, pp.120-124, 2001.
- [12] P.D. van der Wal et al. ,”High-K Dielectrics for Use as ISFET Gate Oxide”, in *Sensors*, Proceedings of IEEE, 2004.
- [13] H.K.Liao et al.,” Study of amorphous tin oxide thin films for ISFET applications”, *Sensors and Actuators B*, vol.50, pp.104-109, 1998.
- [14] Luc Bousse, Piet Bergveld, “The Role Of Buried OH Sites In The Response Mechanism Of Inorganic-Gate pH-Sensitive ISFETs”, *Sensors and Actuators*, vol. 6, pp.65-78, 1984.
- [15] P. Woias, L.Meixner, P. Frostl, ”Slow pH response effects of silicon nitride ISFET sensors”, *Sensors and Actuators B*, vol. 48, pp.501-504, 1998.
- [16] J.C. Chou, K.Y. Huang, J.S. Lin, ”Simulation of time-dependent effects of pH-ISFETs ” *Sensors and Actuators B*, vol. 62, pp.88-91, 2000.
- [17] Luc Bousse et al. , ”Comparison of the hysteresis of Ta<sub>2</sub>O<sub>5</sub> and Si<sub>3</sub>N<sub>4</sub> pH-sensing insulators”, *Sensors and Actuators B*, vol.17, pp. 157-164, 1994.
- [18] J.C. Chou, Y.F. Wang, ”Preparation and study on the drift and hysteresis properties of the tin oxide gate ISFET by the sol-gel method”, *Sensors and Actuators B*, vol.86, pp.58-62, 2002.
- [19] S. Jamasb, S. D. Collins, R. L. Smith, ”A Physical Model for Threshold Voltage Inreproducibility in Si<sub>3</sub>N<sub>4</sub>-Gate H<sup>+</sup>-Sensitive FET’S ( pH ISFET’s )”, *IEEE Transactions on Electron Devices*, vol. 45, no. 6, pp.1239-1245, Jun, 1998.
- [20] H. Scher, Elliott W. Montroll, ”Anomalous transit-time dispersion in amorphous solid”, *Physical Review B*, vol. 12, no.6, pp.2455-2477, Sep., 1975.
- [21] G. Pfister, H. Scher, ” Time-dependent electrical transport in amorphous solid: As<sub>2</sub>Se<sub>3</sub>”, *Physical Review B*, vol. 15, no. 4, pp.2062-2082, Feb., 1977.
- [22] J. Kakalios, R. A. Street, W. B. Jackson, ”Stretched-Exponential Relaxation Arising from Dispersive Diffusion of Hydrogen in Amorphous Sillicon”, *Physical Review Letters*, vol. 59, no.9, pp.1037-1040, Aug. 1987.
- [23] 吳浩青, 李永舫, ”電化學動力學”, 科技圖書公司, 2001年2月.

- [24] S. Jamasb, S. D. Collins, R. L. Smith, "A Physically-based Model for Drift in  $\text{Al}_2\text{O}_3$ -gate pH ISFETs" in International Conference on Solid-State Sensors and Actuators Chicago, June, 1997.
- [25] S. Jamasb, S. D. Collins, R. L. Smith, "A physical model for drift in pH ISFET", Sensors and Actuators B, vol. 49, pp.146-155, 1998.
- [26] George T. Yu, S.K. Yeh, "Hydrogen ion diffusion coefficient of silicon nitride thin films", Applied Surface Science, vol. 202, pp.68-72, 2002.



# Chapter 3

## Experiment and Measurement

### 3.1 Introduction

To investigate the properties of the Polyimide and Nafion™ as protective membrane above solid-state reference electrode, the miniaturized reference electrodes for pH-ISFET is fabricated in this chapter. The organization of the chapter 3 is as follows. We first will introduce the characteristics of polyimide and Nafion™ materials. The fabrication process flow of ISFET will be described in section 3. The section 4 contains illustration of key steps in this experimental process. Section 5 is the measurement system setup which is used for investigating the characteristics of different polyimide/Nafion™-based structures.

### 3.2 The characteristics of the Polyimide and Nafion™

#### 3.2.1 Polyimide

Polyimide (PI) is widely used in electronics and aerospace because of their excellent thermal, electrical, chemical, and mechanical properties. It consists of an organic dianhydride and a diamine [1]. These two components react to a polyadduct with high viscosity and high density. In this study, we employ polyimide as protective membrane above metal reference electrode because it exhibits several advantages, such as thermal reproducibility, good chemical resistance, high viscosity, excellent mechanical properties, and characteristic orange/yellow color. Therefore we use polyimide membrane to protect metal reference electrodes from chemical attack and the problems of liquid/solid interface.

### 3.2.2 Nafion

According to the lectures, Nafion™ is a perfluorinated polymer that contains small proportions of sulfonic or carboxy ionic functional groups and with this functional groups, Nafion has the features of unique equilibrium ionic selectivity and the ionic transport. Fig. 3-1 shows the its chemical structure and model, we can see that Nafion™ can be divided into three parts: (A) a hydrophobic fluorocarbon backbone C-F (B) an interfacial region of relatively large fractional void volume (C) the clustered regions where the majority of the ionic exchange sites, counter ions, and absorbed water exists [2-5]. Because of the high concentration  $\text{SO}_3^-$  ion clusters, Nafion™ exhibits a high conductivity to cations, i.e. high cation exchange. Furthermore, Nafion™ is modified from Teflon, so Nafion™ is extremely resistant to chemical attack and high working temperature.

According to the above introduction, we use Nafion™ to be the protective membrane above polyimide membrane. In order to examine if the Nafion™ coating will influence  $\text{H}^+$  sensitivity, we coated Nafion™ membrane above the metal reference electrode to test the reproducibility and linearity first.

### 3.3 Fabrication process flow of ISFET

All procedures of experiment were accomplished in NDL (National Nano Device Laboratory) and NFC (Nano Facility Center). In this study, the ISFET devices were made on a p-type Si (100) wafer. The fabrication procedures are listed as follows and the process is illustrated in Fig. 3-2:

(a)

1. RCA clean
2. Wet oxidation of silicon dioxide (6000 Å, 1050°C, 65mins)

(b)

3. Defining Source/Drain region (Mask<sup>#1</sup>)
4. BOE wet etching of silicon dioxide
5. Dry oxidation of silicon dioxide as screen oxide (300 Å, 1050°C, 12mins)
6. Source/Drain implantation (Dose=5E15(1/cm<sup>2</sup>), Energy=25KeV)
7. Source/Drain annealing (950°C, 30mins)

(c)

8. PECVD oxide deposition (1 μm)

(d)

9. Defining contact hole and gate region (Mask<sup>#2</sup>)
10. BOE wet etching of silicon dioxide
11. Dry oxidation of gate oxide (100 Å, 850°C, 60mins)

(e)

12. Defining of contact hole (Mask<sup>#3</sup>) and wet etching of silicon dioxide by HF
13. Defining of Sensing layer (Mask<sup>#4</sup>) and sensing layer (ZrO<sub>2</sub>) deposition by Sputtering (300 Å).
14. ZrO<sub>2</sub> sintering (600°C, 30mins)

(f)

15. Define the contact and solid reference electrode region (Mask<sup>#5</sup>)
16. Ti/Pt deposition (150 Å /350 Å) by sputtering or Al evaporation (5000 Å)

(g)

17. Backside Al evaporation (5000 Å)
18. Pt and Al sintering 400°C, 30mins

(h)

19. The polyimide/Nafion<sup>TM</sup> membrane-based material was coated onto metal

electrode surface

### 3.4 Key steps illustration

#### 3.4.1 Gate region formation

In step 1, RCA clean is a standard set of wafer cleaning steps which needs to be performed before high temp processing steps (oxidation, diffusion, CVD) of silicon wafers in semiconductor manufacturing. The purpose of the RCA clean is to reduce the possible pollution (such as dust particles, grease, organics, diffusion ions, and native oxide) from the wafer surface. Careful RCA clean will ensure the integrity of device electricity. In step 2, 6000 Å thickness wet oxide is deposited as barrier layer for S/D implant. The energy and the density of S/D implant are 25KeV and  $5E15$  ( $1/cm^2$ ) with phosphorous dopant, respectively. After S/D implanting, we have to activate the dopant by following a 950°C, 30 mins  $N^+$  annealing.

Next, we have to deposit 1 μm thickness oxide by PECVD. In standard MOSFET process, we don't need to deposit oxide. However, it is necessary to execute for protecting the pH-ISFET device. During a long period of electrolyte immersing, ions may diffuse and affect the electrical characterization of ISFET, so a thicker oxide can eliminate the effect. It is a significant difference compare with standard MOSFET processes. After oxide depositing by PECVD, we grow dry oxide with thickness 100 Å as gate oxide.

#### 3.4.2 Sensing layer deposition

In step 13, we deposit  $ZrO_2$  sensing layer by sputtering. Various sensing material with different deposition techniques decides the characteristics of drift and sensitivity. It has been proved the  $ZrO_2$  film deposited by sputtering has good characteristics as a

pH-ISFET sensing layer. Therefore, in this study, we still use  $ZrO_2$  as the sensing layer and research the suitable solid-state reference electrode. Table 3-1 is the sputtering parameters.

### 3.4.3 Polyimide/Nafion<sup>TM</sup> membrane-based reference electrodes

In step 16, we have to deposit titanium (Ti) as the adhesion layer before depositing Pt because the adhesion between Pt/SiO<sub>2</sub> is very poor. The Ti layer can improve the surface adhesion and Pt layer can protect the titanium from oxidation and corrosion. In step 19, this procedure is the most important part in our experiment. Polyimide/Nafion<sup>TM</sup> membrane-based reference electrodes have been fabricated by combining silicon fabrication and drop-coating method. To investigate the Polyimide/Nafion<sup>TM</sup> membrane-based material on the improvement of reference electrode performance, two type metal electrodes (Ti/Pt and Al) were prepared. Then the Polyimide/Nafion<sup>TM</sup> membrane-based material was coated onto an exposed area of metal electrode to produce a solid-state reference electrode. After that, we coat Nafion<sup>TM</sup> (NF) above polyimide as a protective membrane. Besides the two-layer structure, a mix composition of Nafion<sup>TM</sup> and polyimide is also prepared for this study. The test structures are listed in Table 3-2. Following is our process flow:

1. Dropping the polyimide solution onto the metal electrode at room temperature.
2. Dried under a dust-free ambient air condition for 24 hours, the solution become colloid.
3. In order to drive off solvent, the polyimide was baked in two steps on hot-plate, first at 120°C for 10 minutes and subsequently at 300°C for 2 mins.
4. Dropping Nafion<sup>TM</sup> 2% solution above polyimide. In the case of dropping Nafion<sup>TM</sup>, the polyimide must be covered with Nafion<sup>TM</sup> completely.
5. Dried under a dust-free ambient air condition for 30 mins.



### 3.5 Packing and measurement system

Before executing measurement, a container is bonded to the gate region of ISFET using epoxy resin. Entire sensing region and solid-state reference electrode must be included in the opening under the container. In order to investigate the characteristics of different polyimide/Nafion<sup>TM</sup> membrane-based reference electrodes, we measure the  $I_{DS}$ - $V_{GS}$  curves for the pH-ISFET by using HP4156A as measurement tool and the measurement setup is shown in Fig. 3-3. In the setup of HP-4156A, substrate voltage is grounded to avoid the body effect and the reference electrode sweeps to different voltage.

For getting accurate result of measurement, all measuring conditions of the experiments were carried out at a constant temperature of 25°C using a temperature control system, and the entire measurement procedures were executed in a dark box because light will produce serious influence on the pH-ISFET [7]. The measured pH values are 1, 3, 5, 7, 9, 11, 13, and the pH buffer solutions were supplied by Riedel-deHaen corp. Preparation of NaCl solution is also needed in Na<sup>+</sup> ions measurement. The NaCl salts are electronic grade and solutions are prepared in DI water with different mole concentrations, 10<sup>-3</sup>M, 10<sup>-2</sup>M, 10<sup>-1</sup>M, 1M. When preparation of NaCl solution, it have to know the solubility of NaCl at room temperature is about 37g NaCl per 100g water. In order to reduce the preparation error of mole concentration, we prepare 1M solution, and the other mole concentraions are diluted by DI water.

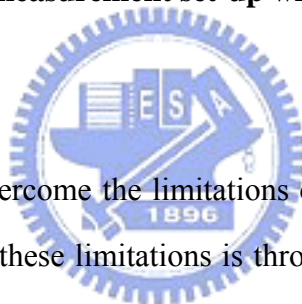
#### 3.5.1 Current-Voltage (I-V) measurement set-up

In our measurement, a HP-4156A semiconductor parameter analyzer system was set up to measure the I-V characteristic curves, in which include  $I_{DS}$ - $V_{GS}$  and  $I_{DS}$ - $V_{DS}$  curves at controlled temperature. We have to take care when dropping the pH-buffer

solution at the sensing region. Because the sensing region is small, we have to pay attention to preventing generation of air bubbles at the interface. In order to make sure that the devices are under a steady state, every pH buffer solution is immersed for 60s before measuring.

From  $I_{DS}$ - $V_{GS}$  curves, we can extract the pH sensitivity (mV/pH) of  $ZrO_2$  pH-ISFET. At first, we find the point of maximum transconductance, i.e. the maximum slope of  $I_{DS}$ - $V_{GS}$  curves, and get the corresponding current value ( $I_{DS}$ ). At the constant  $I_{DS}$  of maximum transconductance, we can find that with different pH values the reference electrode voltage ( $V_G$ ) will shift linearly and the shifted voltage per pH value is the sensitivity, as illustrated in Fig. 3-4.

### 3.5.2 Current-Voltage (I-V) measurement set-up with solid-state reference electrodes



In this study, we try to overcome the limitations of the glass reference electrode, one of the ways to overcome these limitations is through the all-solid-state reference electrodes. In this situation, we replace the glass reference electrode with solid-state reference electrode. The reproducibility of the output voltage ( $V_G$ ) is what we concern about in this study first. Hence, as the same with measuring for sensitivity, every pH value is immersed for 60 seconds before  $I_{DS}$ - $V_{GS}$  measurement. Then the reproducibility of output voltage is measured for 120 seconds with 30 seconds a measurement point. From the reproducibility of output voltage, we can observe the linearity of test structures for different pH buffer solutions.

### 3.5.3 Drift measurement set-up with solid-state reference electrodes

The drift characteristics were measured with pH = 7 buffer solution and the same condition samples period of 30 seconds, 1 minute, 10 minutes and 1 hour. 33

measuring points in the time frame of 7 hours were measured by polyimide/Nafion<sup>TM</sup> membrane-based solid-state reference electrodes. The detection principle is in a similar manner to that of the pH measurement and is shown in Fig. 3-5.

### 3.6 References

- [1] M. Sato, T. Yamamoto, M. Takeuchi, K. Yamanouchi, Humidity sensitivity of Lamb waves on composite polyimide:ZnO:Si<sub>3</sub>N<sub>4</sub> structure, Jpn. J. Appl. Phys. 32 Part 1, pp. 2380-2383, 1993.
- [2] John Payne "Nafion® - Perfluorosulfonate Ionomer", April, 2005 from <http://www.psrc.usm.edu/mauritz/nafion.html> .
- [3] Daivid T.V. Anh, W. Olthuis, P. Bergveld, "Hydrogen peroxide detection with improved selectivity and sensitivity using constant current potentiometry", Sensors and Actuators B, vol. 91, pp. 1-4, 2003.
- [4] Patrick J. Kinlen, John E. Heider, David E. Hubbard, "A solid-state pH sensors based on a Nafion-coated iridium oxide indicator electrode and a polymer-based silver chloride reference electrode" Sensors and Actuators B, vol. 22, pp. 13-25, 1994.
- [5] J.P. Tsao, C.W. Lin, "Preparations and Characterizations of the Nafion/SiO<sub>2</sub> Proton Exchange Composite Membrane", Journal of Materials Science and Engineering, vol. 34, No. 1, pp. 17-26, 2002.
- [6] K. M. Chang, K. Y. Chao, T. W. Chou, and C. T. Chang, "Characteristics of Zirconium Oxide Gate Ion-sensitive Field-Effect Transistors" Japanese Journal of Applied Physics Vol. 46 No. 7A pp. 4334-4338, 2007.
- [7] Paik-Kyun Shin, "The pH-sensing and light-induced drift properties of titanium dioxide thin films deposited by MOCVD", Applied Surface Science, vol. 214, pp. 214-221, 2003.

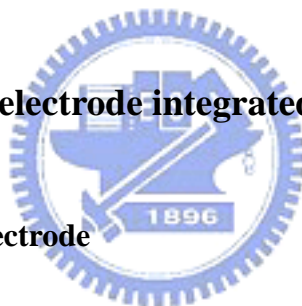
## Chapter 4

### Results and Discussion

#### 4.1 Introduction

The aim of this research is to investigate the miniaturized solid-state reference electrode. In this chapter, Section 2 begins with background on the history and development of the solid-state reference electrodes. The experimental results and discussion of the solid-state reference electrodes with the polyimide/Nafion<sup>TM</sup> membrane-based materials are described in section 3. Finally, conclusion is reported in section 4.

#### 4.2 Solid-state reference electrode integrated with ISFET



##### 4.2.1 Solid-state reference electrode

D. haramé was first to incorporate a silver/silver chloride (Ag/AgCl) structure on the ISFET chip [1]. In microelectrochemical sensors, thin-film Ag/AgCl electrodes without any internal reference electrolyte are often referred as “quasi-reference electrodes”. Most investigations have been focused on the miniaturization of the Ag/AgCl electrode. However, several factors limit the durability of the Ag/AgCl electrode. Foremost is the well-known non-negligible diffusion of the chlorine ions when the Ag/AgCl electrode directly contacts to the electrolyte solution. Moreover, the electrode is susceptible to changing activity of its primary ion [e.g.  $a(\text{Cl}^-)$  in Ag/AgCl system] and the existence of interfering redox materials. Hence, the lifetime of such structure is very short and the potential reproducibility is very poor. In other words, the potential at the solid/liquid interface is thermodynamically undefined and

will lead to significant errors in pH measurement. In addition, its use is thus severely restricted. To solve these problems of bare Ag/AgCl electrode as mentioned above, another approach was attempted and devoted to miniaturize and scale down the mature macro liquid-junction reference electrode, yet preserving its basic structure and operation principle. This approach was carried out to incorporate the liquid-filled solid-state reference electrode as an integrated part of the ISFET chip, using IC technology and micro-machining. However, to seal a small volume of saturated potassium chloride (KCl) electrolyte is still a mass production challenge [2]. Recently, various modifying methods have been proposed to improve the Ag/AgCl electrode, such as KCl membrane and Nafion<sup>TM</sup> coating [3], where chloride ions were trapped within the KCl membrane.

According to previous experiment in our group, it showed that the polymer-based materials can make REFET have low sensitivity. It means that the surface potential maintains almost a constant value, i.e. the surface potential will be stable. On the basis of the experimental results, we applied the polyimide/Nafion<sup>TM</sup> membrane-based materials to the metal reference electrodes. We choose NF, PI, PI/NF, and PI-mix-NF structures as the protective membrane of metal reference electrode. Comparing with the Ag/AgCl reference electrode, such solid-state reference electrodes will not have the problem of chloride diffusion.

As described in the previous section, an electrochemical sensor needs a reference electrode to define a stable accurate electrochemical potential as the measurement reference. It is therefore important that the potential of the reference electrode to be constant and invariant with solution composition. Hence, we can observe the behavior of these solid-state reference electrodes. Properties such as the drift, hysteresis, and reproducibility are some indicators to characterize the reference electrodes.

## 4.2.2 The glass reference electrode (GRE)

In this experiment, for the reason of a standard reference line, we first measure the sensitivity of ZrO<sub>2</sub>-pH-ISFET by glass reference electrode. In chapter 1, we have introduced the potential of glass electrode is very stable and accurate. Fig. 4-1 shows the sensitivity and sensitivity linearity of ZrO<sub>2</sub>-pH-ISFET measured by glass reference electrode is about 59 mV/pH. The value is very close to the theoretical maximum sensitivity of 59.2mV/pH. Furthermore, we can observe that  $I_{DS} - V_{GS}$  curves are shifted parallel with the pH concentration of the buffer solutions in the non-saturation region with  $V_{DS} = 1V$ . It is obviously that the threshold voltage shift towards positive values with increasing pH values.

## 4.3 The experimental results and discussion of solid-state reference electrodes



### 4.3.1 Potential reproducibility and linearity

A good reference electrode is a prerequisite for providing a stable reference potential. An unstable reference electrode potential results in the shift of the working electrode potential and affects the output current. Reproducibility is a test of the manufacturability of the fabrication technology. In this study, we first tested the potential reproducibility and linearity of ZrO<sub>2</sub>-pH-ISFET with the polyimide/Nafion<sup>TM</sup> membrane-based solid-state reference electrode. The reproducibility of the ZrO<sub>2</sub>-pH-ISFET in buffer solutions with pH = 1, 3, 5, 7, 9, 11, and 13 at a constant temperature of 25°C is obtained using a HP4156A semiconductor parameter analyzer for 120 seconds with 30 seconds a measurement point. We also used the linear fit program to fit our experimental data.

Fig. 4-2 ~ Fig. 4-17 show that the reproducibility and linearity of

ZrO<sub>2</sub>-pH-ISFET by all kinds of polyimide/Nafion<sup>TM</sup> membrane-based solid-state reference electrodes. The discussions of the measuring results of reproducibility and linearity are listed as follows:

- (1) For bare metal reference electrodes, we can see that the gate voltage ( $V_G$ ) of each pH value is very unstable within 120 seconds and linearity is also very bad. The unstable phenomenon is caused by solid/liquid interface and other chemical reactions.
- (2) By Nafion<sup>TM</sup> membrane coating, we can see that potential reproducibility become better and stable. In Fig. 4-3 and Fig. 4-11, we also find that the reproducibility in acid electrolyte is more stable than in basic electrolyte. The possible reason for this phenomenon is that Nafion<sup>TM</sup> is a cation-exchange membrane, and the H<sup>+</sup> ions in acid are more than in basic, therefore the thermodynamic equilibrium at the solid/liquid in acid electrolyte will achieve quickly than in basic electrolyte.
- (3) From the experimental results, it is obviously that the baked PI membrane could greatly improve the reproducibility and linearity. The improvement was considered that the solvent in polyimide membrane was removed after two-step baking.
- (4) The solid-state reference electrode with Ti/Pt/PI-mix-NF structure showed a poor reproducibility and linearity. The results were considered to be caused by the poor mixed structure and a large surface roughness. Furthermore, the difference in viscosity and density between polyimide and Nafion<sup>TM</sup> is very large.
- (5) From the experimental results, we conclude that Pt/baked PI/NF structure could greatly improve the reproducibility of solid-state reference electrode potential. The reproducibility and linearity is very stable between pH 1 to pH 13. These results mean that the low sensitivity sensing layer of REFET also work at the solid-state reference electrodes. From the experimental results,

the Ti/Pt/PI/NF structure seems to have the potential to solve the unstable problem of the solid-state reference electrodes.

### 4.3.2 pH sensitivity

The pH sensitivity of the ZrO<sub>2</sub>-pH-ISFET in buffer solutions with pH = 1, 3, 5, 7, 9, 11, and 13 at a constant temperature of 25°C is obtained using a HP4156A semiconductor parameter analyzer. Furthermore, the alkali metal ions are easy to be found in electrolytes, we also investigate the Na<sup>+</sup> sensitivity of ISFET.

Fig. 4-18 ~ Fig. 4-35 show that the H<sup>+</sup> and Na<sup>+</sup> sensitivity of ZrO<sub>2</sub>-pH-ISFET by all kinds of polyimide/Nafion<sup>TM</sup> membrane-based solid-state reference electrodes. The sensing performances of sensitivity for different test structures were summarized in Table 4-1. The discussions of the measuring results of sensitivity are listed as follows:

- (1) For bare metal reference electrodes, the experimental results show that the I<sub>DS</sub> - V<sub>GS</sub> curves are irregular and unstable, bare Al solid-state reference electrodes especially.
- (2) The experimental results show that the I<sub>DS</sub> - V<sub>GS</sub> curves which were measured by Al solid-state reference electrodes with polyimide/Nafion<sup>TM</sup> membrane coating are not very parallel and unstable. However, we need a stable reference potential for measurement. Therefore the I<sub>DS</sub> - V<sub>GS</sub> curves are difficult to be regarded as a standard reference line. The main reason is that the redox reactions at the surface of aluminum metal. Fundamentally, redox reactions are a family of reactions that are concerned with the transfer of electrons between species.
- (3) Fig. 4-27 shows that the sensitivity is a little increased by Nafion<sup>TM</sup> membrane coating. However, the sensitivity of Ti/Pt/NF structure is only 27.5 mV/pH in pH 1 ~ pH 9 and is still difficult in application.
- (4) From the experimental results, we can conclude that the ZrO<sub>2</sub>-pH-ISFET



with Ti/Pt/baked PI/NF membrane solid-state reference electrode has a higher sensitivity of 56.5 mV/pH in the pH 1 ~ pH 13.

- (5) Fig. 4-34 and Fig. 4-35 show  $\text{Na}^+$  sensitivity and sensitivity linearity of Ti/Pt/PI/NF structure with and without baked PI is 7.5 mV/pNa and 10.25 mV/pNa, respectively. It shows that the  $\text{ZrO}_2$  sensing film is more selective to  $\text{H}^+$  than  $\text{Na}^+$ .

### 4.3.3 Drift characteristics

Drift is typically characterized by a relatively slow, monotonic, and temporal change in the threshold voltage of the ISFET device under constant conditions such as temperature, pH value, and electrolyte concentration. The drift is an inevitable phenomenon of pH-ISFET, some studies already indicate that drift behavior exists during the entire measurement process [4]. To make sure that the device is under a stable state, the ISFET must be immersed in the buffer solution for 1h before drift measurement. The measuring time kept up for 7 h at a constant temperature of 25°C. We can calculate the drift of ISFET from 1 to 7 h to gain the drift rate.

Fig. 4-38 ~ Fig. 4-44 show that the drift of  $\text{ZrO}_2$ -pH-ISFET by all kinds of polyimide/Nafion<sup>TM</sup> membrane-based solid-state reference electrodes in pH = 7 buffer solution for 7 h. In addition, the drift of Ti/Pt/PI/NF structure with and without baked PI showed in Fig. 4-46 and Fig. 4-47 were measured for 24 h, respectively. The drift rate amount of various solid-state reference electrodes is summarized in Table 4-2. The discussions of the measuring results of drift are listed as follows:

- (1) According to the Fig. 4-45, we can see that Ti/Pt/PI/NF structure has an obviously small drift. it is possible to eliminate the drift rate by this structure. Furthermore, experimental results indicate the Ti/Pt/PI/NF structure of reference electrode with baked PI membrane exhibited an obviously small drift rate (1.05 mV/h) than same structure without baked PI membrane.

- (2) From the experimental results, the solid-state reference electrode with Ti/Pt/PI-mix-NF structure showed a serious drift rate. The results were considered to be caused by the poor mixed structure and a large surface roughness. This unstructured compound could result in serious hydration.
- (3) Fig. 4-46 and Fig. 4-47 show the drift of Ti/Pt/PI/NF membrane reference electrode with and without baked PI and the results indicate drift rates of 1.08 mV/h and 1.57 mV/h for 24 h measurement, respectively.

## 4.4 Conclusions

In this study, we successfully applied the polyimide/Nafion<sup>TM</sup> membrane-based material for solid-state reference electrode. The structure of polyimide/Nafion<sup>TM</sup> membrane-based solid-state reference electrode is simple and easy to fabricate by drop-coating method. Our analysis indicated the polyimide/Nafion<sup>TM</sup> membrane-based material can work at the solid-state reference electrodes and the unstable voltage problems of solid-state reference electrode are greatly solved by Ti/Pt/baked PI/NF structure. The reproducibility within 120 seconds is very stable and the sensitivity is extremely close to the performance of glass reference electrode. It exhibited an excellent pH response of 56.5 mV/pH and the Na<sup>+</sup> sensitivity of this structure is only a little influenced by different Na<sup>+</sup> concentrations with the value 7.5 mV/pH. Furthermore, the experimental data indicated that the Ti/Pt/baked PI/NF structure has a drift smaller than other test structures obviously.

From the experimental results, we confirm the kind of polymer-based material have a big potential to integrate a miniaturized solid-state reference electrodes integrate into ISFET chip. The cheap and simple production of miniaturized all-solid-state reference microelectrodes could substitute classical reference electrodes in practical applications.

## 4.5 References

- [1] I-Yu Huang, Ruey-Shing Huang, "Fabrication and characterization of a new planar solid-state reference electrode for ISFET sensors", *Thin Solid Films*, vol. 406, pp.255-261, 2002.
- [2] I-Yu Huang, Ruey-Shing Huang, Lieh-Hsi Lo, "Improvement of integrated Ag/AgCl thin-film electrodes by KCl-gel coating for ISFET applications", *Sensors and Actuators B*, vol. 94, pp.53-64, 2003.
- [3] Chen Dong-chu, et al., "Preparation of Nafion Coated Ag/AgCl Reference Electrode and Its Application in the pH Electrochemical Sensor", *Journal of Analysis Science*, vol. 21, pp. 432-434, Aug., 2005.
- [4] Z. Yule, Z. Shouan and L. Tao, "Drift characteristic of pH-ISFET output", *Chin. J. Semicond.* 15, pp. 838-843, 1994.
- [5] K. M. Chang, K. Y. Chao, T. W. Chou, and C. T. Chang, "Characteristics of Zirconium Oxide Gate Ion-sensitive Field-Effect Transistors" *Japanese Journal of Applied Physics* Vol. 46 No. 7A pp. 4334-4338, 2007.

## Chapter 5

### Future Work

In our experiment, characteristics of various solid-state reference electrodes are studied. Based on the observed result, Ti/Pt/Polyimide/Nafion<sup>TM</sup> membrane is a good candidate for solid-state reference electrode. But the coating process is not optimized in this experiment.

For the purpose of mass manufacture, the yield and reliability are the most important issues. In our experiment, the performance sometimes will fail and unstable during coating and measurement. So, the optimized coating method, including the influence of baking temperature or dropping manners, needs to be studied further. The properties of these polymer materials and other new polymer stuffs are also need to be more understood.

Additionally, we will change the sensing layer for ChemFET and ENFET that have more biomedical applications. Hence, the device will become a useful tool in the future.

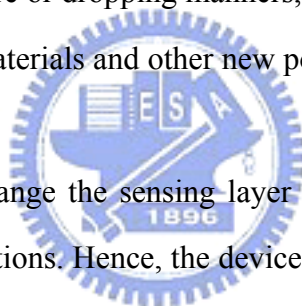


Table 1-1 Sensitivity for different sensing layers

Sensing layer	Test range (pH)	Sensitivity (mV/pH)	Reference
ZrO <sub>2</sub>	1-13	57.5	5
SiO <sub>2</sub>	4-10	25-48	6
Si <sub>3</sub> N <sub>4</sub>	1-13	46-56	6
Al <sub>2</sub> O <sub>3</sub>	1-13	53-57	6
Ta <sub>2</sub> O <sub>5</sub>	1-13	56-57	6
SnO <sub>2</sub>	2-10	58	7

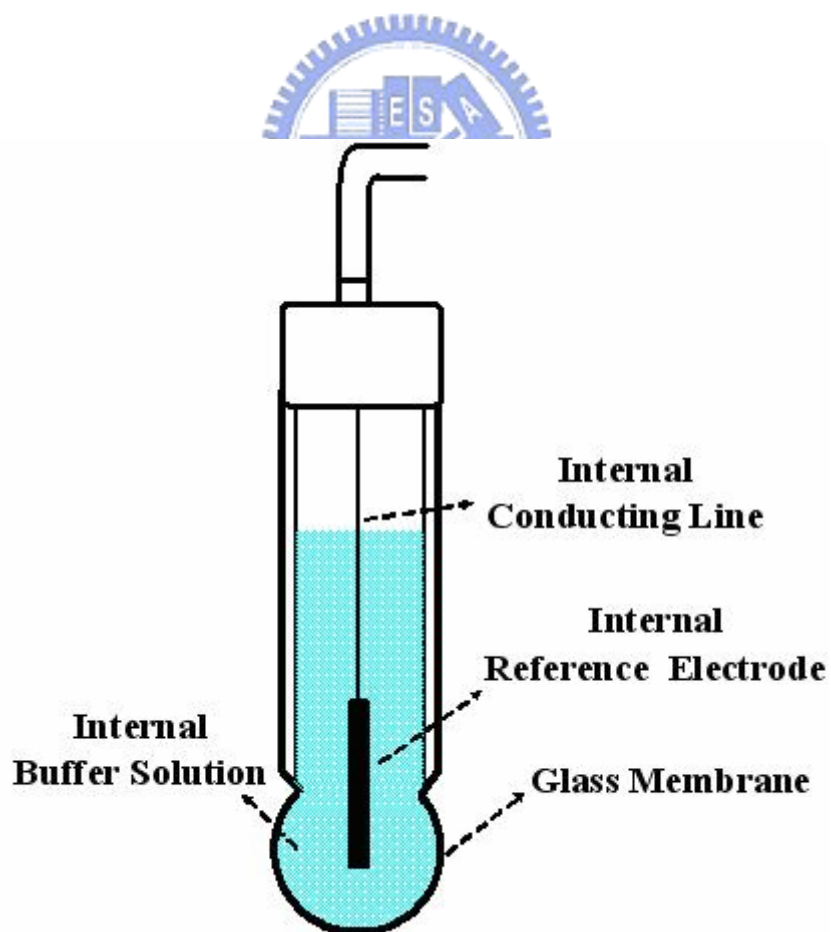


Fig. 1-1 Conventional pH glass electrode

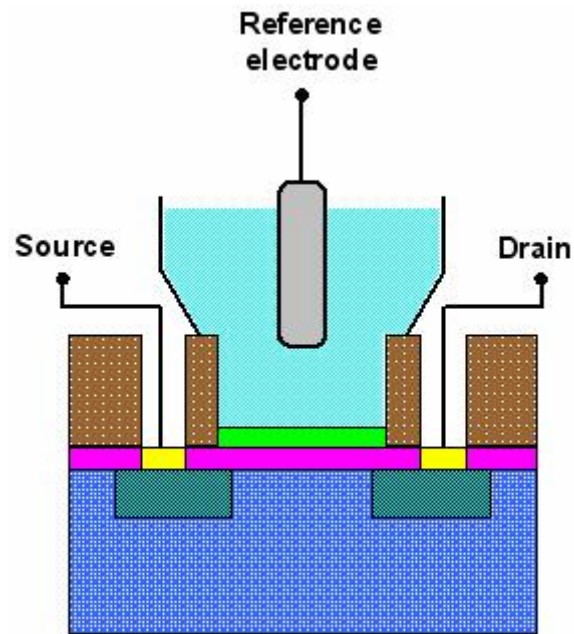
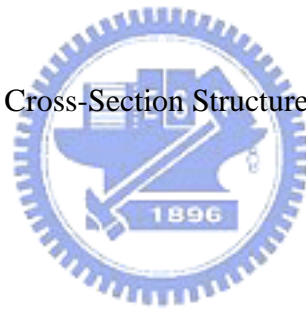


Fig. 1-2 Cross-Section Structure of ISFET



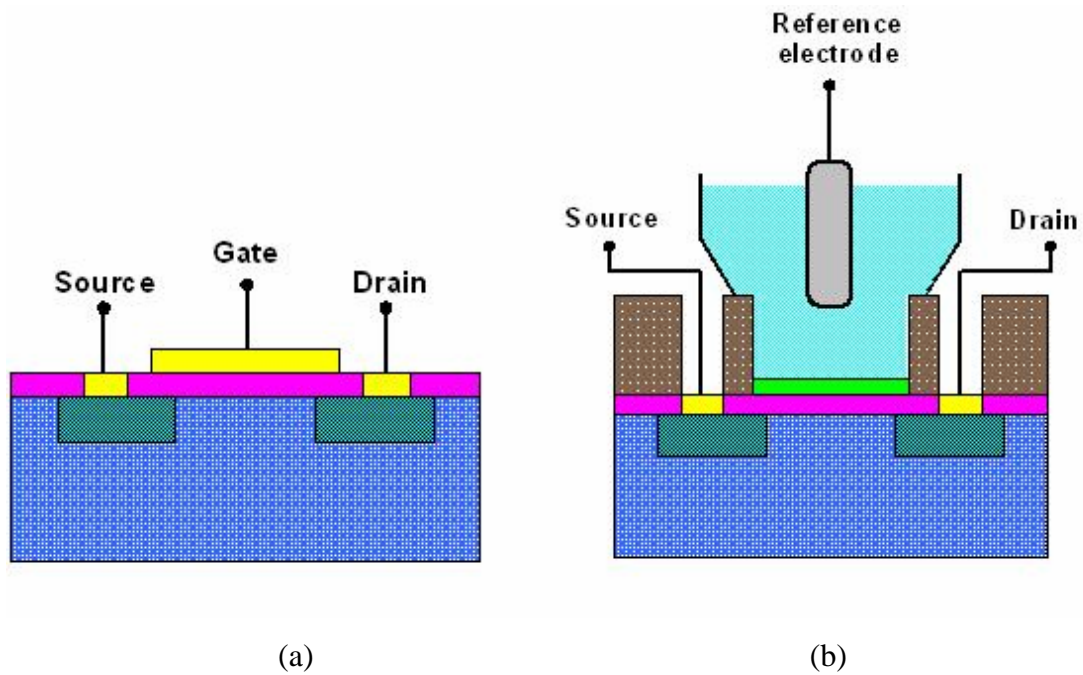


Fig. 2-1 Schematic representation of a MOSFET (a) and an ISFET (b) cross-section structure

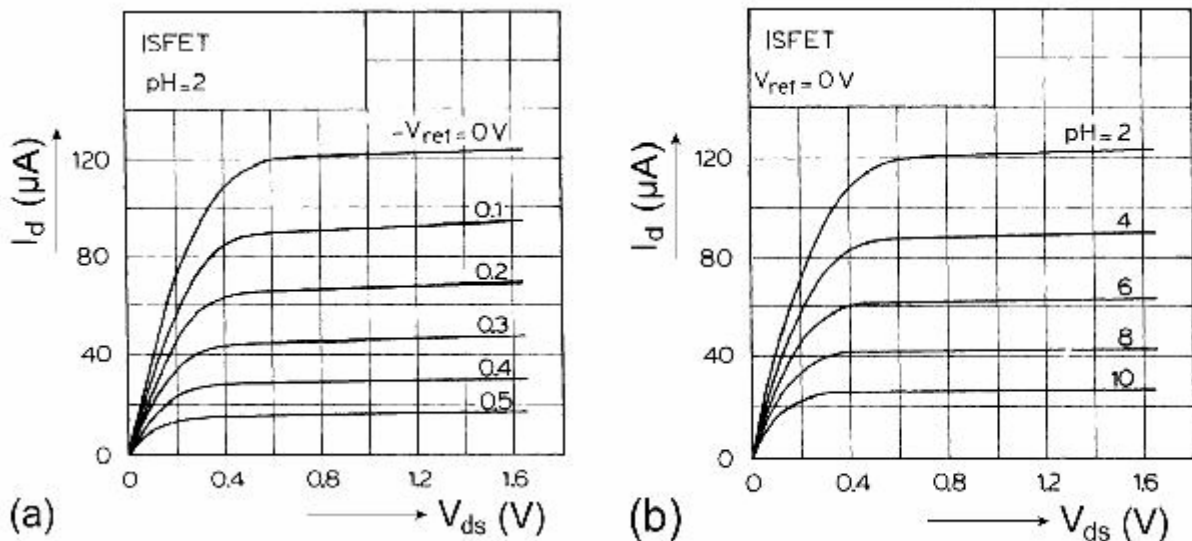


Fig. 2-2  $I_D$ - $V_{DS}$  curve of an ISFET with  $V_{gs}$  (a), and pH (b) as a parameter

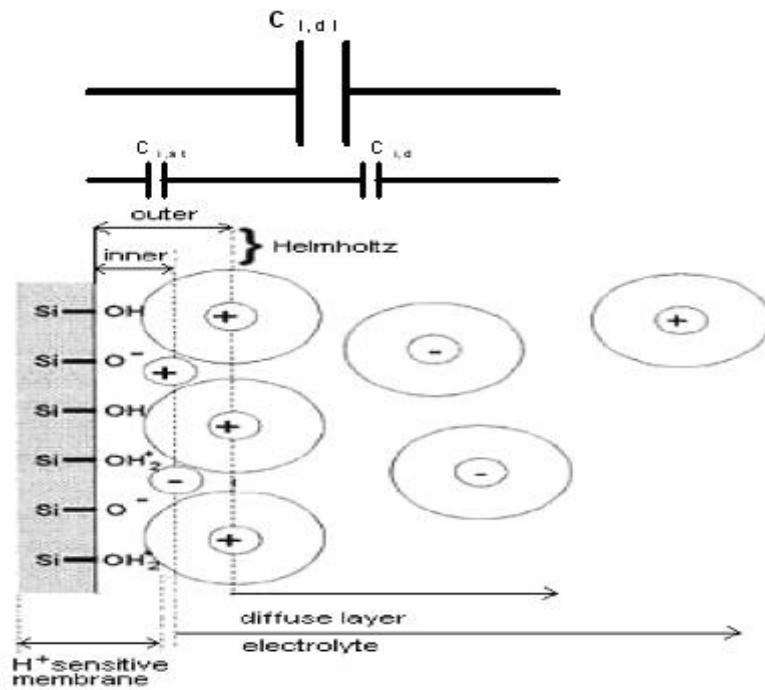


Fig. 2-3. Electrode and electrolyte interface

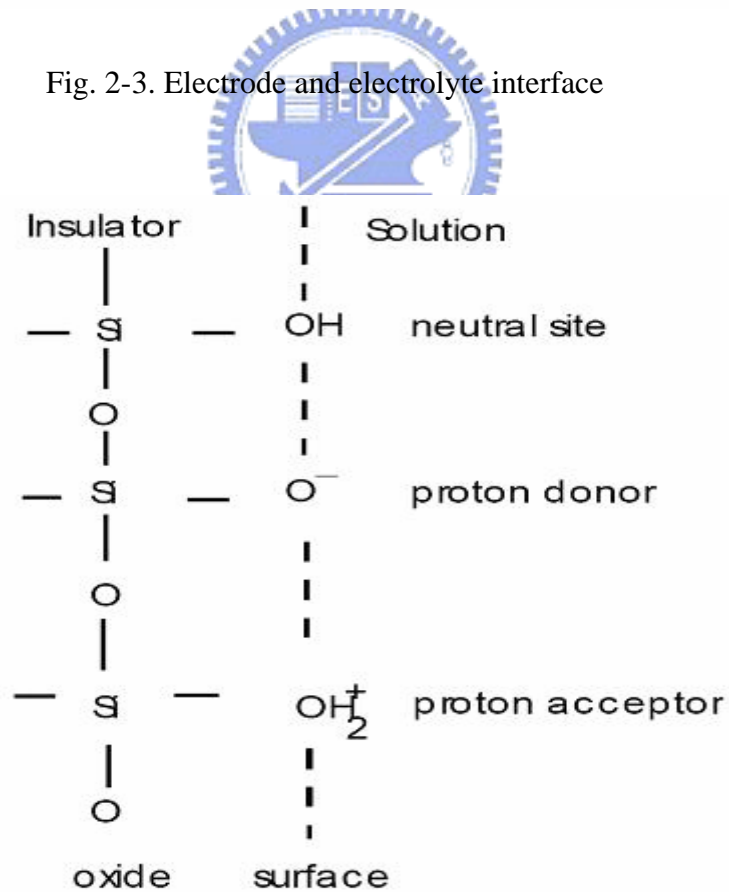


Fig. 2-4 Schematic representation of site-binding model



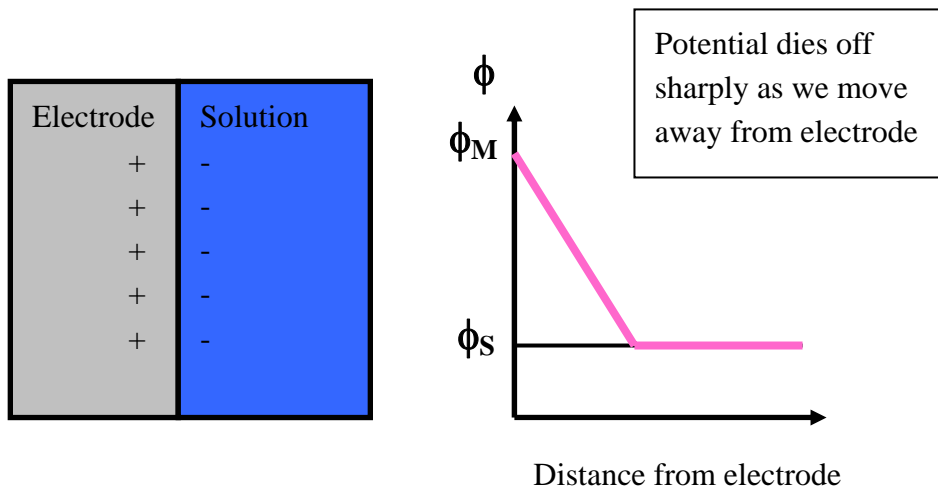


Fig. 2-5 Helmholtz model

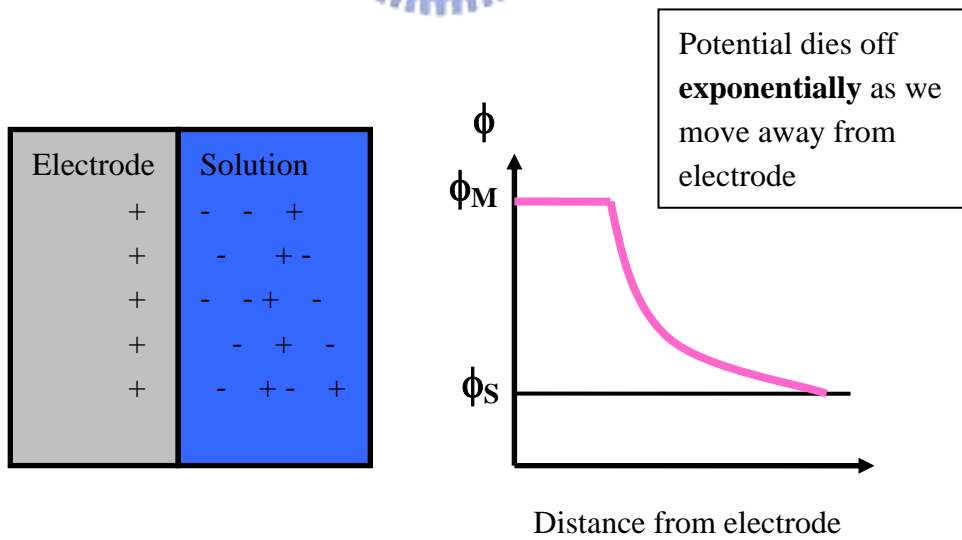


Fig. 2-6 Gouy-Chapman model

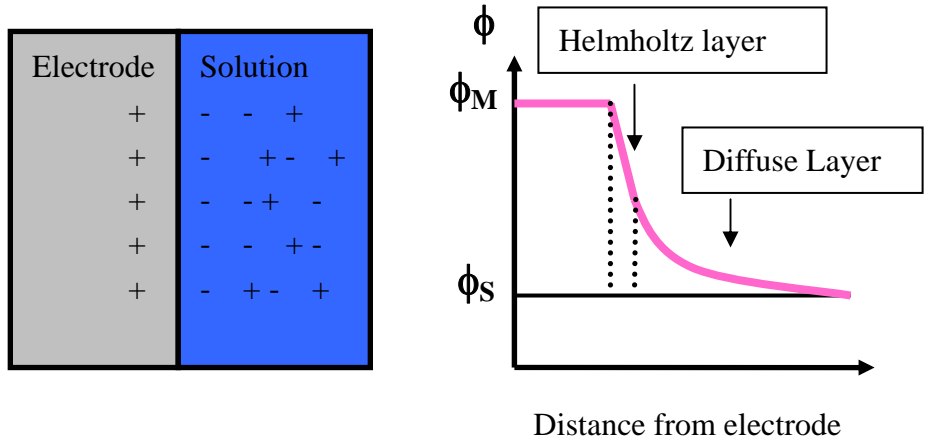


Fig. 2-7 Gouy-Chapman-Stern model

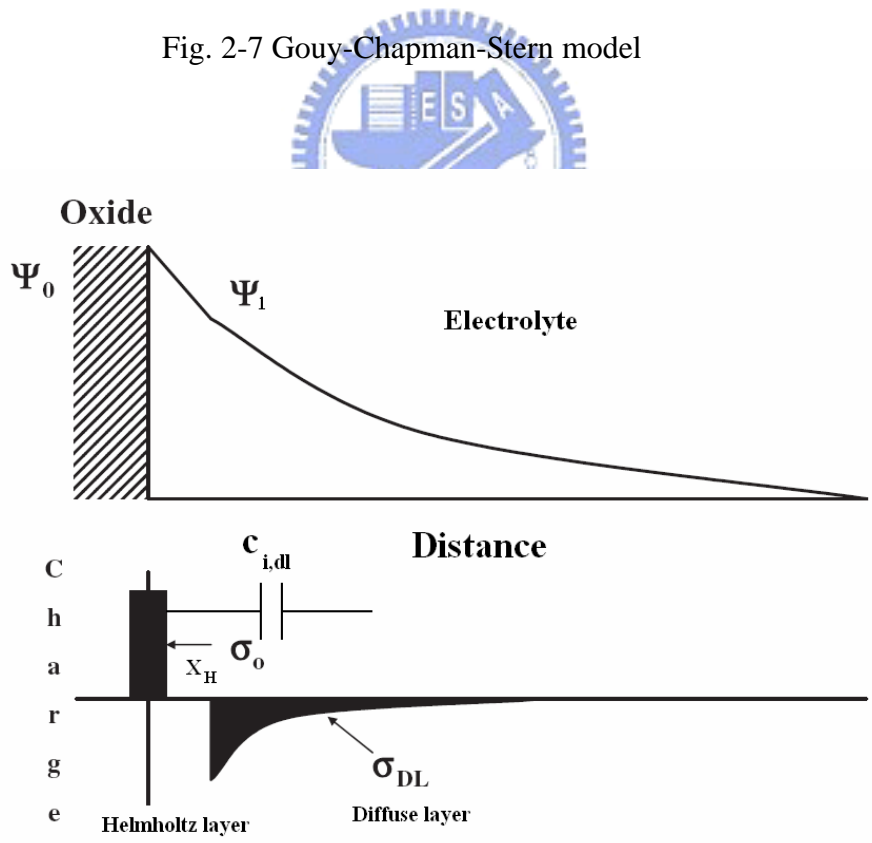


Fig. 2-8 Potential profile and charge distribution at an oxide/electrolyte solution interface

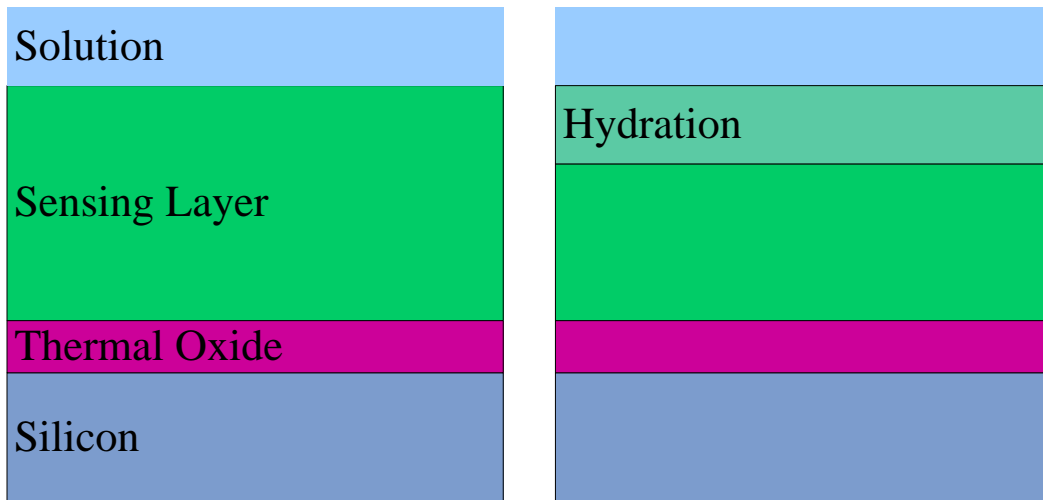


Fig. 2-9 Series combination of the (a) initial (b) hydrated insulator capacitance

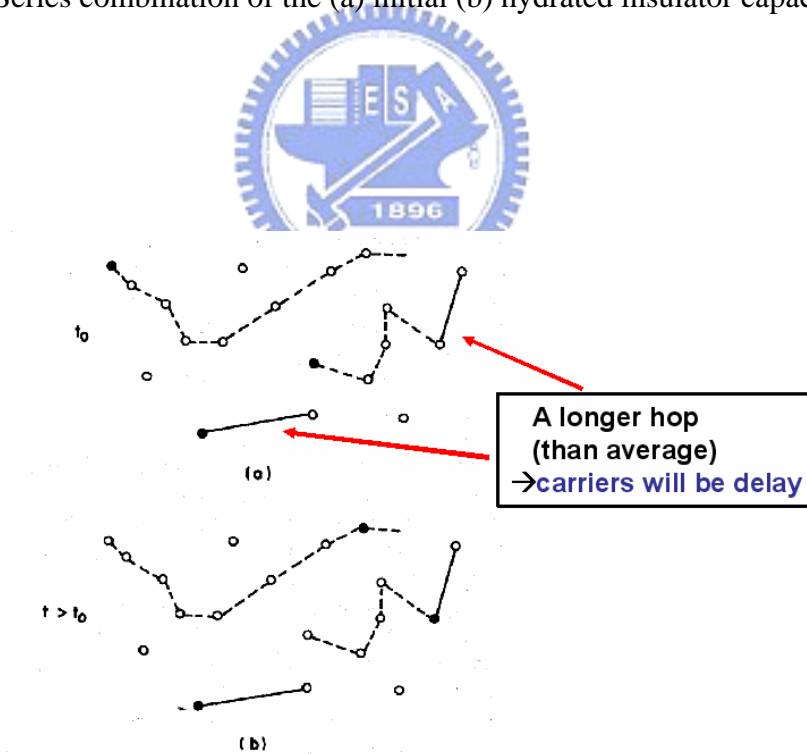


Fig. 2-10 Schematic representation of carriers hopping through a random array of sites

Table 3-1 ZrO<sub>2</sub> Sputtering parameters

<b>parameters of ZrO<sub>2</sub> sputter</b>
<b>Power : 110 W</b>
<b>Ar / O<sub>2</sub> flow rate : 24 / 8 ( sccm )</b>
<b>Density : 6.51</b>
<b>Acoustic impedance : 14.72</b>
<b>Tooling factor : 0.533</b>
<b>Rate : 0.01 Å / s</b>
<b>Pre-sputter 60W for 10 min</b>
<b>Pressure : 7.6×10<sup>-3</sup> torr</b>

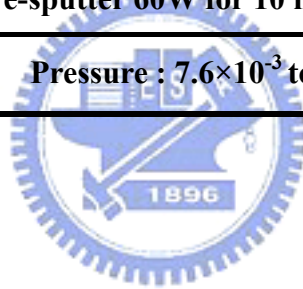
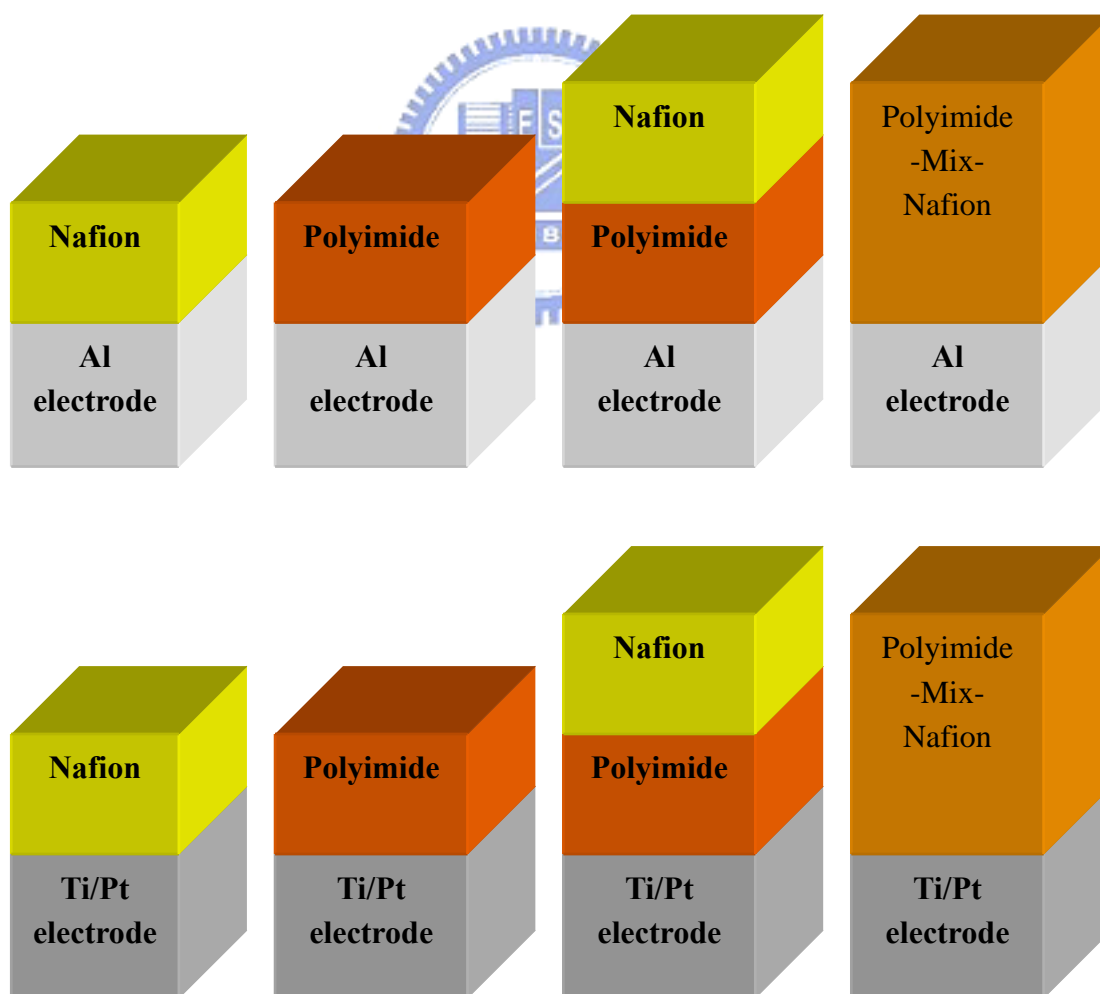


Table 3-2 Test structures of solid-state reference electrodes

Solid-state RE test structures	Protective membrane coating (NF = Nafion™, PI = Polyimide)			
	Al electrode	NF	PI	PI-mix-NF
		Baked PI	Baked PI-mix-NF	Baked PI/NF
Ti/Pt electrode	NF	PI	PI-mix-NF	PI/NF
		Baked PI	Baked PI-mix-NF	Baked PI/NF



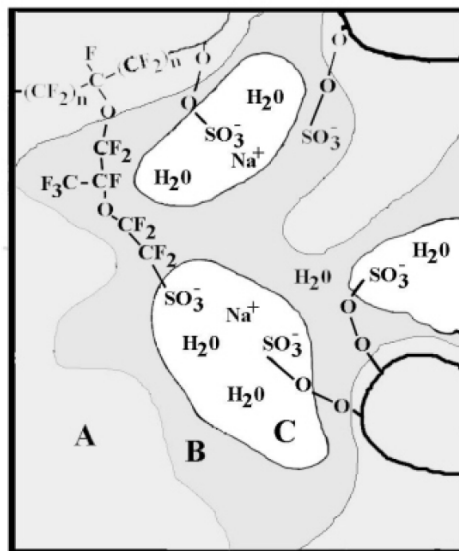
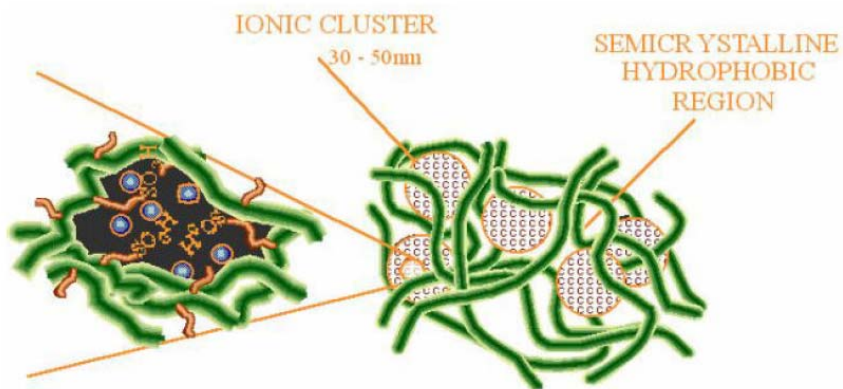
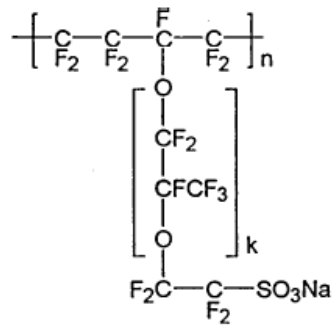
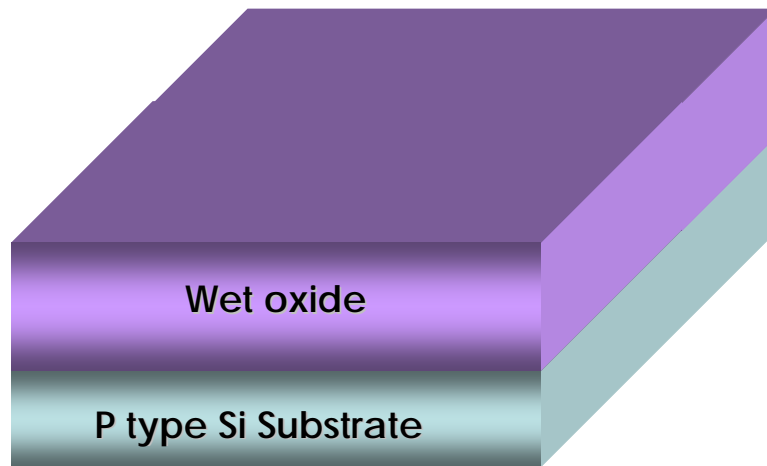
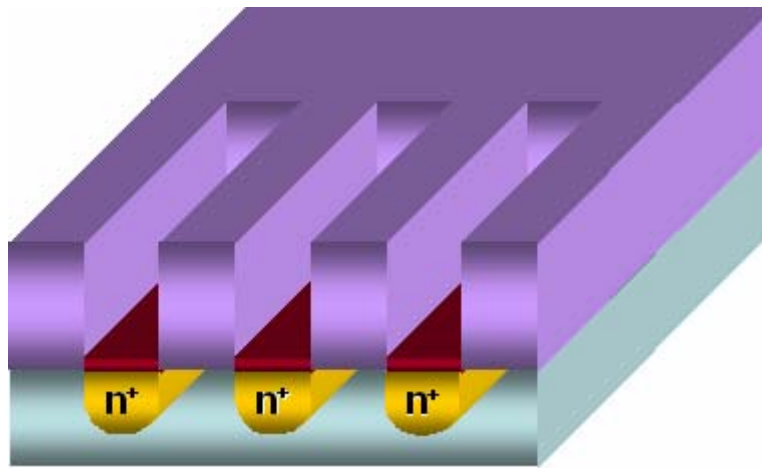


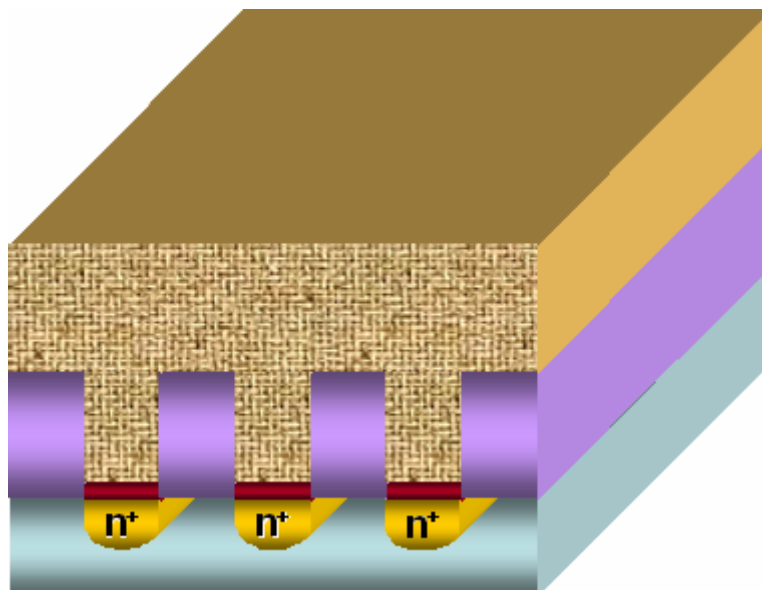
Fig. 3-1 Chemical structure and model of Nafion™



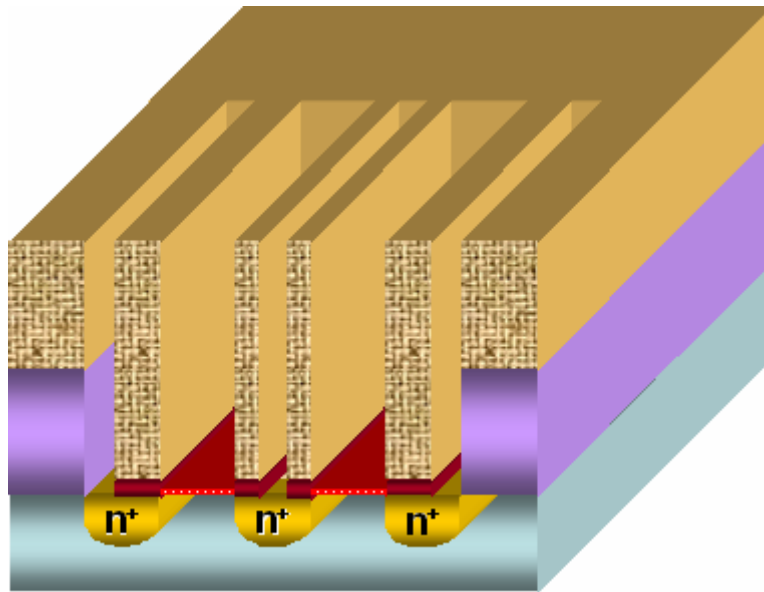
(a)



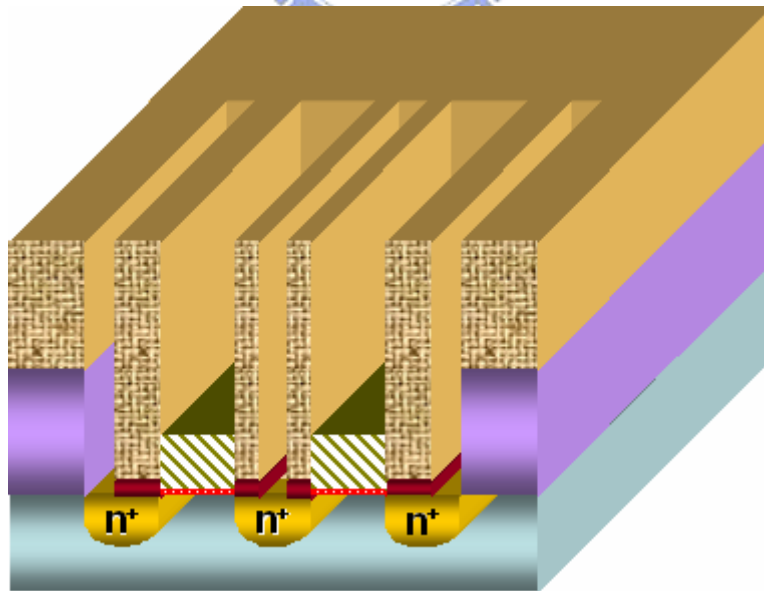
(b)



(c)

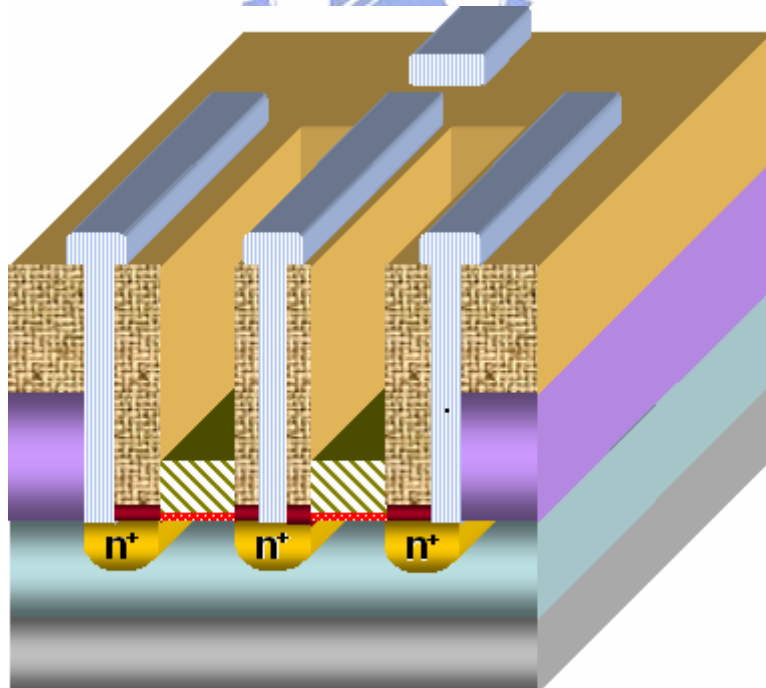
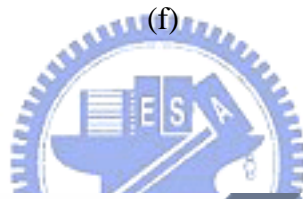
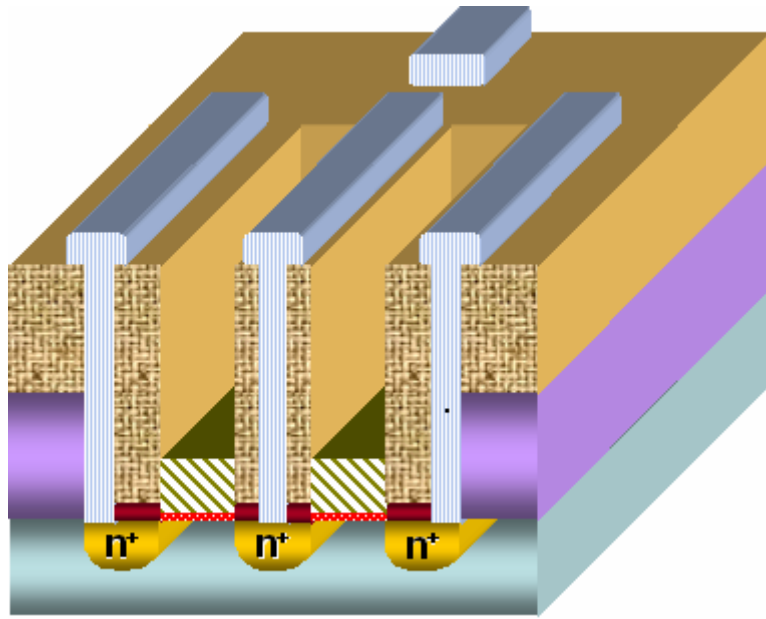


(d)

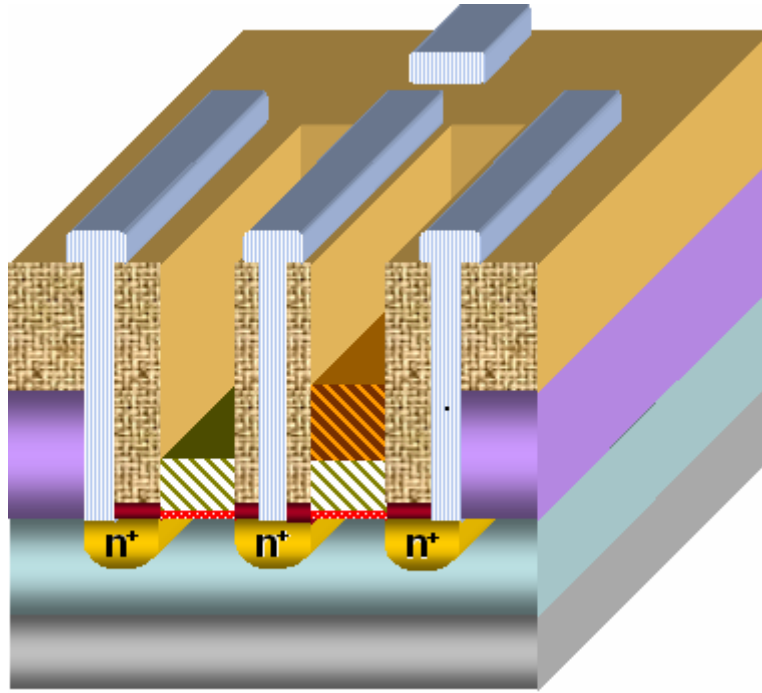


(e)





(g)



(h)

Fig. 3-2 Fabrication Process Flow

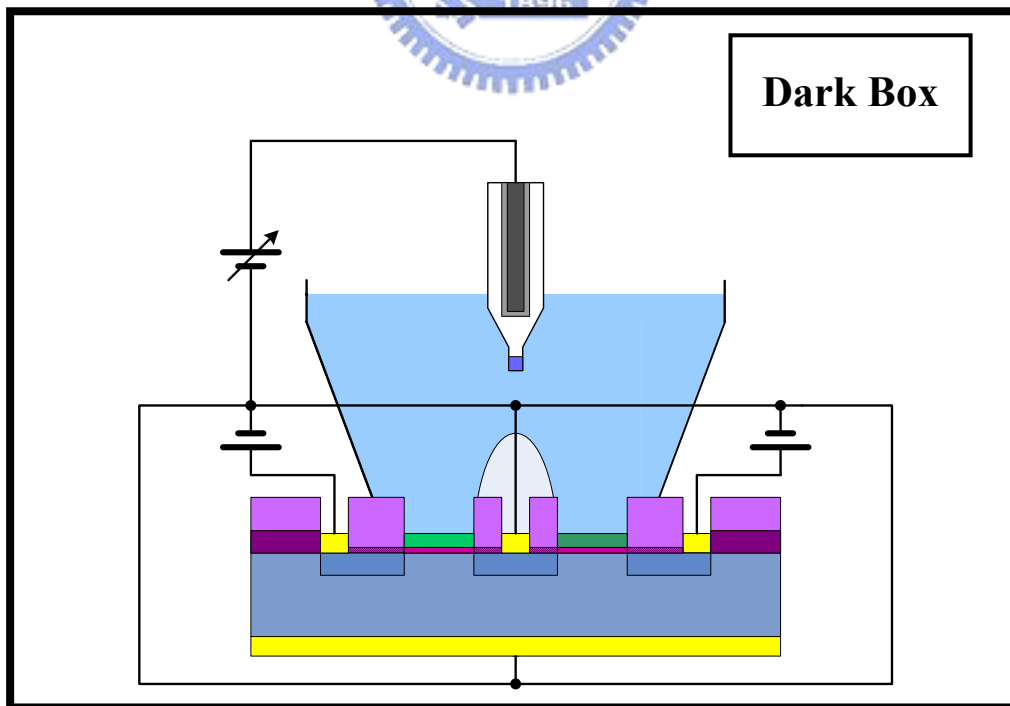


Fig. 3-3 Measurement set-up

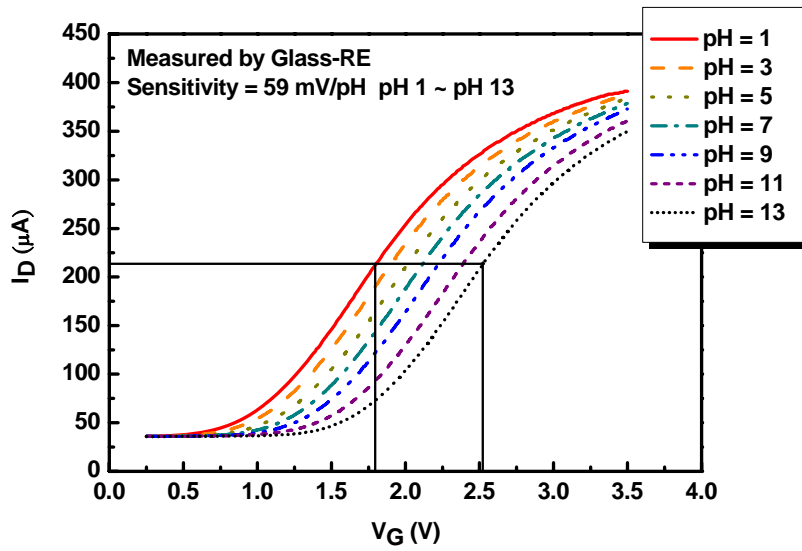


Fig. 3-4 Detection principle of sensitivity

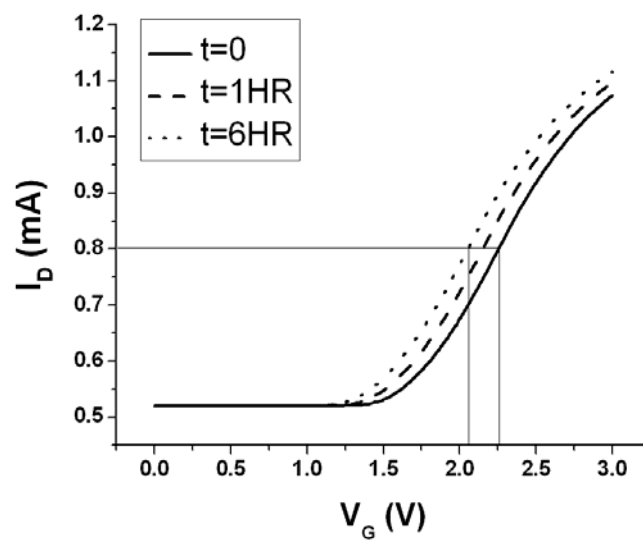
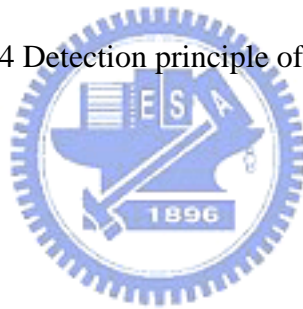


Fig. 3-5 Detection principle of drift

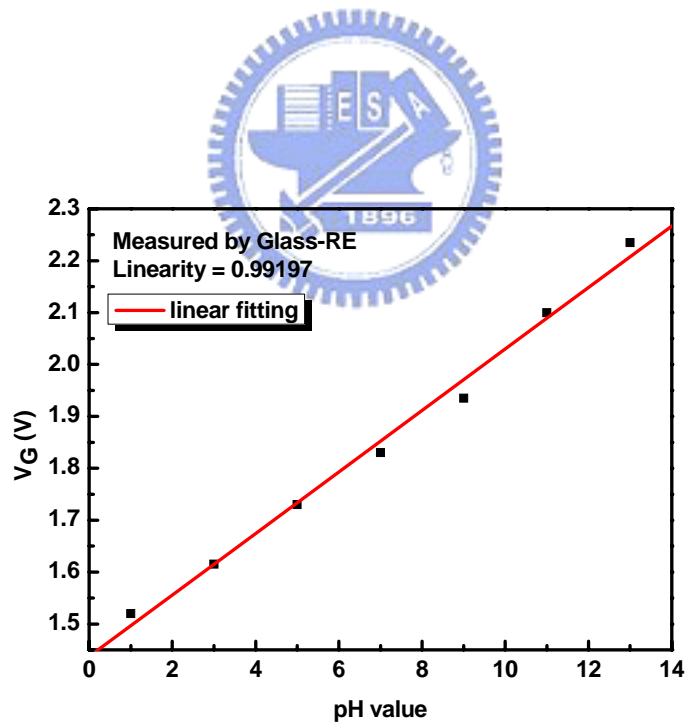
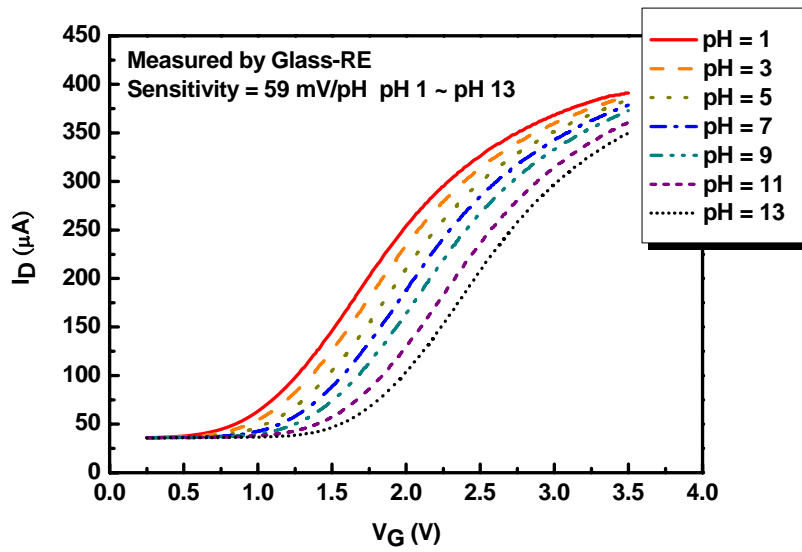


Fig. 4-1 The  $I_{DS} - V_G$  curves and sensitivity linearity of  $ZrO_2$ -pH-ISFET measure by glass reference electrode

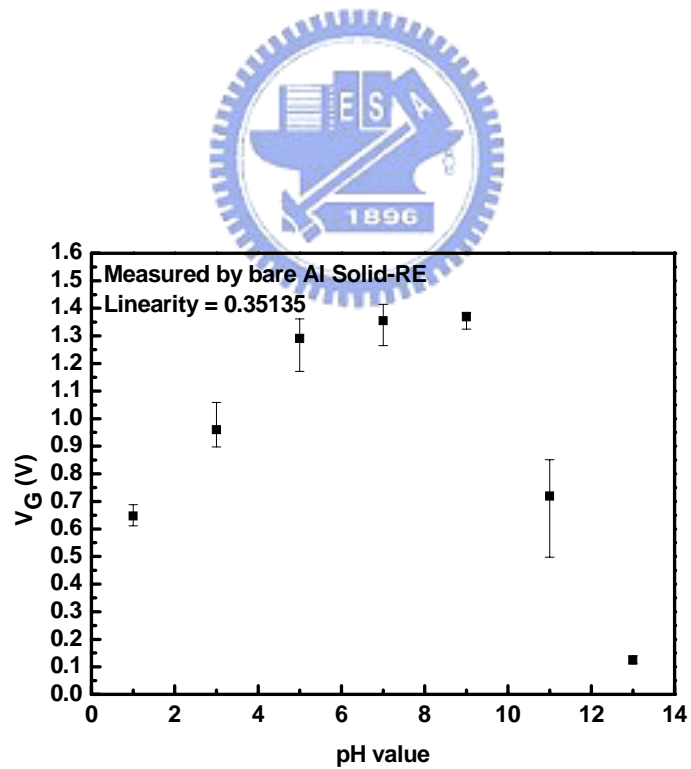
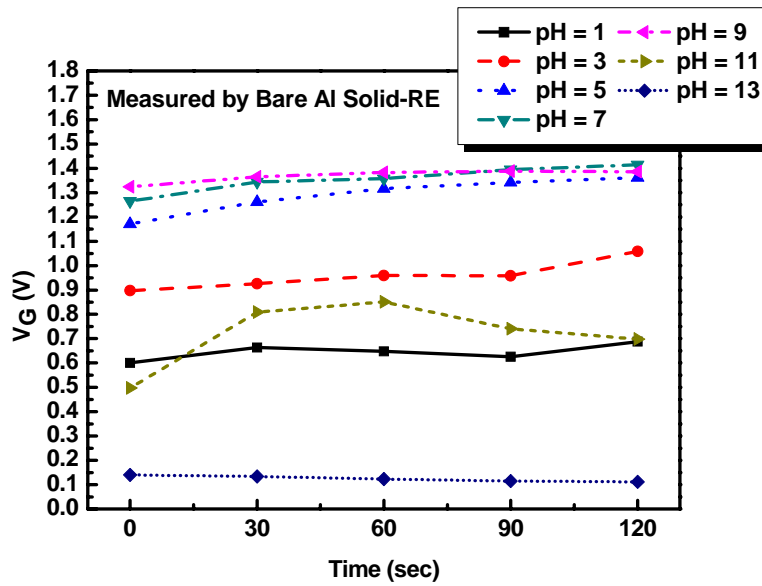


Fig. 4-2 Reproducibility and sensitivity linearity of  $ZrO_2$ -pH-ISFET measured by bare Al solid-state reference electrode

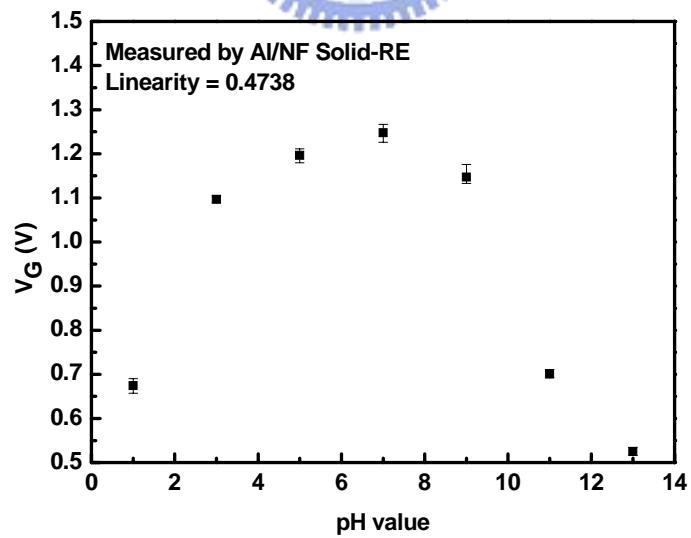
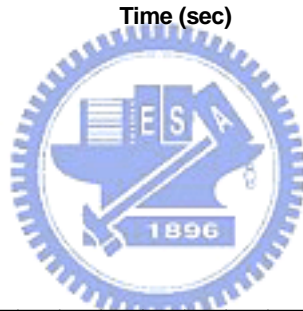
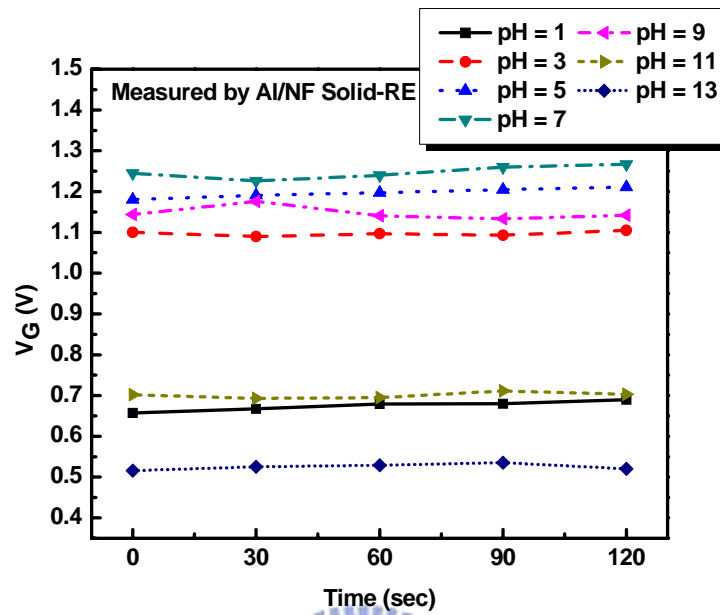


Fig. 4-3 Reproducibility and sensitivity linearity of  $ZrO_2$ -pH-ISFET measured by Al/NF solid-state reference electrode

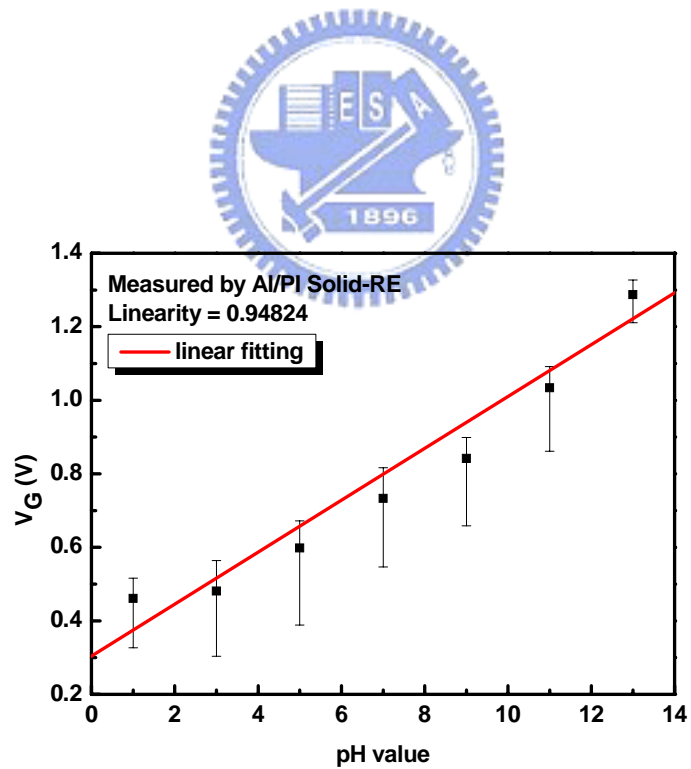
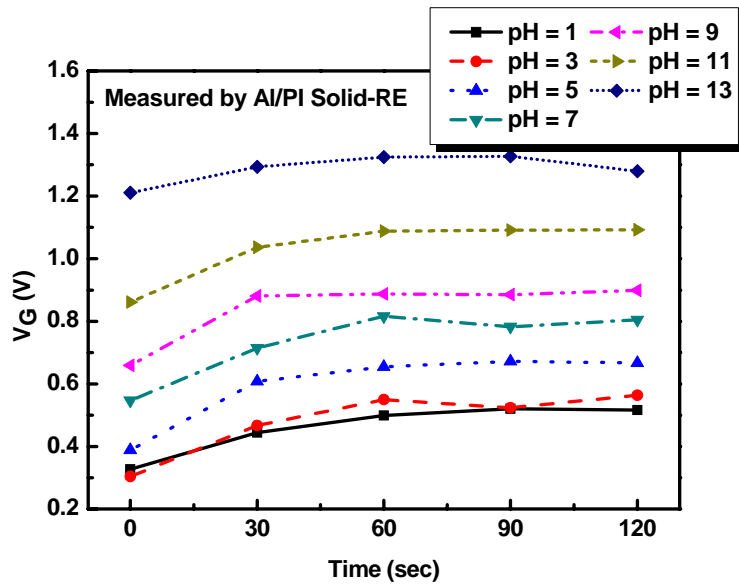


Fig. 4-4 Reproducibility and sensitivity linearity of  $ZrO_2$ -pH-ISFET measured by Al/PI solid-state reference electrode

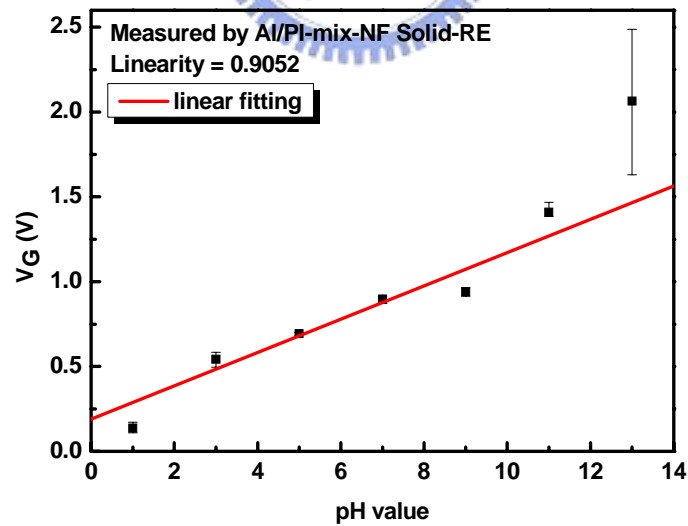
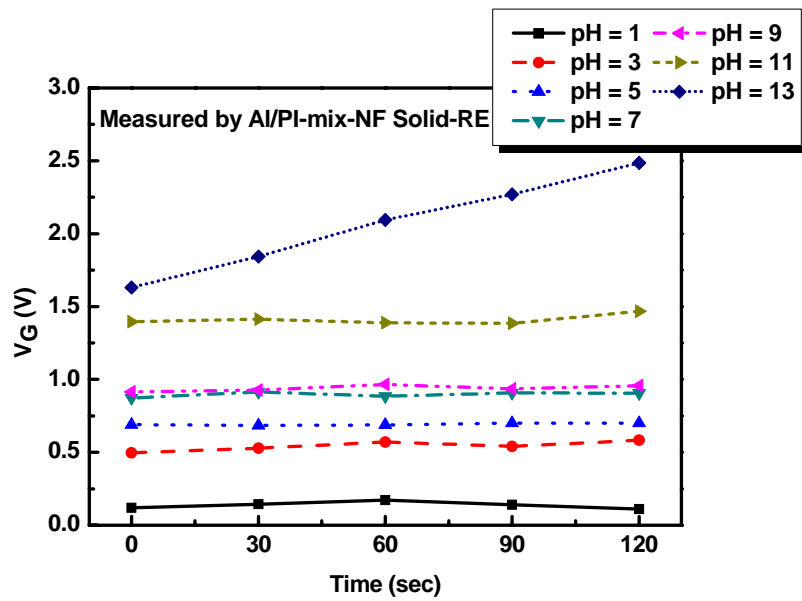


Fig. 4-5 Reproducibility and sensitivity linearity of  $ZrO_2$ -pH-ISFET measured by Al/PI-mix-NF solid-state reference electrode



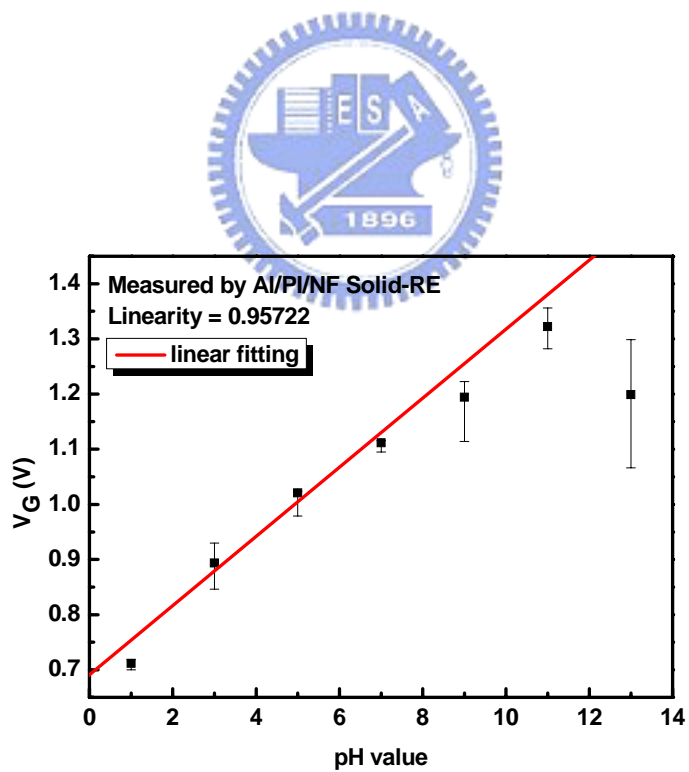
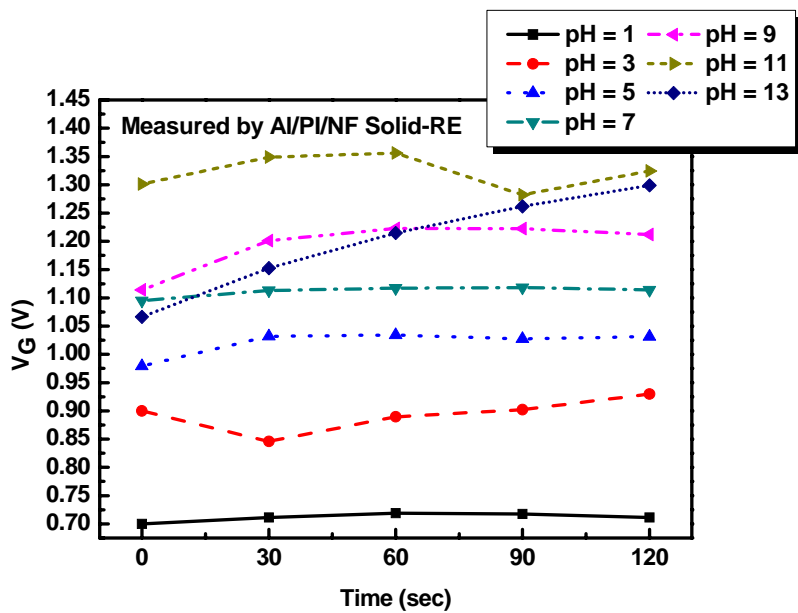


Fig. 4-6 Reproducibility and sensitivity linearity of  $ZrO_2$ -pH-ISFET measured by Al/PI/NF solid-state reference electrode

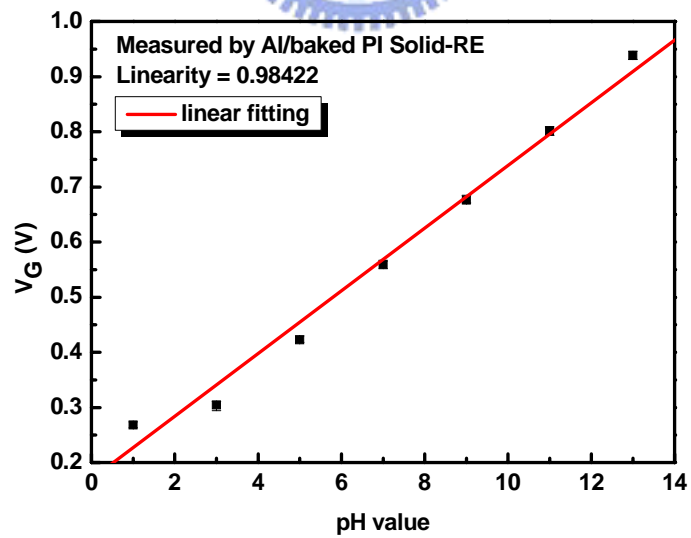
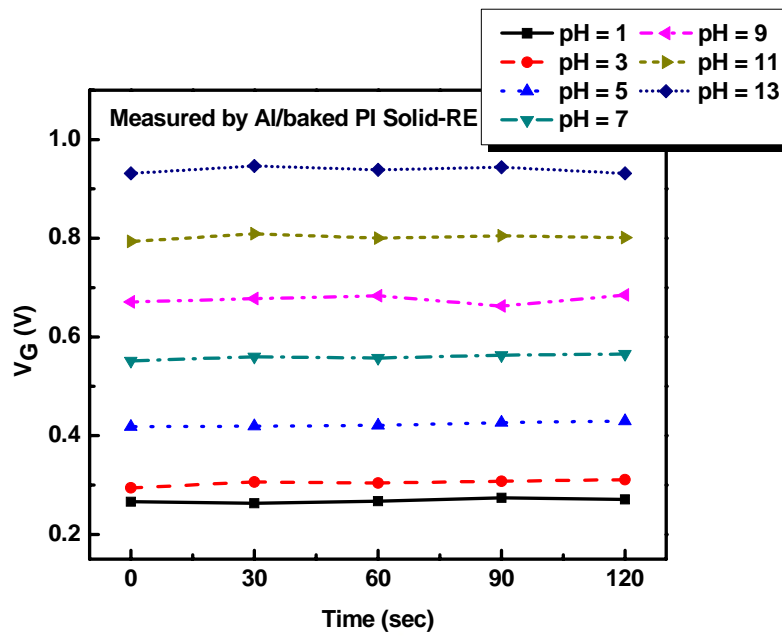


Fig. 4-7 Reproducibility and sensitivity linearity of  $ZrO_2$ -pH-ISFET measured by Al/baked PI solid-state reference electrode

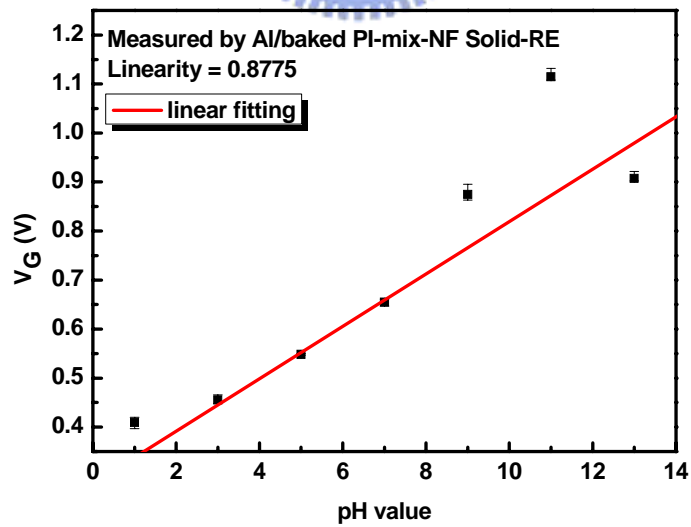
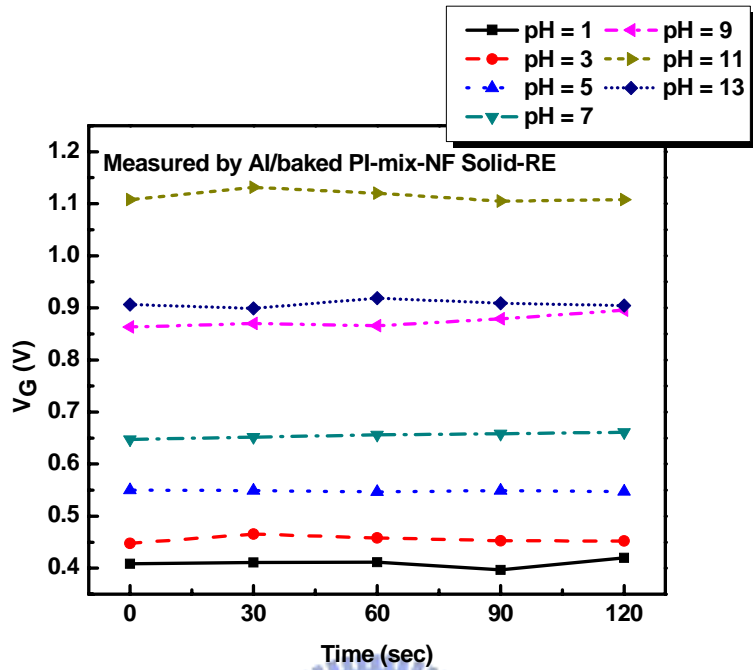


Fig. 4-8 Reproducibility and sensitivity linearity of  $ZrO_2$ -pH-ISFET measured by Al/baked PI-mix-NF solid-state reference electrode

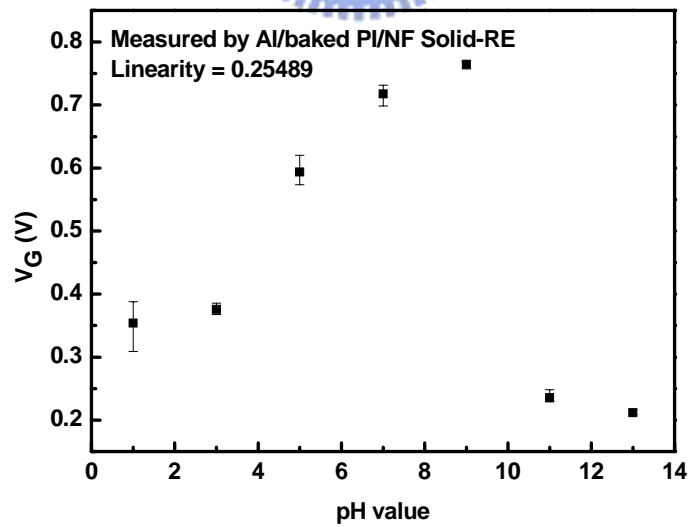
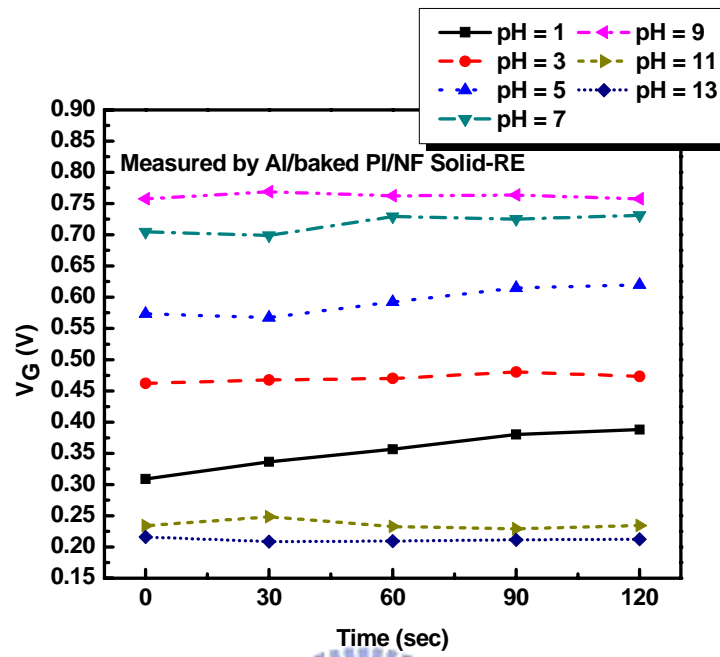


Fig. 4-9 Reproducibility and sensitivity linearity of  $ZrO_2$ -pH-ISFET measured by Al/baked PI/NF solid-state reference electrode

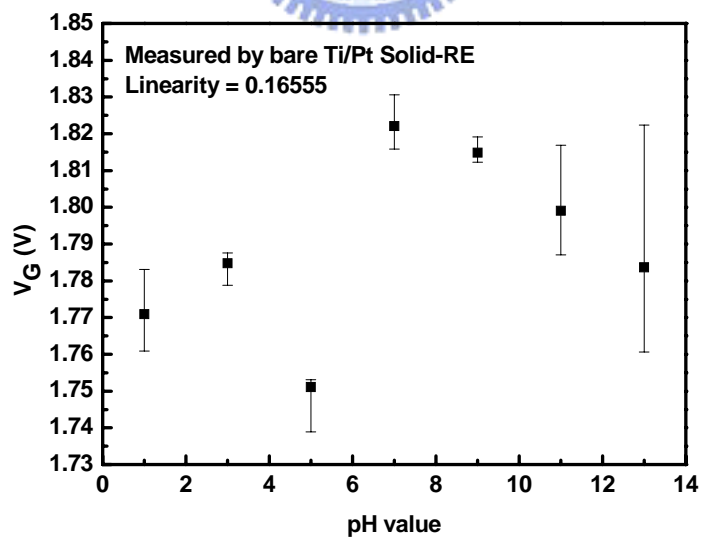
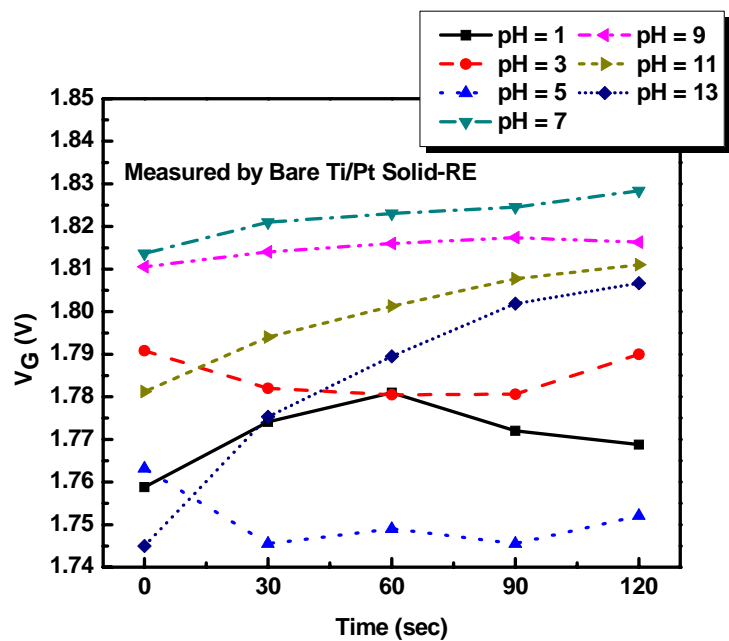


Fig. 4-10 Reproducibility and sensitivity linearity of  $ZrO_2$ -pH-ISFET measured by bare Ti/Pt solid-state reference electrode

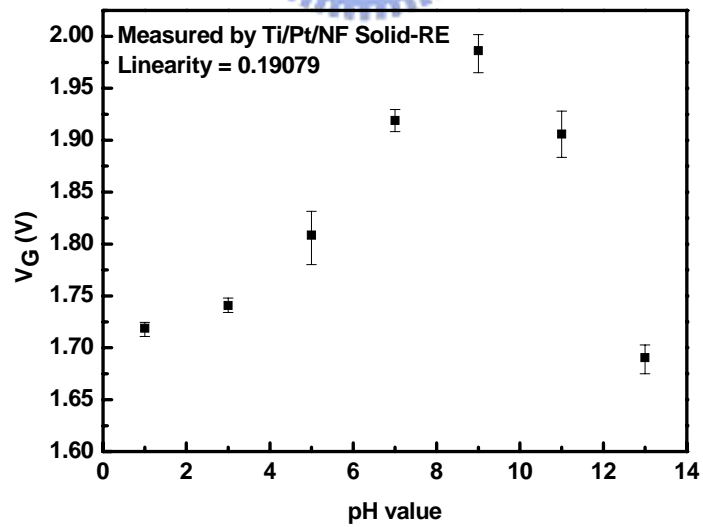
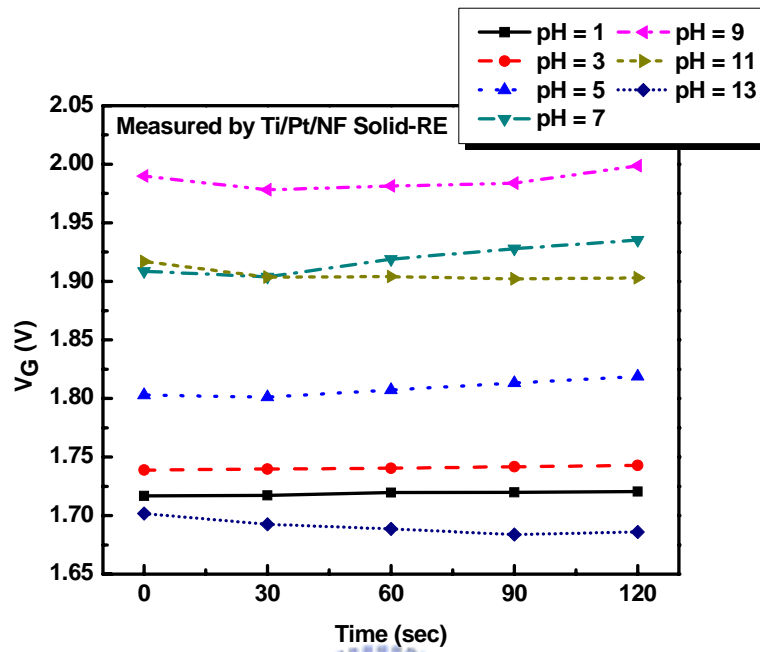


Fig. 4-11 Reproducibility and sensitivity linearity of  $ZrO_2$ -pH-ISFET measured by Ti/Pt/NF solid-state reference electrode

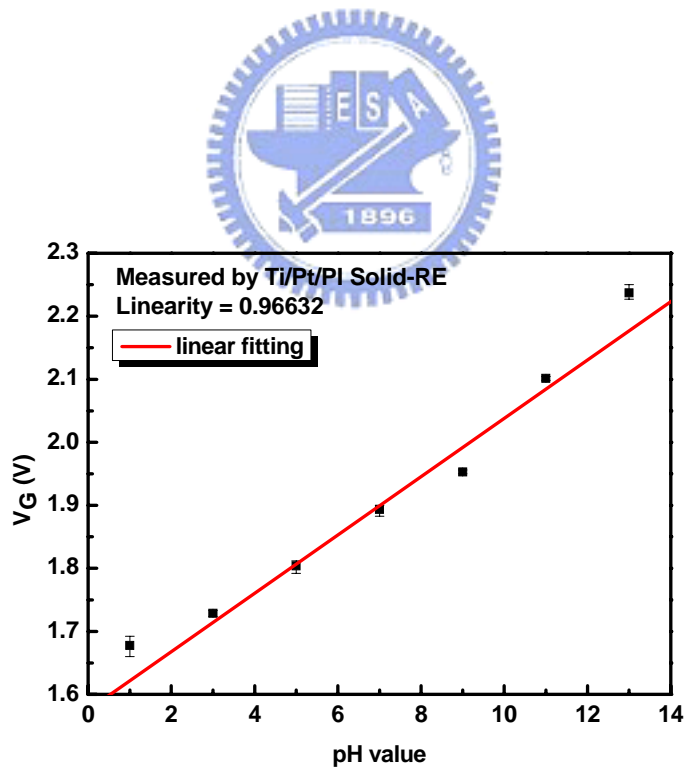
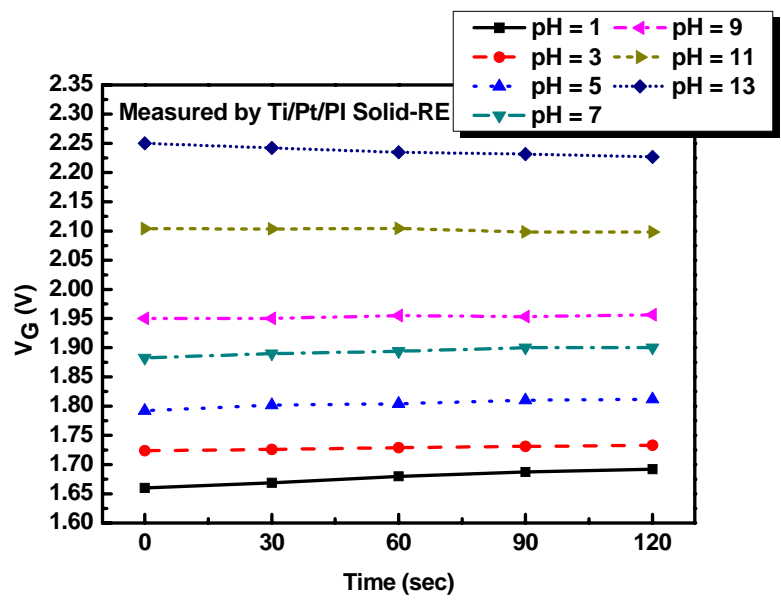


Fig. 4-12 Reproducibility and sensitivity linearity of  $ZrO_2$ -pH-ISFET measured by Ti/Pt/PI solid-state reference electrode

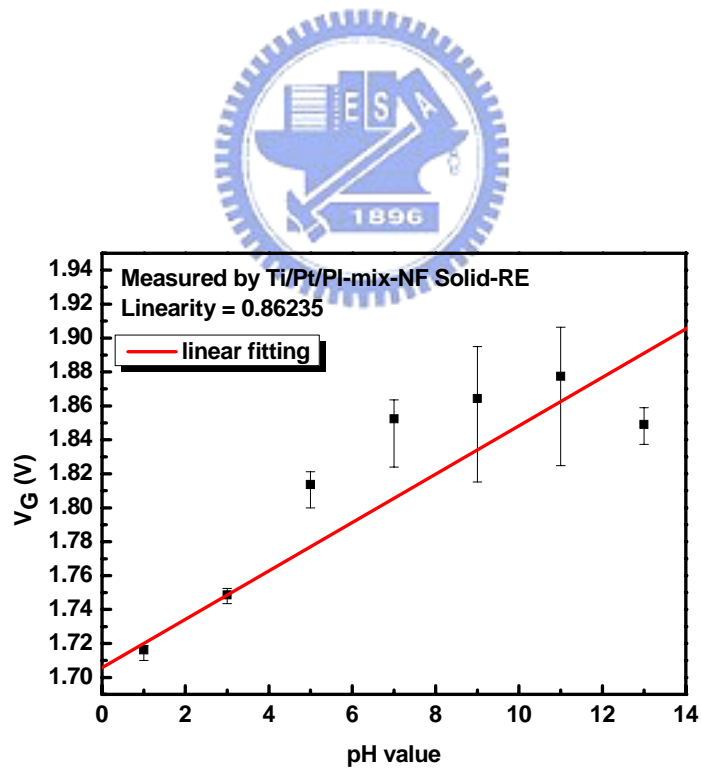
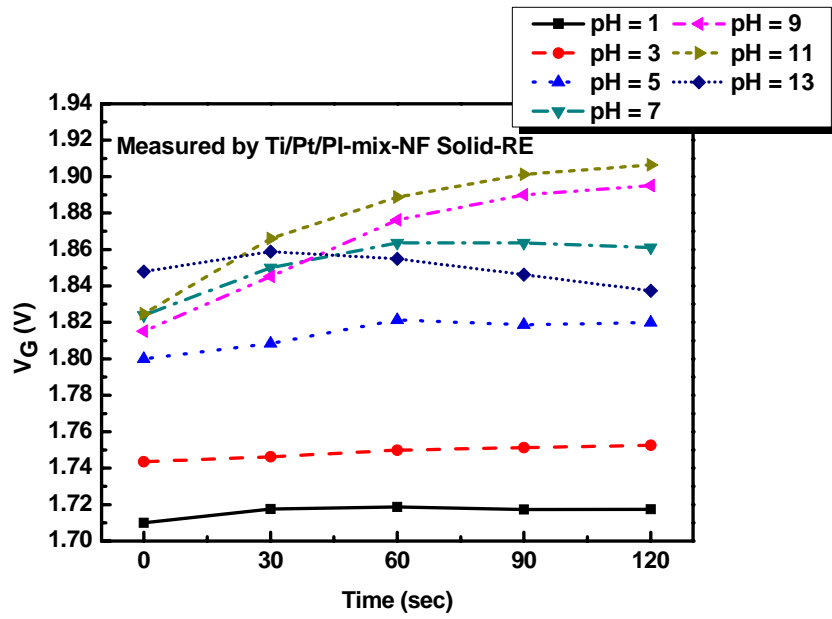


Fig. 4-13 Reproducibility and sensitivity linearity of  $ZrO_2$ -pH-ISFET measured by Ti/Pt/PI-mix-NF solid-state reference electrode



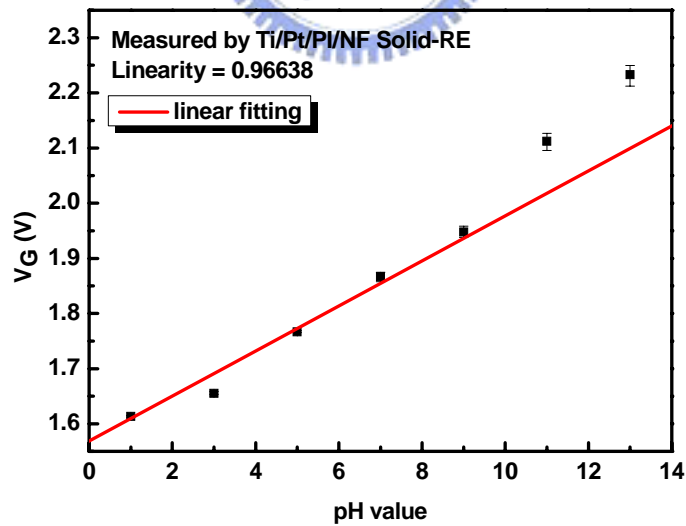
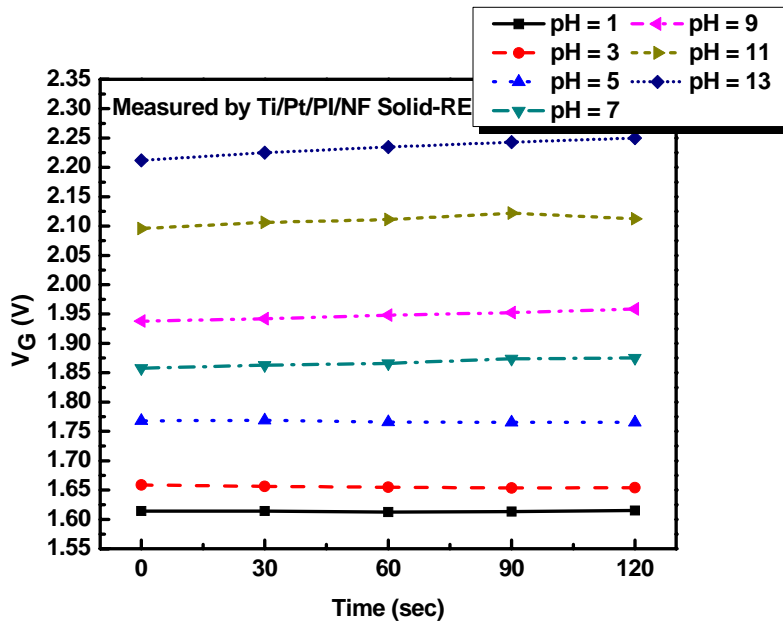


Fig. 4-14 Reproducibility and sensitivity linearity of  $ZrO_2$ -pH-ISFET measured by Ti/Pt/PI/NF solid-state reference electrode

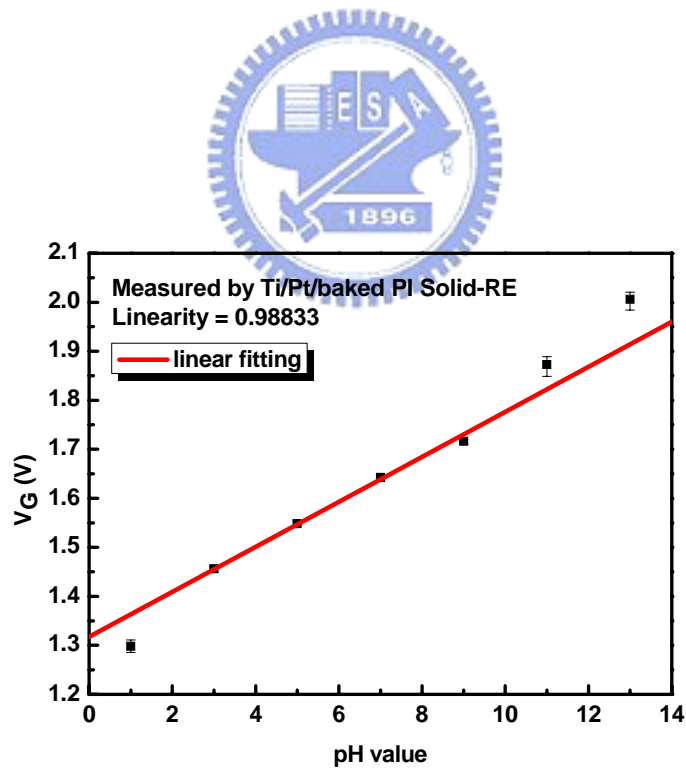
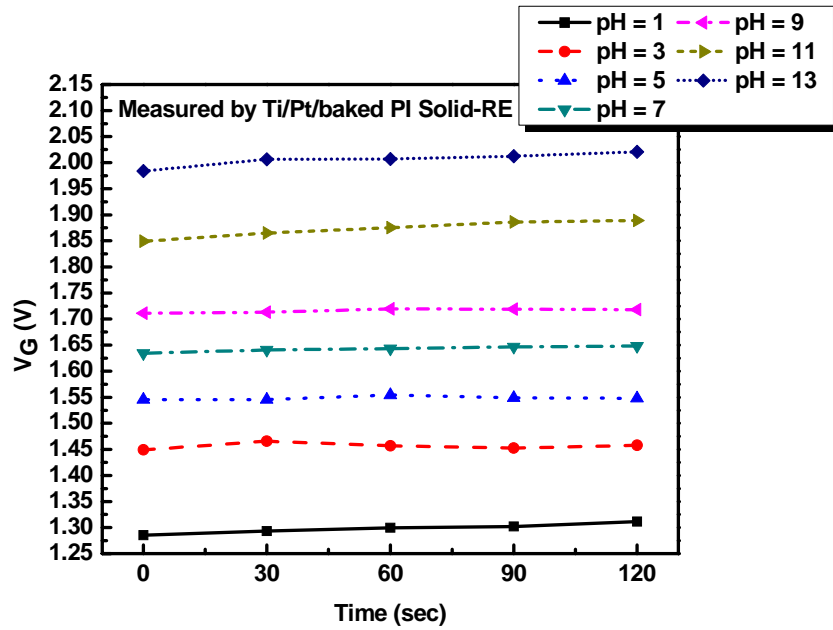


Fig. 4-15 Reproducibility and sensitivity linearity of  $ZrO_2$ -pH-ISFET measured by Ti/Pt/baked PI solid-state reference electrode

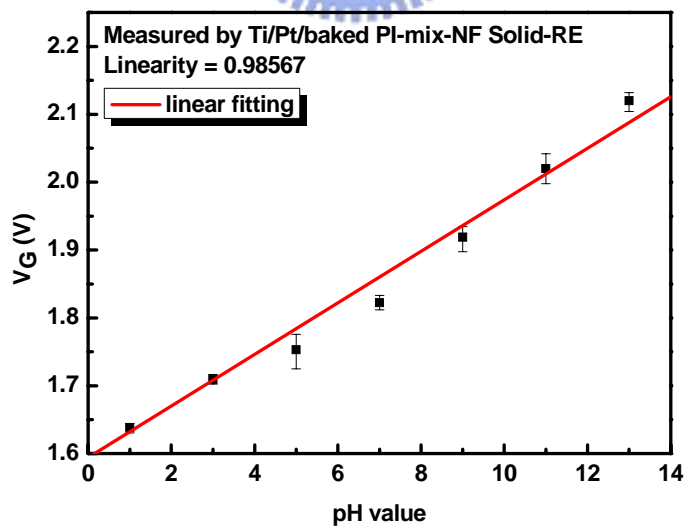
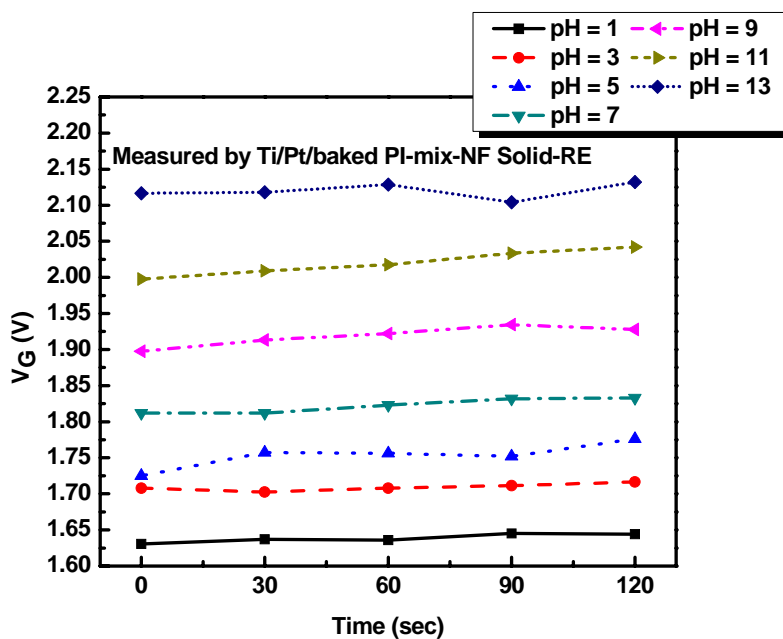


Fig. 4-16 Reproducibility and sensitivity linearity of  $ZrO_2$ -pH-ISFET measured by Ti/Pt/baked PI-mix-NF solid-state reference electrode

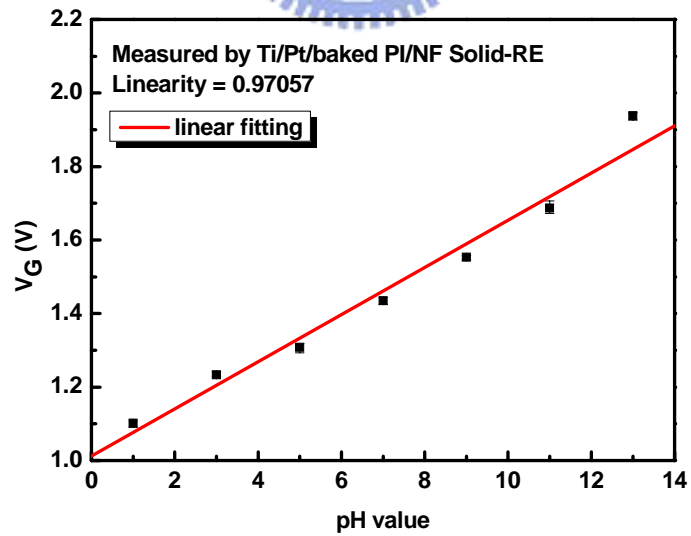
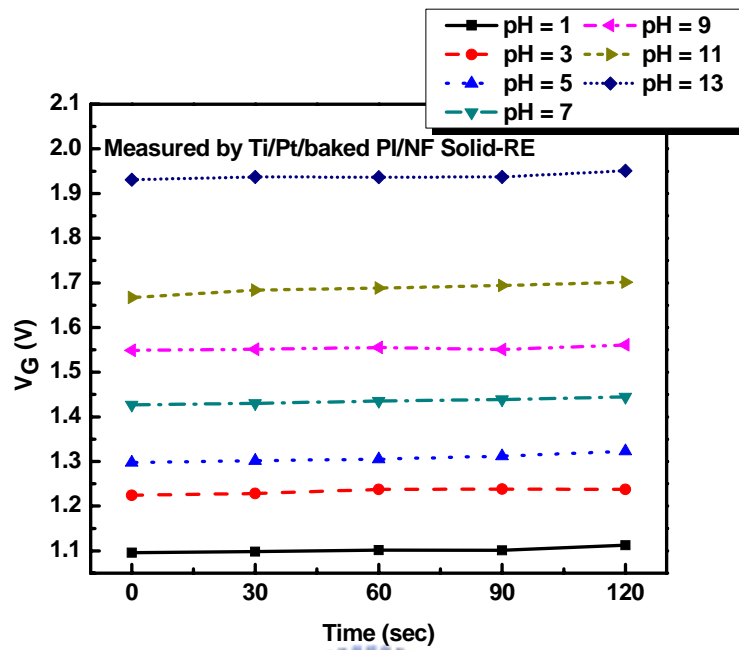


Fig. 4-17 Reproducibility and sensitivity linearity of  $ZrO_2$ -pH-ISFET measured by Ti/Pt/baked PI/NF solid-state reference electrode

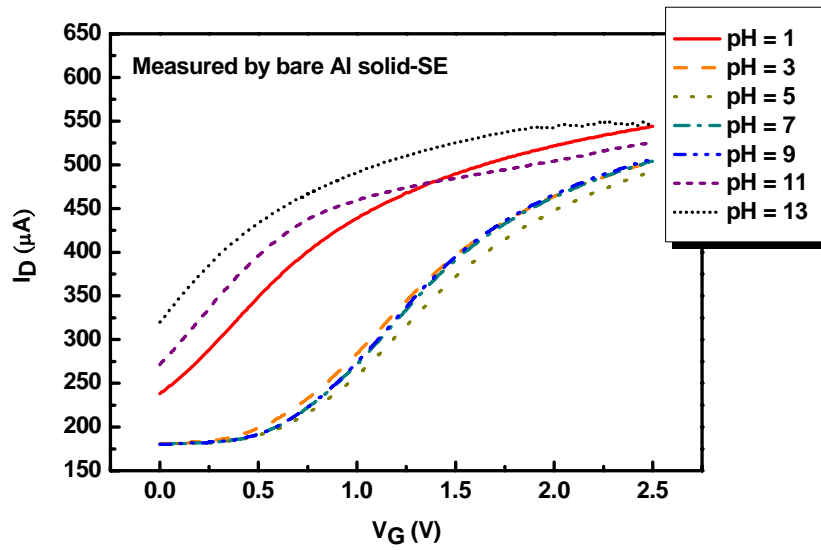


Fig. 4-18 Sensitivity of  $ZrO_2$ -pH-ISFET measured by bare Al solid-state reference electrode

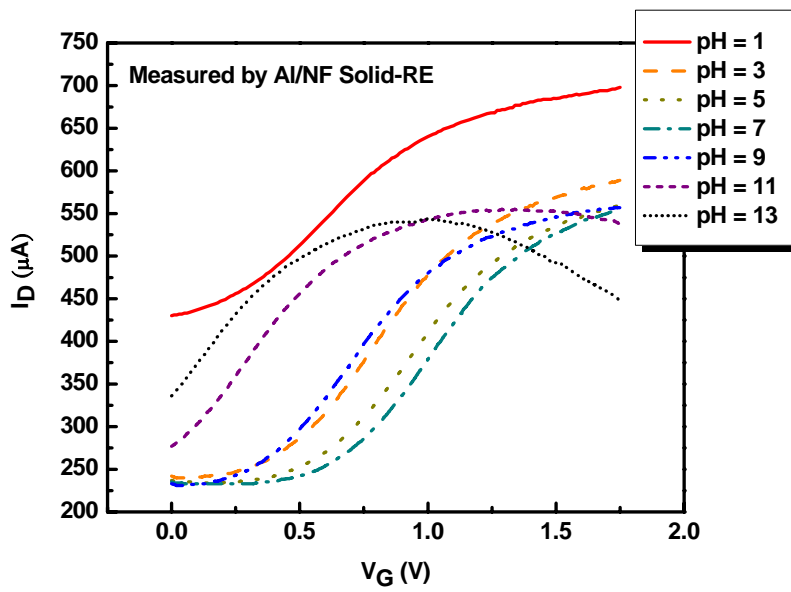
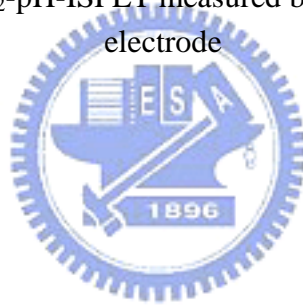


Fig. 4-19 Sensitivity of  $ZrO_2$ -pH-ISFET measured by Al/NF solid-state reference electrode

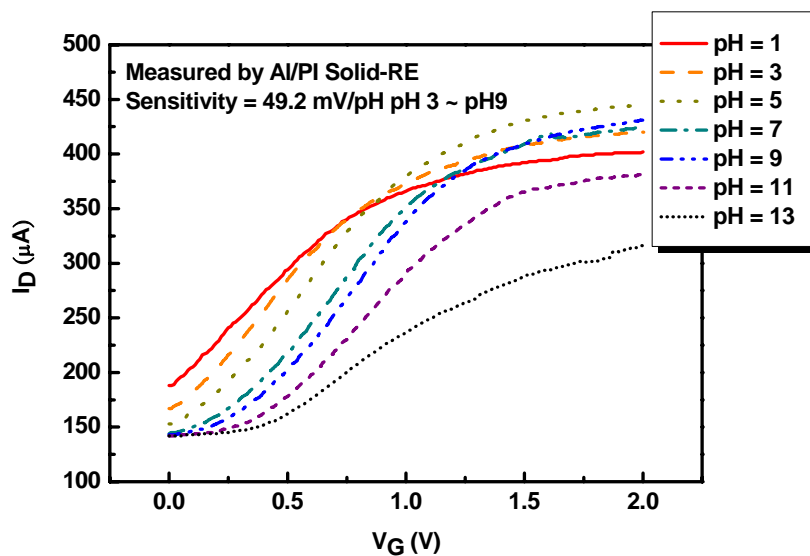


Fig. 4-20 Sensitivity of  $ZrO_2$ -pH-ISFET measured by Al/PI solid-state reference electrode

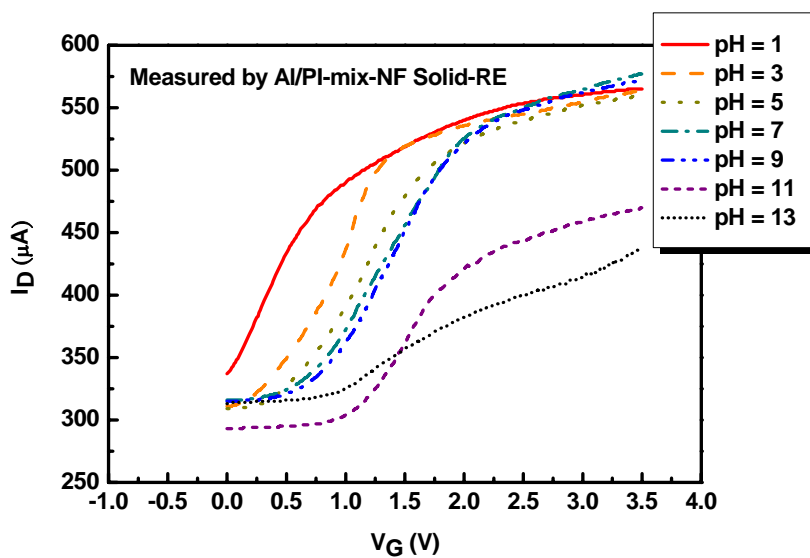
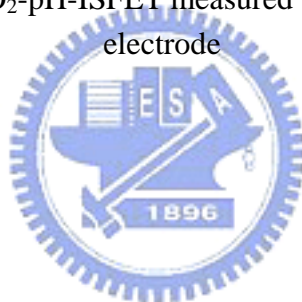


Fig. 4-21 Sensitivity of  $ZrO_2$ -pH-ISFET measured by Al/PI-mix-NF solid-state reference electrode

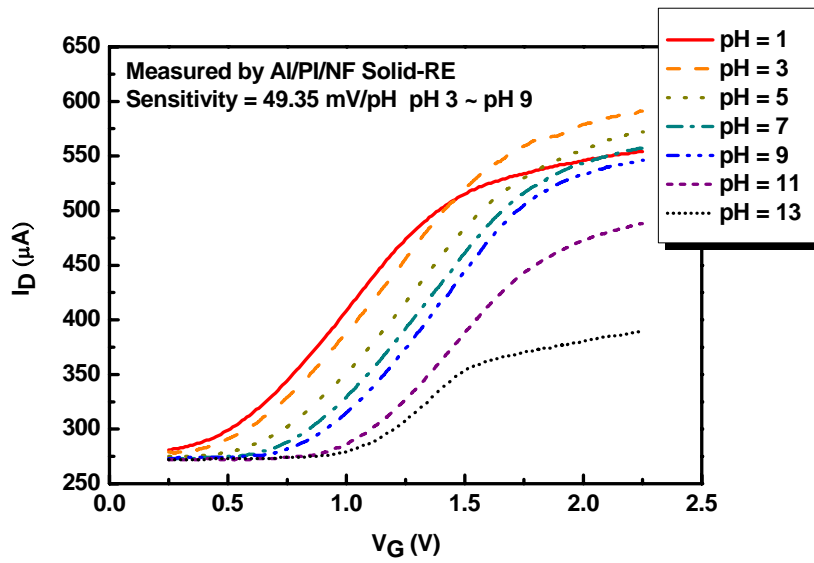


Fig. 4-22 Sensitivity of ZrO<sub>2</sub>-pH-ISFET measured by Al/PI/NF solid-state reference

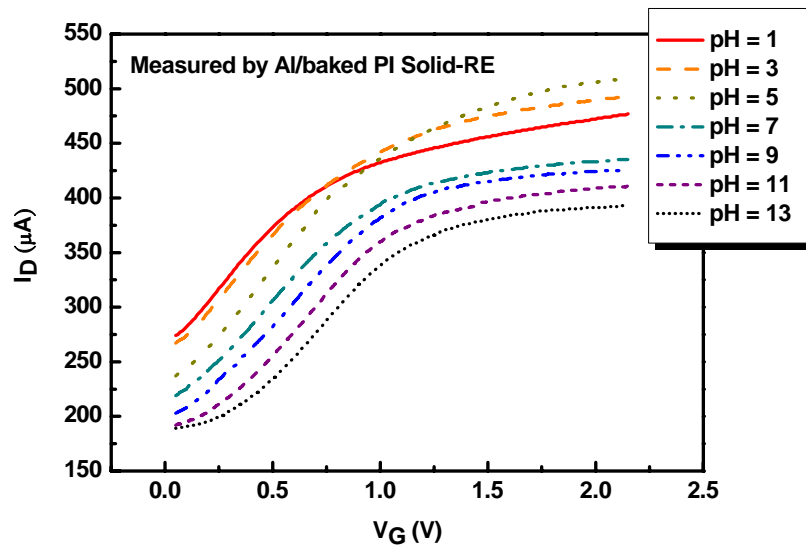
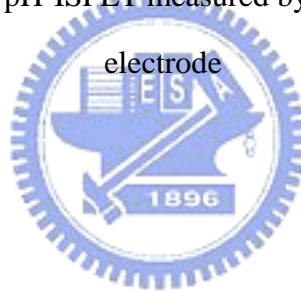


Fig. 4-23 Sensitivity of ZrO<sub>2</sub>-pH-ISFET measured by Al/baked PI solid-state reference electrode

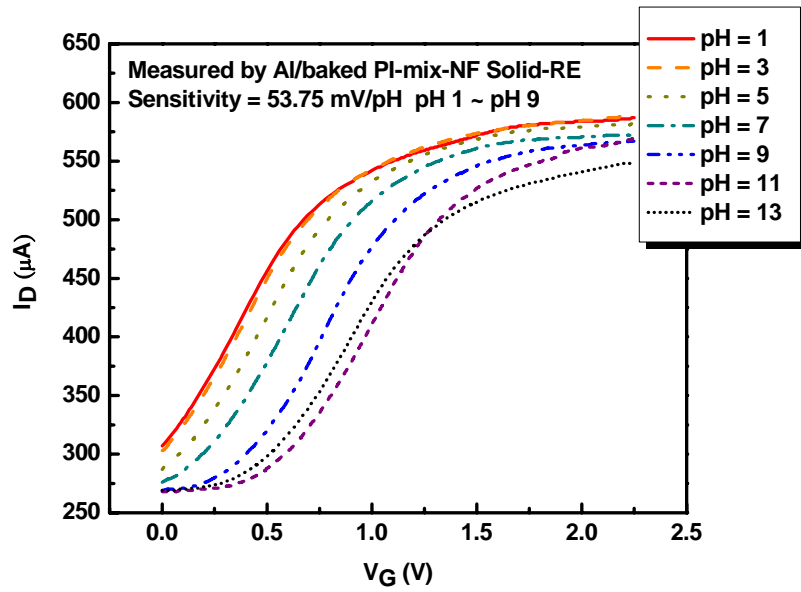


Fig. 4-24 Sensitivity of  $ZrO_2$ -pH-ISFET measured by Al/baked PI-mix-NF solid-state reference electrode

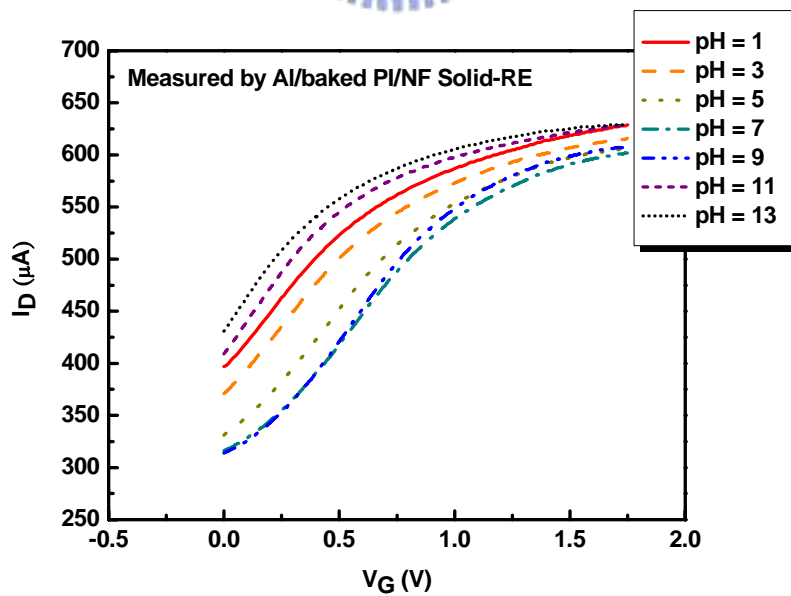
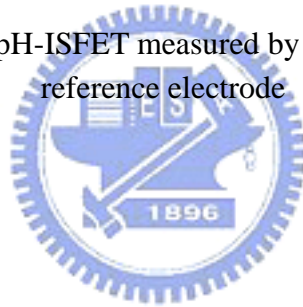


Fig. 4-25 Sensitivity of  $ZrO_2$ -pH-ISFET measured by Al/baked PI/NF solid-state reference electrode



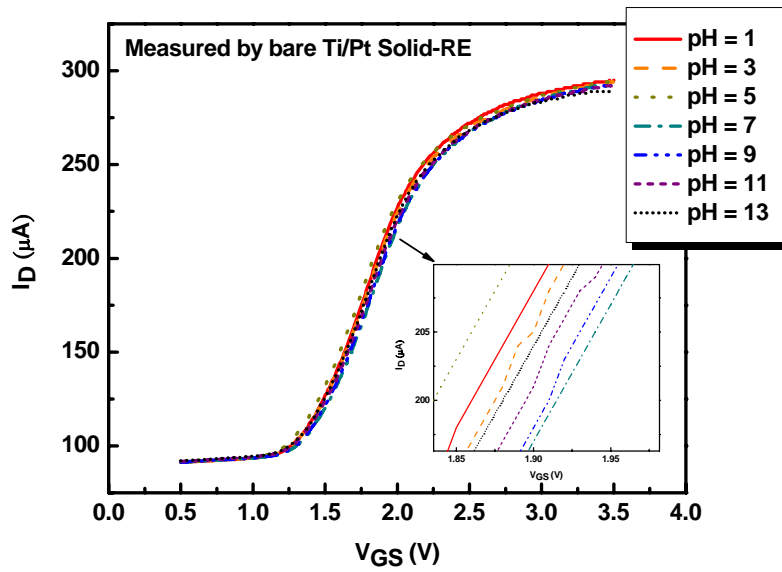


Fig. 4-26 Sensitivity of  $ZrO_2$ -pH-ISFET measured by bare Ti/Pt solid-state reference electrode

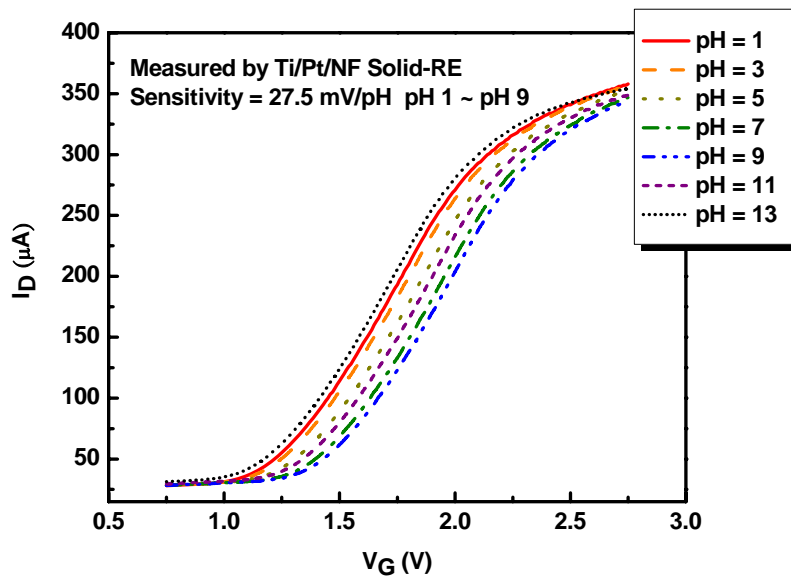
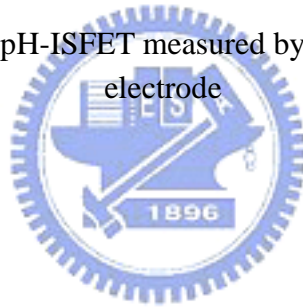


Fig. 4-27 Sensitivity of  $ZrO_2$ -pH-ISFET measured by Ti/Pt/NF solid-state reference electrode

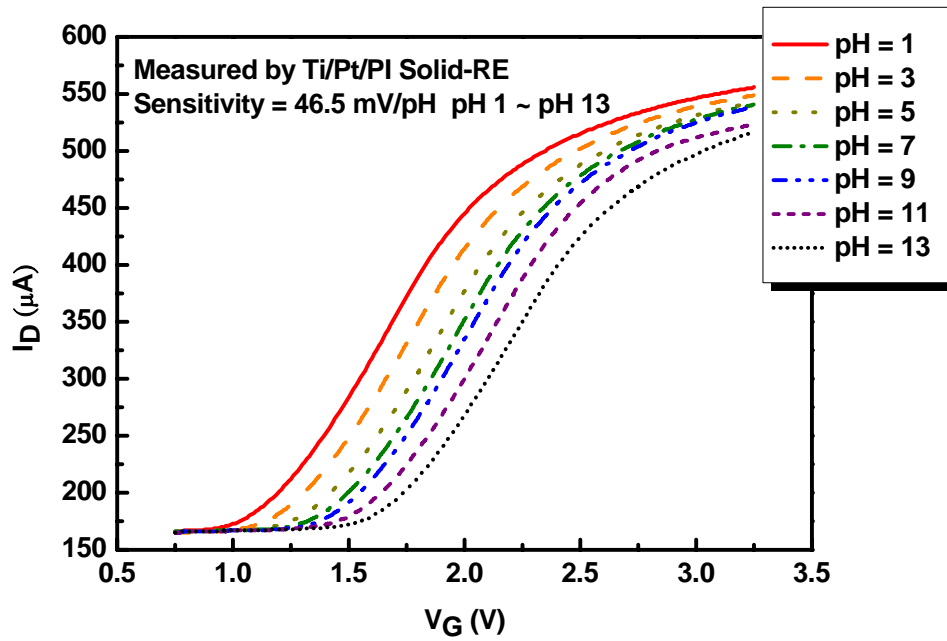


Fig. 4-28 Sensitivity of ZrO<sub>2</sub>-pH-ISFET measured by Ti/Pt/PI solid-state reference electrode

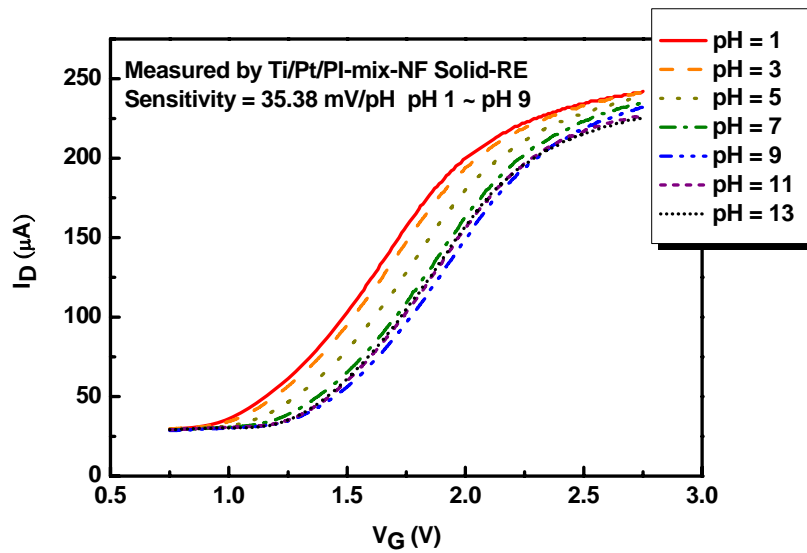


Fig. 4-29 Sensitivity of ZrO<sub>2</sub>-pH-ISFET measured by Ti/Pt/PI-mix-NF solid-state reference electrode

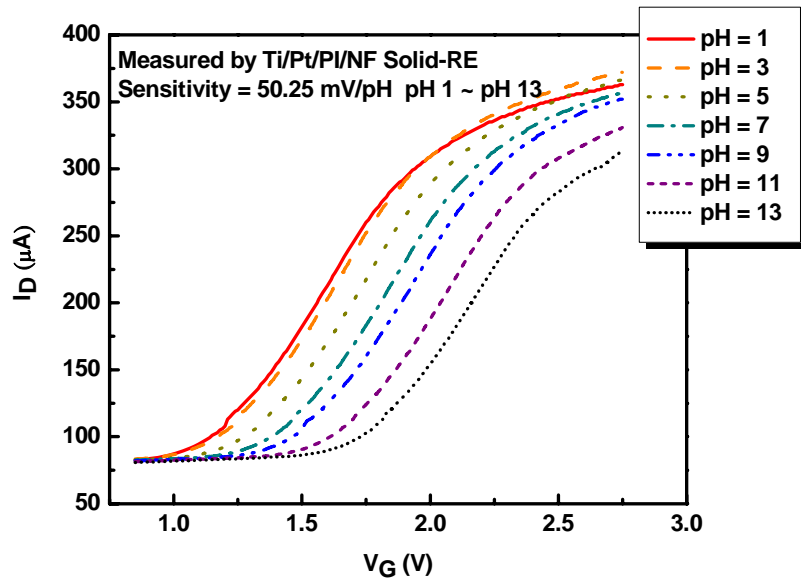


Fig. 4-30 Sensitivity of  $ZrO_2$ -pH-ISFET measured by Ti/Pt/PI/NF solid-state reference electrode

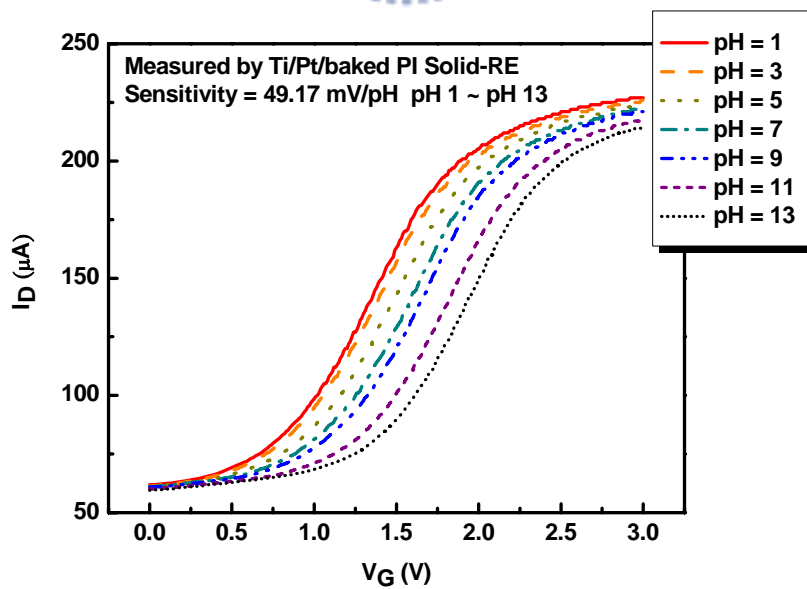
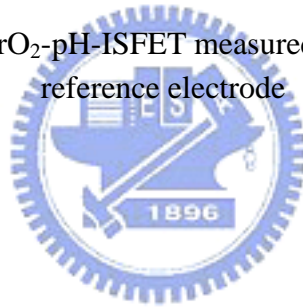


Fig. 4-31 Sensitivity of  $ZrO_2$ -pH-ISFET measured by Ti/Pt/baked PI solid-state reference electrode

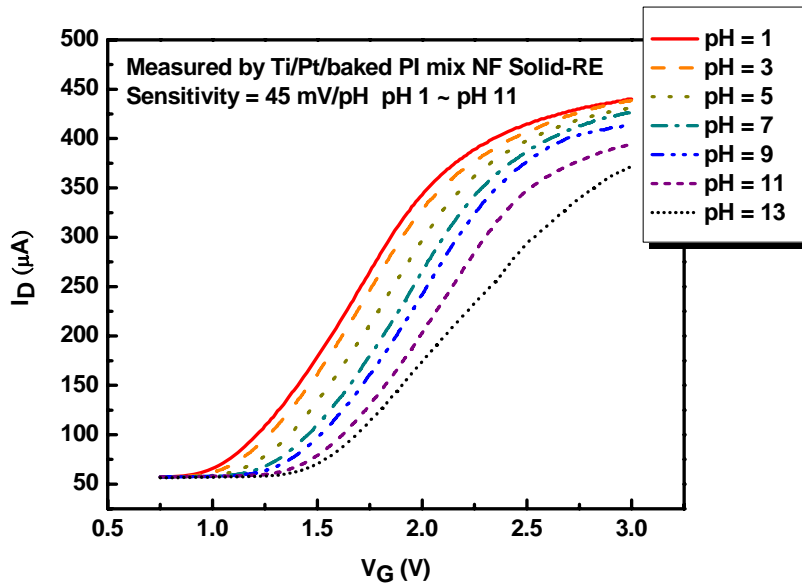


Fig. 4-32 Sensitivity of  $ZrO_2$ -pH-ISFET measured by Ti/Pt/baked PI-mix-NF solid-state reference electrode

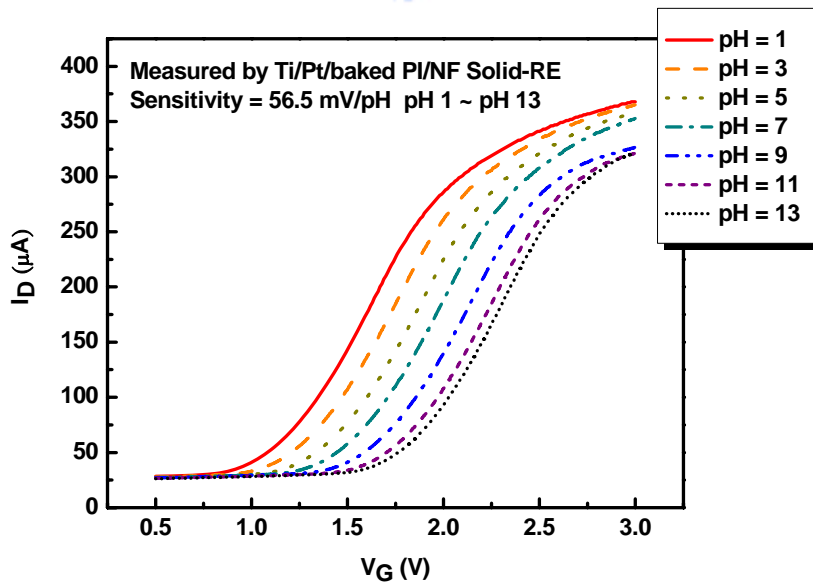
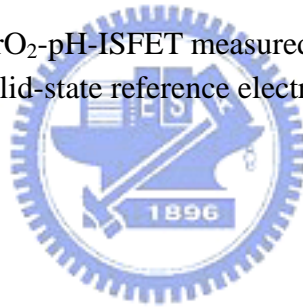


Fig. 4-33 Sensitivity of  $ZrO_2$ -pH-ISFET measured by Ti/Pt/baked PI/NF solid-state reference electrode

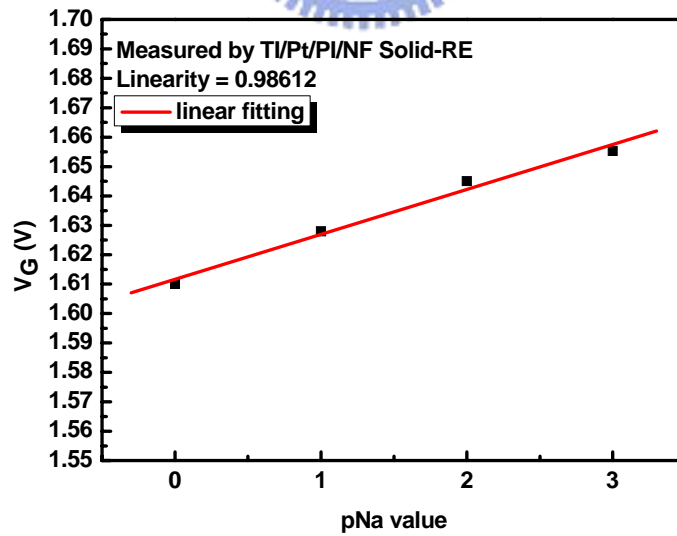
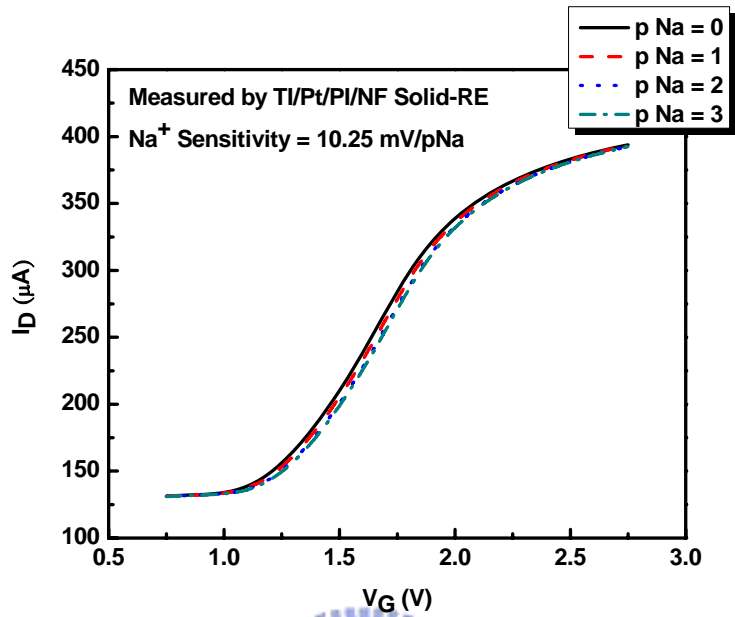


Fig. 4-34  $\text{Na}^+$  sensitivity and sensitivity linearity of  $\text{ZrO}_2$ -ISFET by Ti/Pt/PI/NF solid-state reference electrode

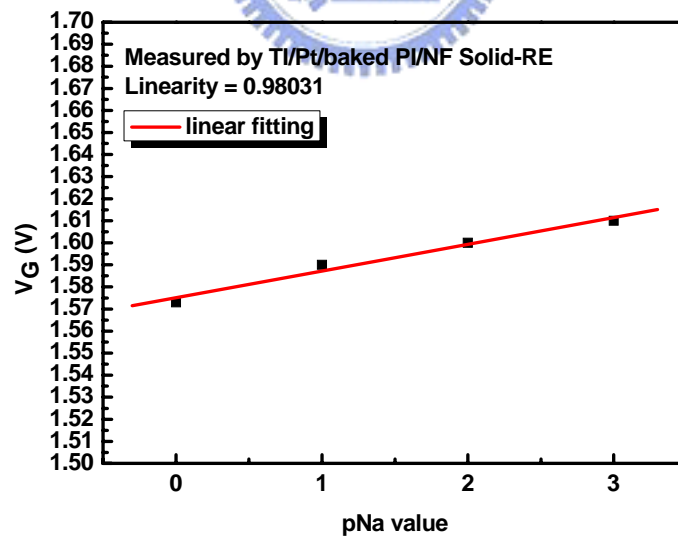
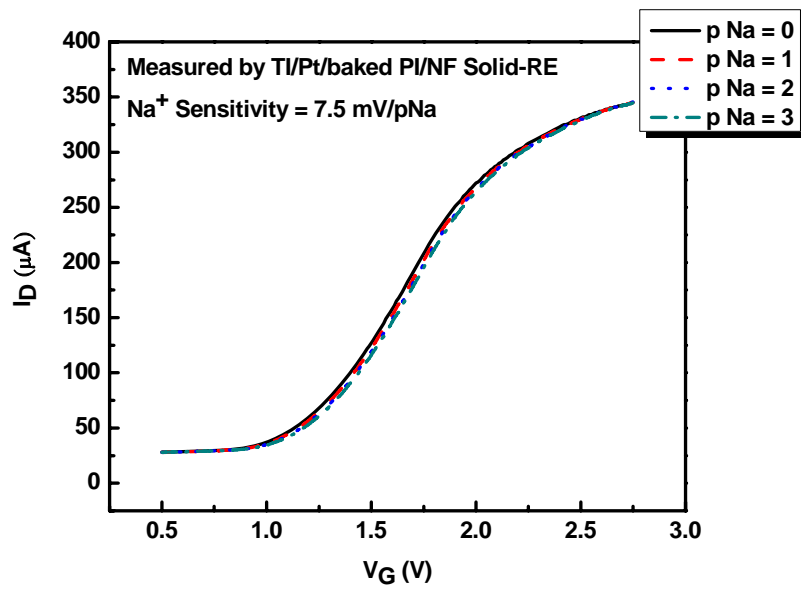


Fig. 4-35  $\text{Na}^+$  sensitivity and sensitivity linearity of  $\text{ZrO}_2$ -ISFET by Ti/Pt/baked PI/NF solid-state reference electrode

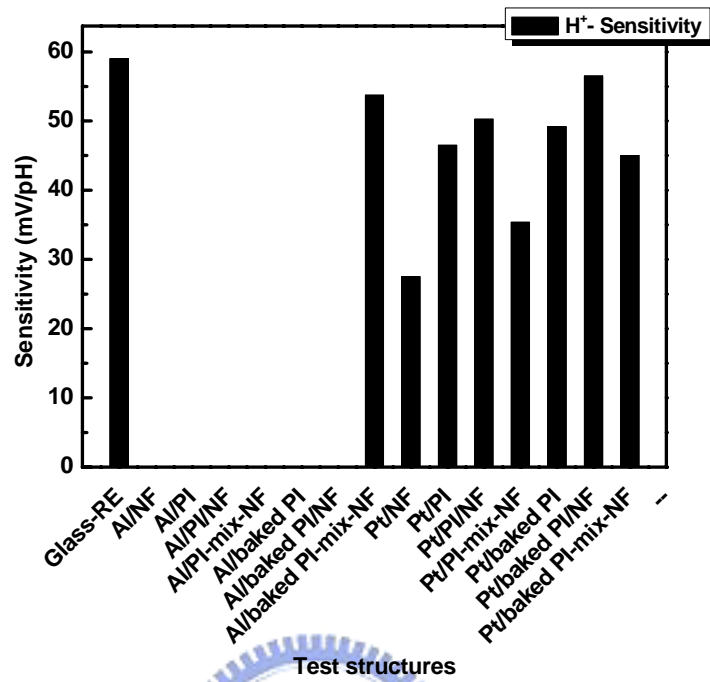


Fig. 4-36 Summary of H<sup>+</sup>-sensitivity for different test structures

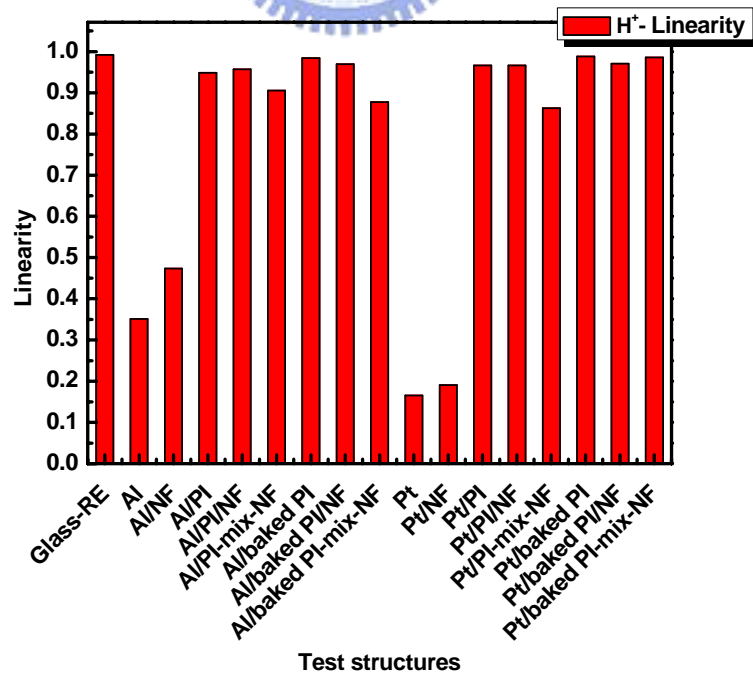


Fig. 4-37 Summary of H<sup>+</sup>-linearity for different test structures

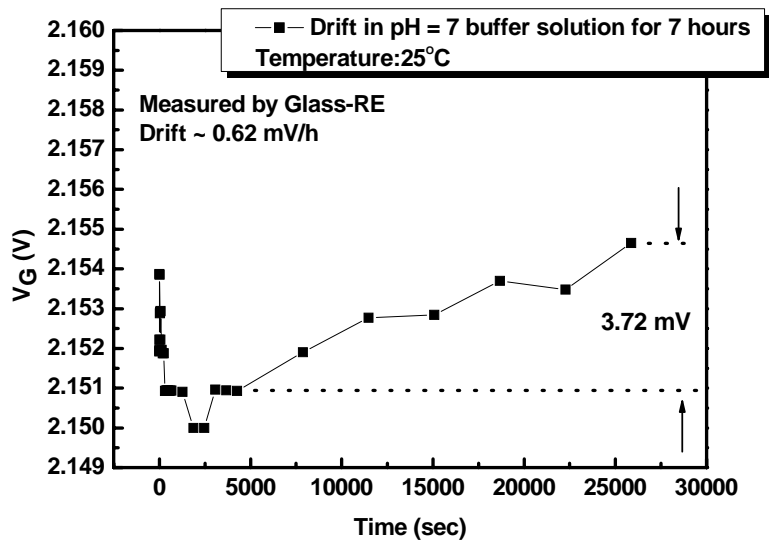


Fig. 4-38 Drift of  $ZrO_2$ -pH-ISFET measured by glass reference electrode for 7 hours

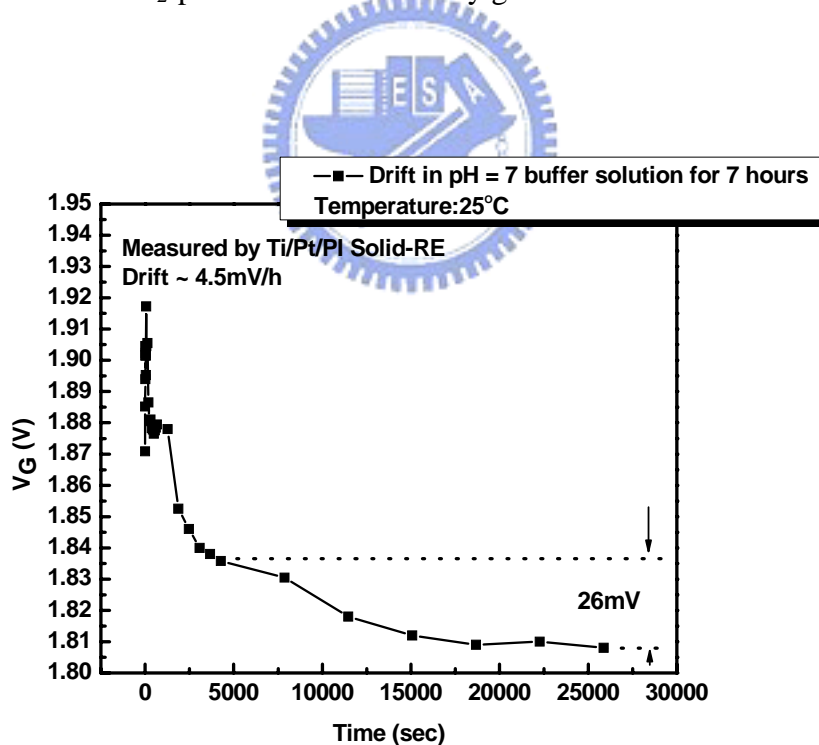


Fig. 4-39 Drift of  $ZrO_2$ -pH-ISFET measured by Ti/Pt/PI solid-state reference electrode for 7 hours



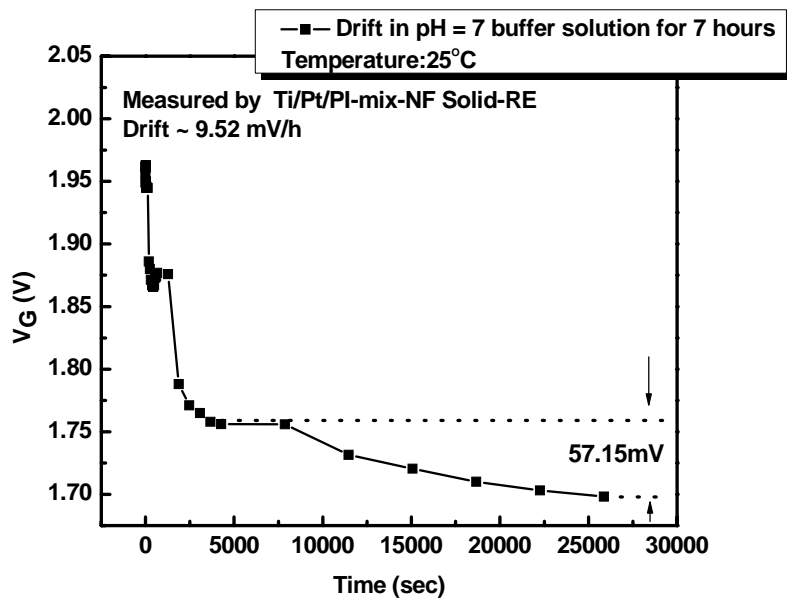


Fig. 4-40 Drift of ZrO<sub>2</sub>-pH-ISFET measured by Ti/Pt/PI-mix-NF solid-state reference electrode for 7 hours

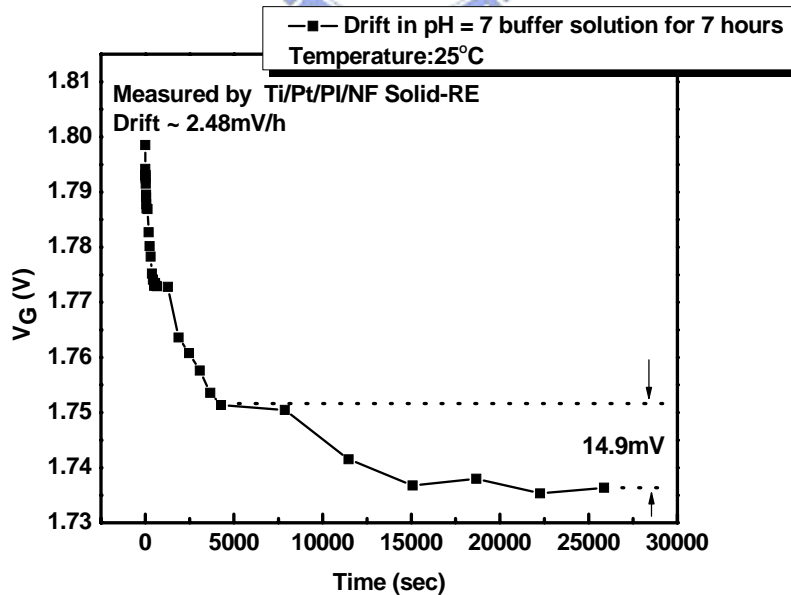


Fig. 4-41 Drift of ZrO<sub>2</sub>-pH-ISFET measured by Ti/Pt/PI/NF solid-state reference electrode for 7 hours

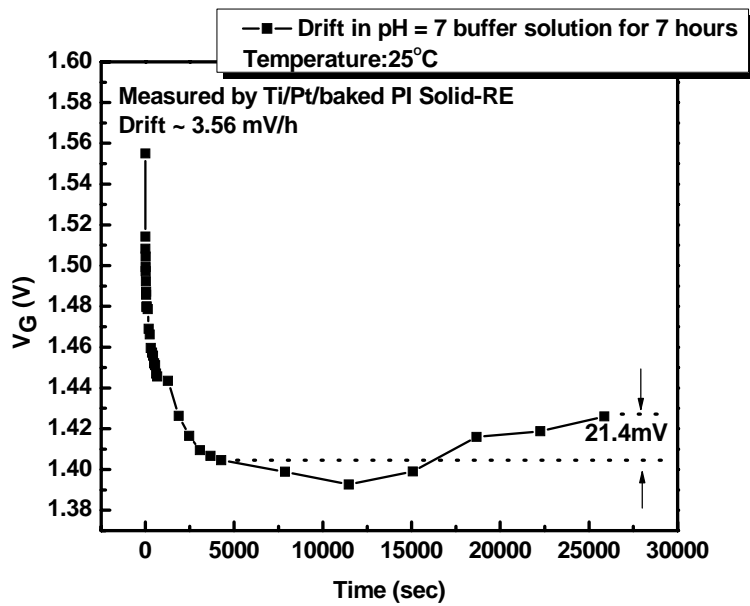


Fig. 4-42 Drift of  $ZrO_2$ -pH-ISFET measured by Ti/Pt/baked PI solid-state reference electrode for 7 hours

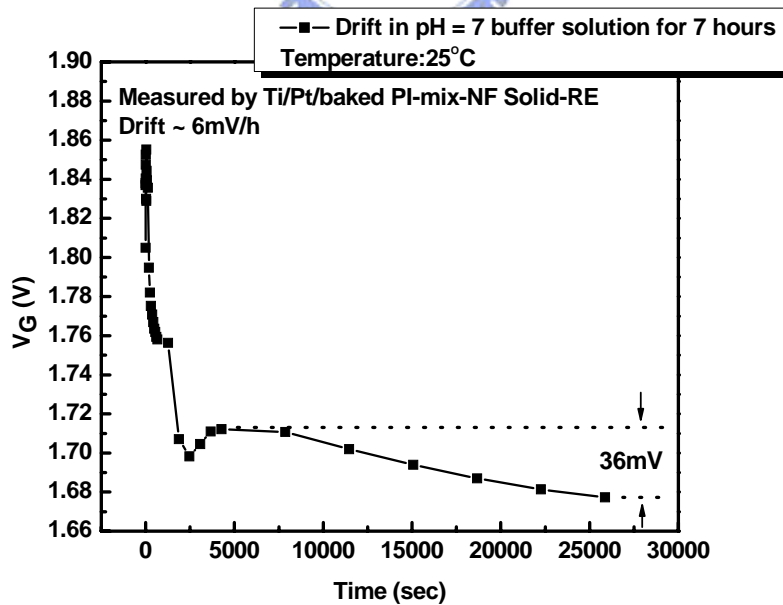
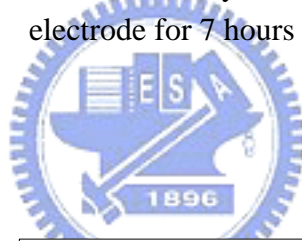


Fig. 4-43 Drift of  $ZrO_2$ -pH-ISFET measured by Ti/Pt/baked PI-mix-NF solid-state reference electrode for 7 hours

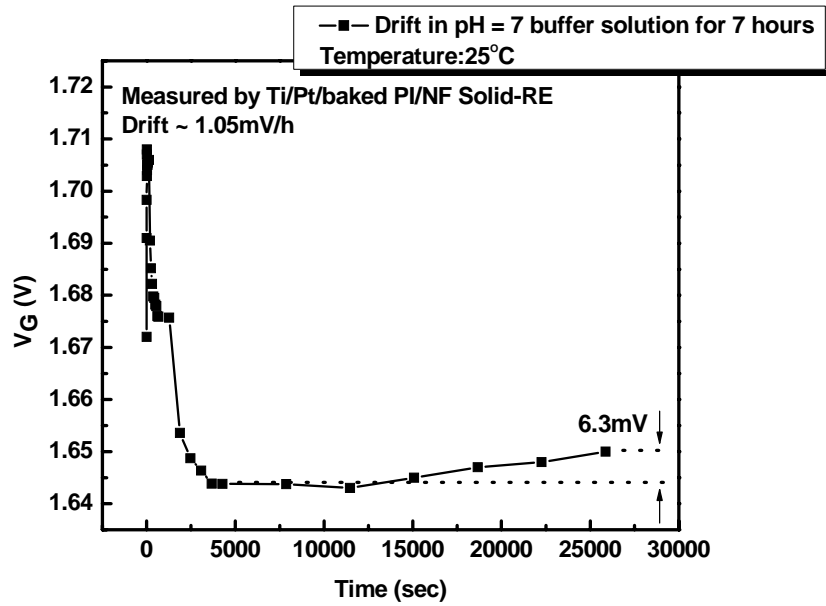


Fig. 4-44 Drift of  $ZrO_2$ -pH-ISFET measured by Ti/Pt/baked PI/NF solid-state reference electrode for 7 hours

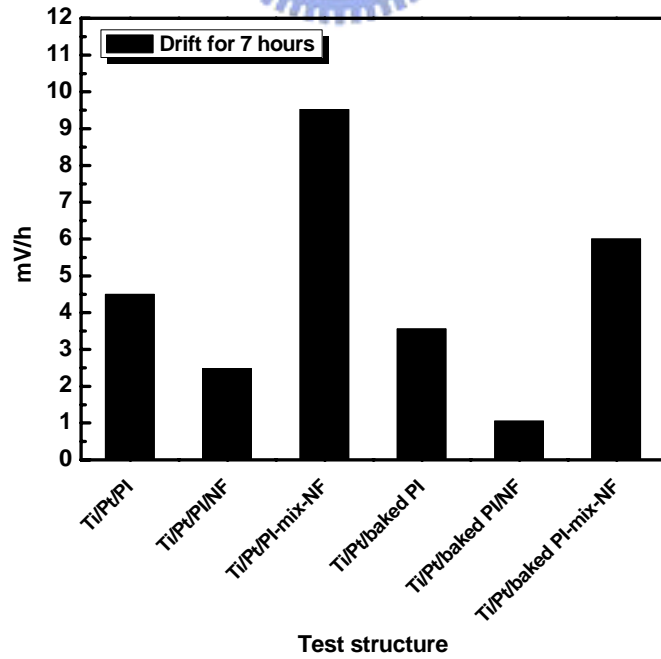


Fig. 4-45 Summary of drift for different test structures

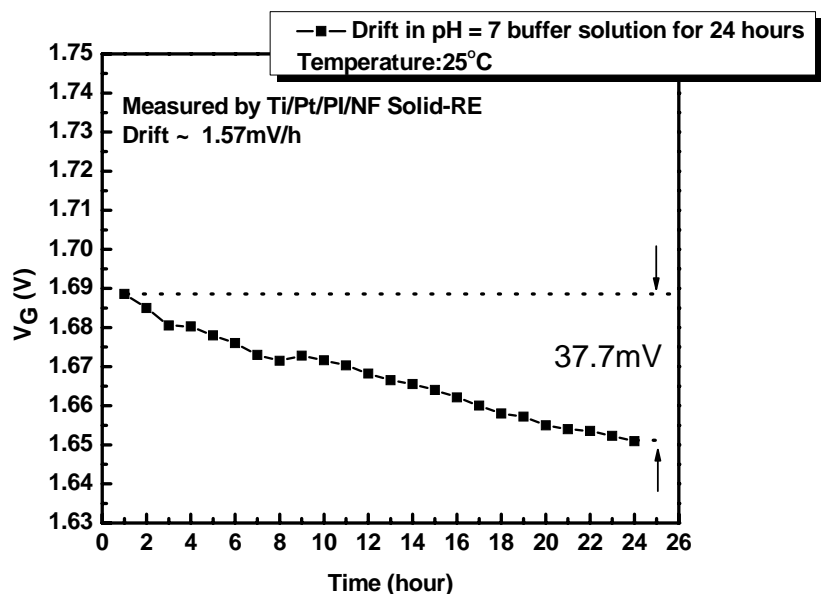


Fig. 4-46 Drift of  $ZrO_2$ -pH-ISFET measured by Ti/Pt/PI/NF solid-state reference electrode for 24 hours

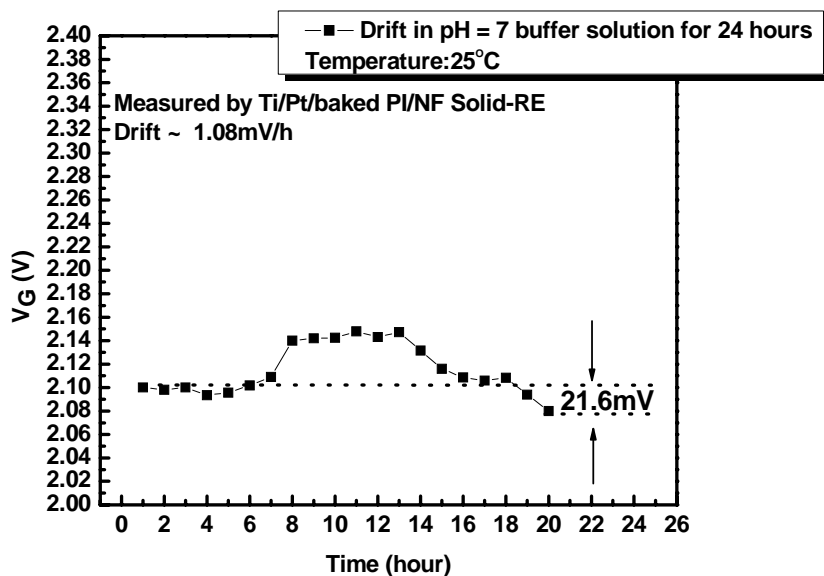
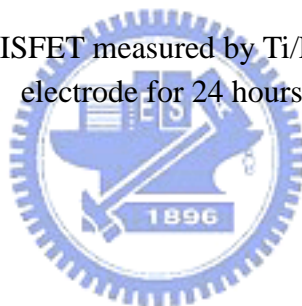


Fig. 4-47 Drift of  $ZrO_2$ -pH-ISFET measured by Ti/Pt/baked PI/NF solid-state reference electrode for 24 hours

Table 4-1 Summary of H<sup>+</sup> sensitivity for different test structures

Solid-state RE test structure		H <sup>+</sup> Sensitivity(mV/pH)			
		Without baking	pH range	With baking	pH range
Al	NF	NA			
	PI	49.2	pH 3 ~ pH 9	NA	
	PI-mix-NF	NA		53.73	pH 1 ~ pH 9
	PI/NF	49.35	pH 3 ~ pH 9	NA	
Ti/Pt	NF	27.5	pH 1 ~ pH 9		
	PI	46.5	pH 1 ~ pH 13	49.17	pH 1 ~ pH 13
	PI-mix-NF	35.38	pH 1 ~ pH 9	45	pH 1 ~ pH 11
	PI/NF	50.25	pH 1 ~ pH 13	58.5	pH 1 ~ pH 11

Table 4-2 Summary of drift for different Ti/Pt test structures

Solid-state RE test structure	Drift for 7 hours		Drift for 24 hours	
	Without baking	With baking	Without baking	With baking
Ti/Pt/PI	4.5 mV/h	3.56 mV/h		
Ti/Pt/PI-mix-NF	9.52 mV/h	6 mV/h		
Ti/Pt PI/NF	2.48 mV/h	1.05 mV/h	1.57 mV/h	1.08 mV/h

## 簡 歷

姓 名：何 彥 忠

性 別：男

出生日期：民國 73 年 07 月 17 日

籍 貫：台灣省台中縣

學 歷：台北市立教育大學

(民國 91 年 7 月~民國 95 年 7 月)

國立交通大學電子工程研究所

(民國 95 年 7 月~民國 97 年 7 月)

碩士論文：以Polyimide高分子材料/Nafion<sup>TM</sup>質子交換膜為結構作

pH-ISFET之微小化固態電極之研究

The study of Nafion<sup>TM</sup>/polymer structure based sensing films  
on pH-ISFET applications